CAPACITANCE-VOLTAGE STUDY ON THE EFFECTS OF LOW ENERGY ELECTRON RADIATION ON $Al_{0.27}Ga_{0.73}N$/GaN HIGH ELECTRON MOBILITY TRANSISTORS

THESIS

Thomas D. Jarzen, Major, USA

AFIT/GNE/ENP/05-05

DEPARTMENT OF THE AIR FORCE
AIR UNIVERSITY

AIR FORCE INSTITUTE OF TECHNOLOGY

Wright-Patterson Air Force Base, Ohio

APPROVED FOR PUBLIC RELEASE; DISTRIBUTION UNLIMITED

The views expressed in this thesis are those of the author and do not reflect the official policy or position of the United States Air Force, Department of Defense, or the United States Government.

AFIT/GNE/ENP/05-05

CAPACITANCE-VOLTAGE STUDY ON THE EFFECTS OF LOW ENERGY ELECTRON RADIATION ON $Al_{0.27}Ga_{0.73}N$/GaN HIGH ELECTRON MOBILITY TRANSISTORS

THESIS

Presented to the Faculty

Department of Engineering Physics

Graduate School of Engineering and Management

Air Force Institute of Technology

Air University

Air Education and Training Command

In Partial Fulfillment of the Requirements for the

Degree of Master of Science (Nuclear Science)

Thomas D. Jarzen

Major, USA

March 2005

APPROVED FOR PUBLIC RELEASE; DISTRIBUTION UNLIMITED

AFIT/GNE/ENP/05-05

CAPACITANCE-VOLTAGE STUDY ON THE EFFECTS OF LOW ENERGY ELECTRON RADIATION ON $Al_{0.27}Ga_{0.73}N$/GaN HIGH ELECTRON MOBILITY TRANSISTORS

Thomas D. Jarzen
Major, USA, B.S., M.S.

Approved:

Dr. James C. Petrosky (Chairman) — 11 MAR 05 date

Dr. Gary C. Farlow (Member) — 10 March 05 date

Dr. Paul Kladitis (Member) — 10 MAR 05 date

Abstract

The effects of radiation on semiconductors are extremely important to the Department of Defense since the majority of the defense informational, navigational and communications systems are now satellite-based. Due to the high radiation tolerance of gallium nitride and a plethora of high temperature, high power and high frequency applications, the prospect that gallium nitride based devices will become key components in a multitude of military satellite-based systems is highly probable.

AlGaN/GaN HEMTs were irradiated at low temperature (~80 K) by 0.45 – 0.8 MeV electrons up to fluences of 1×10^{15} e^-/cm^2. Following irradiation, low temperature capacitance-voltage measurements were recorded providing fluence-dependent measurements; additionally low-temperature post-irradiation capacitance-voltage measurements were recorded at twenty-four hour intervals up to 72 hours in order to investigate the room temperature annealing process. Using previously irradiated devices, the effects of a 9 month and 12 month room temperature anneal were also considered.

Capacitance-voltage measurements indicate that low energy electron radiation results in an increase in the transistor channel drain current. These increases occur both at low and room temperature. The mechanism, clearly shown through capacitance-voltage measurements, causing the increase in drain current is an increase in the carrier concentration in the 2DEG. This result is due to donor electrons from a nitrogen vacancy in the gallium nitride. The devices begin to anneal immediately and show almost complete recovery after 72 hours.

To my family

Acknowledgments

Dr. James Petrosky, my advisor, has been an invaluable asset and mentor by providing vital technical knowledge, experience and assistance. Truly, without his help this project would never have reached completion. Prior to taking his class *radiation effects on electronics*, I did not even know what a semiconductor was other than something that controlled a microwave oven. He has been an outstanding guide through a strange land.

Dr. Gary Farlow of the Wright State University was responsible for providing the means by which the experiments were carried out. Without the timeless efforts he provided towards repairing, maintaining and running the Van de Graff facility during the experiments, there would be no results to present.

Renate Hannaford of the AFIT library was responsible for assisting in a massive literature search on radiation interaction in GaN and AlGaN. Without her assistance, much of this document would have been incomplete.

Larry Callaghan was responsible for wafer dicing and packaging. His consistently quick turn-around on packaging requests proved to be integral, allowing experiments to be conducted when needed.

My Wife, Daughters and Sons, and other family members and friends continuously provided me with the support and encouragement that kept me going through this long and arduous process. Now all my time will once again be theirs.

And, to DMJ and SAJ for without them none of this would have been possible.

Illigitimi non carborundum sunt!

Table of Contents

Page

Abstract iv

Acknowledgments vi

List of Figures ix

List of Tables xv

List of Symbols xvi

List of Abbreviations and Acronyms xviii

I. Introduction 1

- Background 1
- Problem Statement 9
- Hypothesis 9
- Objectives 9
- Scope 9
- Approach 10
- Assumptions 11
- Sequence of Presentation 12

II. Literature Review 13

- Purpose 13
- Fundamentals of Gallium Nitride heterostructures 13
- Importance of Aluminum Gallium Nitride and Gallium Nitride 14
- Radiation Effects of Protons on AlGaN / GaN 17
- Radiation Effects of Electrons in AlGaN / GaN 22
- Capacitance-Voltage Measurements 26
- Research Justification 31

III. Theory 32

- CV Measurements 32
- Heterostructure Energy Band Diagrams 39
- Performing CV Measurements 42
- Radiation Interaction in GaN 44
- Expected Radiation Effects on C-V Curves 47

IV. Experimental Procedures 52

Transistor Background 52
Pre-Irradiation Characterization 56
Irradiation Experiments 61

V. Experimental Results 73

Irradiation Experiment: Sample A19 73
Irradiation Experiments: Sample A16 74
Irradiation Experiments: Sample A1 76
Irradiation Experiments: Sample A2 84
Previously Irradiated Samples: A0408 and A0409 90
Analysis and Discussion 96

VI. Conclusions and Recommendations 104

Conclusions 104
Recommendations for Further Work 105

Appendix A – Visual Basic Data Acquisition Program 107

Appendix B – Pre-characterization C-V Plots (80K / 330K) 115

Appendix C – Carrier Concentration Calculations 117

Bibliography 118

List of Figures

Figure Page

1. Schematic representation of the trapped electron radiation belts [3].....3

2. Cross-Section of a typical AlGaN/GaN HEMT [17].....7

3. Charge carrier velocity versus electric field for various semiconductors [10].....15

4. Transconductance versus gate-source voltage for AlGaN/AlN/GaN HEMTs before and after 1.8 MeV proton irradiation with fluences from 1×10^{13} cm^{-2} to 1×10^{15} cm^{-2} [30].....19

5. Common-source drain current as a function of gate voltage and transconductance of the same transistor pre-irradiation (solid line), post-10^{12} cm^{-2} fluence (dashed line), and post-5×10^{13} cm^{-2} fluence (dotted line) [13].....20

6. Transfer characteristics for AlGaN/GaN HEMTs before and after 1.8 MeV proton irradiation at various fluences [31].....21

7. Transfer characteristics for AlGaN/GaN HEMTs before and after 105-MeV proton irradiation at different fluences [31].....22

8. Sample A0409 FatFET First Irradiation: Change in *I-V* Curves at LiN Temperature (0.45 MeV Electrons) [21].....24

9. Sample A0409 FatFET Second Irradiation: Change in *I-V* Curves at LiN Temperature (0.45 MeV Electrons) [21].....25

10. Typical plot of the variation of the capacitance (pF) of a 500 μm x 500 μm capacitor versus gate voltage (V_G) ranging from –4.7 to +4.7 volts [33].....27

11. Typical C-V curve measured in darkness at room temperature [35].....28

12. 1/C2 characteristics as a function of bias voltage [35].....28

13. High frequency capacitance-voltage curves for a n-type MOS capacitor measure: (a) before irradiation; (b) after 143 Mrad (Si) irradiation; and (c) after 482 Mrad (Si) irradiation [38]. 30

14. Textbook example of a Capacitance-Voltage Curve [38]. 32

15. Diagram of a typical MOS structure [34]. 33

16. Shape of Capacitance-Voltage curves for ideal and real MOS capacitors with *n*-type Si substrate [34]. 34

17. Band bending diagrams for a Metal Oxide Semiconductor under various applied biases a) accumulation, b) depletion, c) inversion [40]. 38

18. Schematic diagram of the energy bands and the quantum well in an AlGaN/GaN MODFET with gate bias of $V_G = 0$. E_C, E_V and E_F are conduction band, valence band and the Fermi level, respectively. The vertical axis is a measure of energy, qV, and the horizontal axis represents the various heterostructure layers. 39

19. Band diagram of AlGaN/GaN MODFET in accumulation due to an applied gate bias of $V_G > 0$. 40

20. Band diagram of AlGaN/GaN MODFET in depletion due to an applied gate bias of $V_G < 0$. 41

21. Band diagram of AlGaN/GaN MODFET in inversion due to an applied gate bias of $V_G << 0$. 41

22. Plot showing the positive and negative sweep direction and the statistically insignificant effects of hysteresis on the measurements. 43

23. Illustration of the standard C-V measurement procedures: (1) Apply Bias, (2) Light On, (3) Light Off Stabilization, (4) Bias Sweep [39]. 44

24. Maximum energy transfer for gallium and nitrogen as a function of the incident energy. The average and minimum displacement energy for both gallium and nitrogen are shown as horizontal lines [18]. 46

25. Normalized 1-MHz C_{HF}-V curves of an MOS capacitor at several times following pulsed electron beam irradiation [3]. 48

26. Doping dependence of MOS-capacitor high frequency C-V characteristics [41]. 50

27. Wafer section JSO1A containing approximately 40 individual chips. Scale to the right is inches for comparison only. 53

28. Close-up of individual chip showing FATFET location in upper left of the image to the right of the CV ring. Contacts labeled G, S and D. Photo taken by Larry Callaghan of AFRL/SN. 54

29. Individual FATFET spatial layout. 54

30. Cross section of FATFET along AB in Figure 13. 55

31. Diced and packaged chip from wafer section JSO1A. Photo taken by Larry Callaghan of AFRL/SN. 56

32. Building 470 laboratory Experimental Setup for Pre-Irradiation C-V Characterization 57

33. Cold Head and Sample Mounting Assembly [18]. 59

34. Comparison of capacitance-voltage measurements for nine devices averaged over seven cycles and measured at 300K and 80K. 59

35. Graphical representation of the impact of grounding the devices and the intrinsic (additional) capacitance added by the cold head mounting system. 61

36. Van de Graaff facility at Wright State University. 62

37. Sample device attached to cold head by clamp and contact leads soldiered to cold head feed-through lines. 63

38. Schematic of the Experimental Setup at the Wright State University Van de Graaff Facility 65

39. Insulation of cold head by sealing with masking tape and paper towels. 1a) Cold head, 1b) Feed through lines, 2) Liquid nitrogen exit port, 3) Liquid nitrogen input, and 4) VDG beam tube. 66

40. Pre- and Post-Irradiation capacitance-voltage measurements of A19 recorded at room temperature. 74

41. A16 Pre- and Post-Irradiation capacitance-voltage measurements recorded at low temperature (~80K) plotted with 60- & 84-hour room temperature anneal curves. 75

42. A16 Pre- and Post-Irradiation capacitance-voltage measurements at room temperature. 76

43. Pre- and Post-Irradiation capacitance-voltage measurements of device A1 recorded at low temperature (~80K) after a fluence of 3.5×10^{12} e/cm^2 with 0.45 MeV electrons. 77

44. Pre- and Post-Irradiation carrier concentrations of device A1 recorded at low temperature (~80K) after a fluence of 3.5×10^{12} e/cm^2 with 0.45 MeV electrons. 77

45. A1 Post-Irradiation capacitance-voltage measurements at low temperature (~80K) after a fluence of 7.9×10^{12} e/cm^2 with 0.45 MeV electrons. 78

46. A1 Post-Irradiation capacitance-voltage measurements at low temperature (~80K) after a fluence of 2.3×10^{13} e/cm^2 with 0.45 MeV electrons. 79

47. Comparison of Sample A1 Pre-Irradiation C-V data with subsequent irradiation C-V data at fluence levels of 3.5×10^{12} e/cm^2, 7.9×10^{12} e/cm^2 and 2.3×10^{13} e/cm^2 with 0.45 MeV electrons. 80

48. A1 Pre- and Post-Irradiation carrier concentrations at low temperature (~80K) after irradiation at fluence levels of 3.5×10^{12} e/cm^2, 7.9×10^{12} e/cm^2 and 2.3×10^{13} e/cm^2 with 0.45 MeV electrons. 81

49. A1 Pre- and Post-Irradiation capacitance-voltage measurements at room temperature after a total fluence of 1.13×10^{14} e/cm^2 and compared with the 36 and 72-hour room temperature anneal curve. 82

50. A1 Pre- and Post-Irradiation capacitance-voltage measurements at low temperature after a total fluence of $1.13x10^{14}$ e/cm^2 compared with the 48 and 72-hour room temperature anneal curves.....83

51. A1 Pre- and Post-Irradiation carrier concentrations at room temperature with carrier concentration of 48-hour room temperature anneal data.....83

52. A2 Post-Irradiation capacitance-voltage measurements at low temperature (~80K) after a fluence of 3.5×10^{12} e/cm^2 with 0.8 MeV electrons. 85

53. A2 Pre- and Post-Irradiation capacitance-voltage measurements at low temperature (~80K) after a fluence of 3.5×10^{12} e/cm^2 with 0.8 MeV electrons..85

54. A2 Pre- and Post-Irradiation capacitance-voltage measurements at low temperature (~80K) after a fluence of 7.9×10^{12} e/cm^2 with 0.8 MeV electrons..86

55. A2 Post-Irradiation capacitance-voltage at low temperature (~80K) after a fluence of 2.3×10^{13} e/cm^2 with 0.8 MeV electrons. 87

56. A2 Pre- and Post-Irradiation capacitance-voltage measurements at low temperature (~80K) after a fluence of 2.3×10^{13} e/cm^2 with 0.8 MeV electrons..87

57. Comparison of irradiation C-V data at fluence levels of 3.5×10^{12} e/cm^2, 7.9×10^{12} e/cm^2 and 2.3×10^{13} e/cm^2 with 0.8 MeV electrons. 88

58. Comparison of Pre-Irradiation C-V data with subsequent irradiation C-V data at fluence levels of 3.5×10^{12} e/cm^2, 7.9×10^{12} e/cm^2 and 2.3×10^{13} e/cm^2 with 0.8 MeV electrons showing negative increase in capacitance. 88

59. A2 Pre- and Post-Irradiation capacitance-voltage measurements at room temperature after a total fluence of $1.14x10^{14}$ e/cm^2 and compared with the 24 & 60 hour room temperature anneal curves. 89

60. A2 Pre-Irradiation capacitance-voltage measurement at low temperature after a total fluence of $1.14x10^{14}$ e/cm^2 compared with the 36 and 60 hour room temperature anneal curves.....90

61. Sample A0408 Pre- and Post-Irradiation C-V curve (0.45 MeV electrons) 91

62. Sample A0408 Pre- and Post-Irradiation Carrier Concentration 92

63. Sample A0409 Pre- and Post-Irradiation C-V curve (0.45 MeV electrons).....93

64. Sample A0409 Pre- and Post-Irradiation Carrier Concentration 93

65. Comparison of CV curves for A0408 after a nine and twelve-month room temperature anneal measured at 80K. 94

66. Comparison of CV curves for A0409 after a nine and twelve-month room temperature anneal measured at 80K. 94

67. Band diagram of AlGaN/GaN MODFET after irradiation by 0.45 MeV electrons showing increase in carrier concentration due to formation of V_N in the GaN that donate electrons to the 2DEG. 101

68. Negative threshold voltage shift in CV curve as a result of 0.45 MeV electron irradiation creating positive interface trapped charge. 101

69. Band diagram of AlGaN/GaN MODFET after irradiation by 0.8 MeV electrons showing decrease in carrier concentration due to formation of V_{Ga} in the GaN that accept electrons from the heterostructure and 2DEG. 102

70. Screen capture image of program graphic user interface.....114

71. Pre-characterization plots of device A1 (80K and 300K).....115

72. Pre-characterization plots of device A2 (80K and 300K).....115

73. Pre-characterization plots of device A16 (80K and 300K).....116

74. Pre-characterization plots of device A19 (80K and 300K).....116

List of Tables

Table Page

1. Physical properties of wide band gap semiconductors [10].....14
2. Competitive advantages of GaN devices [17]. 16
3. Experimental Device Irradiation Values as conducted by Sattler [21].....26
4. Maximum electron energy transferred to lattice atoms [18].....46
5. A19 and A16 Irradiation Experiment Summary (12 January 2005).....69
6. This table compares the corresponding corrected irradiation fluences calculated after the spot size measurements of 20 January.....69
7. A1 Irradiation Experiment Summary (13 January 2005). 71
8. A2 Irradiation Experiment Summary (14 January 2005). 72
9. Comparison of device Pre- And Post-Irradiation Carrier Concentration.....96

List of Symbols

Symbol	Description	Unit
Å	Angstrom	m
c	Speed of Light	m/s
C_{AlGaN}	AlGaN Capacitance	F
C_{ox}	Oxide Capacitance	F
ε_o	Permittivity in Vacuum	F/cm
ε_{Si}	Silicon Dielectric Constant	F/cm
E	Electric Field	V/m
E_C	Conduction Band Energy Level	eV
E_{e^-}	Incident Electron Energy	eV
E_F	Fermi Level	eV
E_i	ith Quantized Energy Level	eV
E_{trans}^{max}	Maximum Elastic Collisional Transfer Energy	eV
E_V	Valance Band Energy Level	eV
G	Conductance	mS/mm
g_m	Transconductance	mS/mm
I_D, I_d	Drain Current	A
I_{DS}	Source-to-Drain Current	A
I_g	Gate Current	A
k	Boltzman's Constant	eV/K
λ_B	de Broglie wavelength	m
λ_D	Debye Length	nm

m_{e^-}	Electron Rest Mass	kg
m_{atom}	Target Atom Mass	kg
n_i	Intrinsic Carrier Concentration	cm^{-3}
$n(z)$	Position-Dependent Electron Charge Concentration	cm^{-3}
$n_s(x)$	Sheet Charge Density	cm^{-2}
N_D^+, N_d	Ionized Donor Concentration	cm^{-3}
N_A^-	Ionized Acceptor Concentration	cm^{-3}
q	Elementary Charge	C
ρ	Density	g/cm^3
T	Temperature	K
$v(x)$	Electron Mean Velocity	cm/s
V_D	Drain Bias	V
V_{DS}	Drain-Source Bias	V
V_{FB}	Flat Band Voltage	V
V_G	Gate Bias	V
V_S	Source Bias	V
W	Transistor Gate Width	μm
W_d, x_d	Depletion Width	m
x	Mole Fraction of Aluminum in AlGaN or AlGaAs	unitless

List of Abbreviations and Acronyms

Abbreviation	Description
2DEG	Two-Dimensional Electron Gas
III-V	Semiconductor from Group III and Group V
AFIT	Air Force Institute of Technology
AFRL	Air Force Research Laboratories
Al	Aluminum
$Al_xGa_{1-x}N$	Aluminum Gallium Nitride
$Al_xGa_{1-x}As$	Aluminum Gallium Arsenide
AlN	Aluminum Nitride
BJT	Bipolar Junction Transistor
C	Carbon
C-V	Capacitance-Voltage
DLTS	Deep Level Transient Spectroscopy
DOD	Department of Defense
E_d	Displacement Energy
E_T	Threshold Energy
FATFET	FET with an extra wide gate contact
FET	Field-Effect Transistor
Ga	Gallium
GaAs	Gallium Arsenide
GaN	Gallium Nitride

GEO	Geosynchronous Earth Orbit
GHz	Gigahertz
GPIB	General Purpose Interface Bus
HEMT	High Electron Mobility Transistor
HFET	Heterojunction Field-Effect Transistor
I_{Ga}	Gallium Interstitial
I_N	Nitrogen Interstitial
InN	Indium Nitride
In	Indium
I-V	Current-Voltage
keV	kiloelectron volt
kHz	kilohertz
LED	Light Emitting Diode
LEO	Low Earth Orbit
LiN	Liquid Nitrogen
LMDS	Local Multipoint Distribution Services
MEO	Medium Earth Orbit
MeV	Megaelectron Volt
MHz	Megahertz
MMDS	Multipoint Microwave Distribution System
MODFET	Modulation-Doped Field-Effect Transistor
MOS	Metal Oxide Semiconductor
MOSFET	Metal Oxide Field-Effect Transistor

MOS-HFET	Metal-Oxide-Semiconductor Heterostructure Field-Effect Transistor
MOVPE	Metal-Organic Vapor-Phase Epitaxy
N	Nitrogen
N_{C-V}	C-V Carrier Concentration
NIEL	Non-Ionizing Energy Loss
PL	Photoluminescence
RADAR	Radio Detection and Ranging
RF	Radio Frequency
RT	Room Temperature
RTD	Resistive Temperature Device
Si	Silicon
SiC	Silicon Carbide
SMU	Source Measurement Unit
SNDD	Sensors Directorate Aerospace Components and Subsystems Technology Electron Devices Branch
UV	Ultraviolet
VDG	Van de Graff
V_{Ga}	Gallium Vacancy
V_N	Nitrogen Vacancy
WSU	Wright State University

CAPACITANCE-VOLTAGE STUDY ON THE EFFECTS OF LOW ENERGY ELECTRON RADIATION ON $Al_{0.27}Ga_{0.73}N$/GaN HIGH ELECTRON MOBILITY TRANSISTORS

I. Introduction

Background

Over the past forty years there has been a steady growth in the use of semiconductor electronic devices in applications where there is exposure or potential exposure to ionizing radiation. Three major areas of concern for National Defense are: (1) satellites that are exposed to space radiation from solar flares, the Van Allen belts, and cosmic rays; (2) sensory and control electronics systems in nuclear power generating plants; and, (3) nuclear explosion radiation survivability of Department of Defense (DOD) equipment [1].

For our extremely technologically dependent Armed Forces, global electronic communication is an essential component of the successful accomplishment of the warfighter's mission. If the ground commander's communications fail, the most likely outcome is either that mission success will be degraded or that the mission will fail entirely. The importance of radiation hardened communications devices is paramount to future mission accomplishment and is an essential component of force protection. In the military today this force protection includes into protecting the DOD satellite communication systems from accidental or targeted failure due to radiation.

Semiconductors used in satellite electronics illuminate concerns about ionizing radiation as a number of satellites in the past have failed to perform as designed. Due to semiconductor's small volume, a single ionizing particle can produce sufficient ionization to change the operational parameters and the proper functioning of satellite components.

The main energetic particles of the space environment are: 1) protons and electrons in the Van Allen belts, 2) heavy ions trapped by the Earth's magnetic field, 3) protons and ions due to cosmic rays and, 4) protons and ions from solar flares. Due to the scope of this research, the discussion is confined only to energetic electrons. The levels of radiation depend on the activity of the sun. The sun follows a solar cycle that lasts on average about 11 years and oscillates between a minimum and maximum intensity. The Van Allen belts are comprised of mostly electrons up to a few MeV in energy. The inner belt ranges from a few 100 kilometers to 6,000 kilometers with the outer belt extends from the fringe of the inner belt in excess of 60,000 kilometers containing high-energy electrons [2]. The main problem is total ionizing dose and may accumulate to several hundred krads throughout the usable lifetime of a satellite's mission in space. Actual calculations of total dose must take into account the satellite altitude, inclination with respect to the Earth's axis and shielding; however, Figure 1 provides a cross-sectional view of the electron flux that a satellite at various Earth orbits might experience. Satellites in low Earth orbit pass through the Van Allen belts several times a day and experience the effects of trapped electrons [2]. The highest flux level, as shown in the figure, is in the range of $0^{\circ} <$ inclination angle $< 30^{\circ}$ with a steady decrease up to 60° and marginal effects above 60°. Geo-synchronous orbits experience only trapped protons with

energies well below the threshold for initiating nuclear reactions [2]. Thus, for successful operation any device must be capable of operating in an environment containing electrons with energies around 1 MeV.

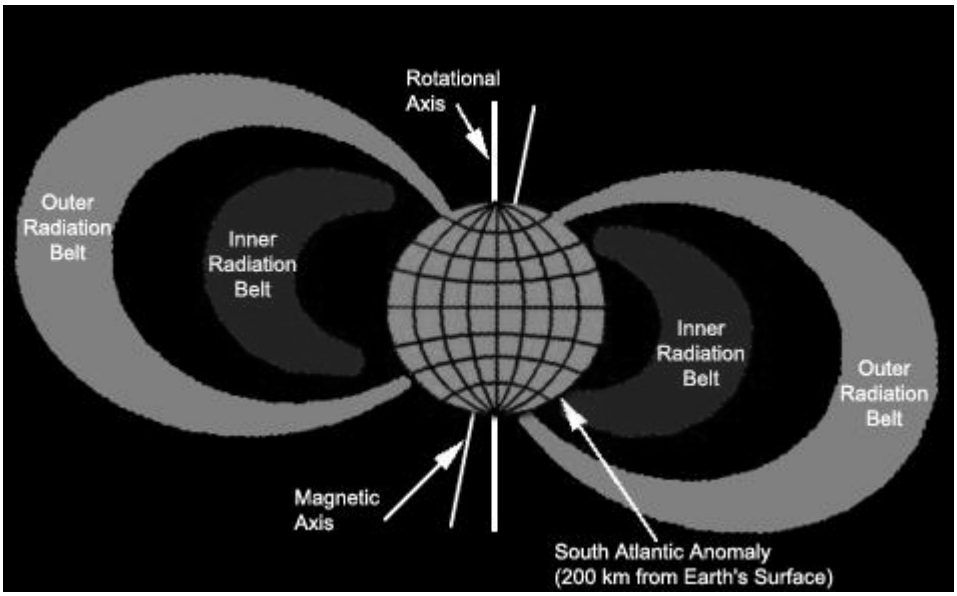

Figure 1. Schematic representation of the trapped electron radiation belts [3].

The semi-permanent effects of exposure to ionizing radiation are the least understood. Research has focused on the electrically measurable symptoms such as the buildup of positive charge in silicon dioxide and the increase of charge at the oxide semiconductor interface. Hardening of semiconductor devices has been accomplished by low-temperature processing, which reduces the physical or crystalline defects, and by developing extremely clean manufacturing processes [1]. The lack of basic knowledge about the damage is so serious that there exist no measurements (electrical, chemical, or physical) that can be made on semiconductor devices and then used to predict the expected behavior in an ionizing radiation environment [1]. Thus, the need for continued research in the field of the effects of ionizing radiation on semiconductor devices is of supreme importance to National Security.

Silicon has been the semiconductor material of choice primarily due to its natural abundance and ability to form an insulating oxide. This has led to an extremely advanced state of fabrication technology for silicon resulting in silicon's dominance in the commercial semiconductor market [4][5]. The second most popular material for building semiconductor devices is gallium arsenide (GaAs) [5][6]. This is due primarily to the superior electron transport and optical properties that GaAs material exhibits over silicon [4][5]. Within the past 10 years, advances in semiconductor growth technology have resulted in the development of devices fabricated from wider band-gap III-V semiconductor materials. Materials such as diamond (C), silicon carbide (SiC), and gallium nitride (GaN), which were previously used as insulators, have now become practical wide band-gap semiconductors that can be used to fabricate faster, more resilient devices and sensors [5].

Gallium Nitride has been referred to as the "final frontier" of semiconductors due to its physical characteristics, fundamental performance capabilities, as well as the unusual location of gallium and nitrogen at the extremes of the Periodic Table for usual semiconductors [7]. Although GaN may not be the final "final frontier," its superiority and potential applications make it a supreme contender for the next generation of semiconductor materials.

GaN is an III-V material since Gallium is from group III and Nitrogen is from group V of the periodic table. For a semiconductor, GaN also has an unusually wide band-gap of 3.49 V as well as a high thermal conductivity, a high melting temperature, a low dielectric constant and a high breakdown voltage. These characteristics mean that GaN possesses the possibility for exceptional performance advances in the areas of high

power and high frequency transistors ranging from 1-50 GHz. This is an order of magnitude greater than GaAs (gallium arsenide) and Si technology [8]. This frequency band is extremely important for covering all forms of mobile communications such as wireless, metropolitan and wide-area networking, point-to-point (LMDS) and point-to-multipoint (MMDS) microwave communications as well as applications in RADAR [7]. Many semiconductor researchers believe that GaN holds the key to reinventing the feasibility, cost and capabilities of such systems [7]. GaN-based devices are being proposed for and have been implemented into a wide variety of modern applications such as high-speed computer development and aircraft/spacecraft sensors and detectors.

Due to gallium nitride's wide bandgap and its intrinsic material properties, GaN-based devices have been theorized to be more resilient than silicon and GaAs-based devices in high temperature, high power, and high frequency conditions [9][10]. Additionally, because of its wide bandgap and high nitride displacement energies, GaN-based devices are definitely more radiation tolerant than GaAs-based devices [11]. Preliminary research conducted by Ionascut-Nedelcescu *et al.* aids in confirming the idea that GaN-based devices are more radiation tolerant than GaAs-based devices [12]. However, few studies focusing on the effects that electron radiation has on AlGaN/GaN high electron mobility transistors (HEMTs) are found in current literature. Recently, however, an increasing volume of literature has surfaced studying the effects of electrons on GaN constituent materials and, to a lesser extent, AlGaN. The majority of radiation studies in the literature have focused on proton irradiation of GaN-based devices [13][14].

There are various types of semiconductor devices intended for many different uses. Transistors are only one specific type of semiconductor application. Of the various types of transistors, the field effect transistor (FET) is the type of device that exploits the effect of high electron mobility: In the bipolar junction transistor (BJT) both holes and electrons participate in the conduction process, in contrast to FETs where predominantly only one of the carriers participates in conduction [15]. Due to this, the effects of radiation vary from one type of transistor to another. The majority of the current studies on GaN-based transistors focus on the heterojunction field-effect transistor (HFET), which is another specific type of FET that is formed by joining two dissimilar semiconductor materials such as GaN and AlGaN. In the family of HFETs there exists a specific transistor design called the HEMT or a modulation-doped field effect transistor (MODFET). The two dissimilar semiconductors are modulation doped which means, for example as in Figure 2, for an AlGaN/GaN HEMT, the AlGaN is doped except for a narrow band along the interface with the undoped GaN. The electrons in the AlGaN then diffuse to the undoped GaN and in the process form a conduction channel in the GaN along the interface between the AlGaN and GaN [16]. This channel is known as a sheet charge or as a two-dimensional electron gas (2DEG). This 2DEG is essentially a thin quantum well that confines carriers and allows for extremely fast carrier transport. This fast carrier transport is fundamentally what makes the HEMT function and of great interest in developing future semiconductor applications [15].

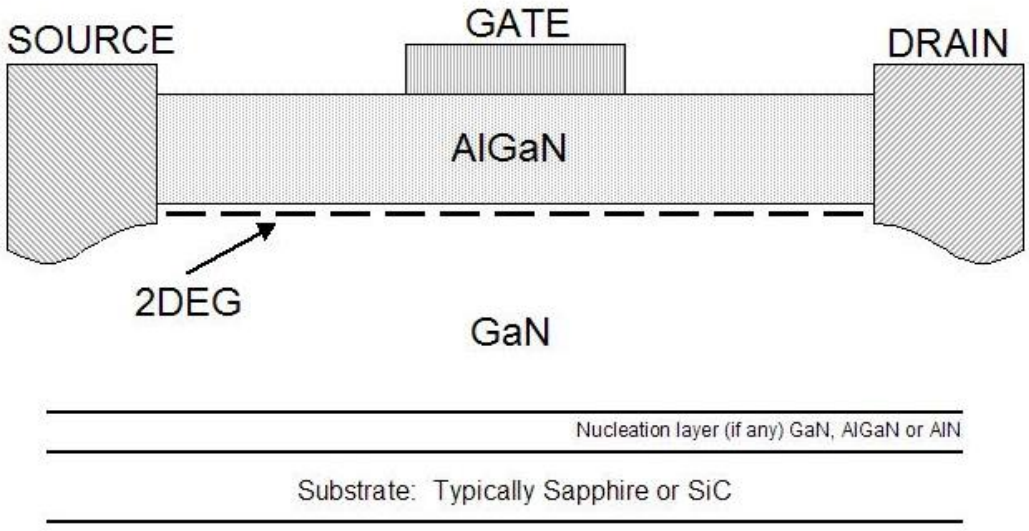

Figure 2. Cross-Section of a typical AlGaN/GaN HEMT [17].

The well-known spontaneous polarization and piezoelectric coefficient in AlGaN/GaN heterostructures results in a positive charge buildup in the AlGaN layer along the heterojunction [17]. This positive charge is believed to attract the negative charge carriers from the n-type GaN region and subsequently creates the 2DEG [17]. The actual cause of the strong n-type nature of the GaN is not well established; however, the native donor is believed to be due to a nitrogen vacancy (V_N) in the gallium nitride. While not conclusive, the majority of the research points to the nitrogen vacancy (rather than an impurity such as Si or O) as the most probable *n*-type self-doping in GaN with carrier concentrations as high as 10^{19} cm^{-3} at 300K [18].

Morkoç proposes that the nitrogen vacancy is the shallow donor in GaN [19]. These native donor and trap levels, as well as unintentional impurities determine the carrier concentration and the ability to control the doping of GaN-based device structures [19]. “Calculations lend support to the assertion that the nitrogen vacancy is most likely a single donor and responsible for the n-type behavior in undoped GaN” [19]. The origin

of the n-type conductivity of the as-grown undoped bulk and heteroepitaxial GaN has been attributed to nitrogen vacancies as well as impurities of Si and/or O. Morkoç [19] reports that W. Kim *et al.* conducted experiments in order to unveil the origin of the auto-doping. They used different ammonia flow rates during growth to show that the background electron concentration decreases as the ammonia flow rate increases. They expected that the concentration of N vacancies would decrease as the amount of ammonia increased. This is indeed what occurred and this result supports the nitrogen vacancy argument. Later research indicated that the oxygen impurities do not substantially account for the electron concentration in unintentionally doped samples of GaN with high electron concentrations. And finally, Morkoç states that Perlin *et al*. "interpreted their first-principles calculations as favoring the notion that nitrogen vacancies are responsible for the large electron concentrations" [19].

Currently, the HEMT has been demonstrated to be the fastest of all transistors and is projected to fill multiple roles in many high-frequency applications [16]. Due to the HEMTs ability to operate at high frequency ($> 10^{10}$ Hz) they are prime candidates for implementation into many modern high-frequency applications. Some of these applications involve integration of GaN-based HEMTs into satellite systems that will be required to operate in earth orbit for several years. During this time on orbit, the satellite and the GaN-based HEMT will be exposed to a wide range of radiation including high-energy electrons in the Van Allen belts which may possess energies up to a few million electron volts (MeV) [20]. Thus, for any GaN-based HEMT to be successfully integrated into a satellite system, it must be able to operate under the influence of a wide range of electron radiation from keVs to MeVs. The first step toward achieving this goal must be

to determine experimentally the specific effects that electrons of a few MeVs have on the operation of AlGaN/GaN HEMTs. Thus, the problem that this thesis will examine is as follows:

Problem Statement

What is the specific cause of the increase in observed drain current in AlGaN/GaN HEMTs after electron irradiation around the 1 MeV energy range?

Hypothesis

The radiation induced increase in drain current is caused by either a change in the channel sheet charge density (increase in carrier concentration in the 2DEG) or a change in the electron mean velocity in the channel.

Objectives

1. Identify device-level electron radiation effects using Capacitance-Voltage measurements.
2. Calculate 2DEG carrier concentrations through fluence dependent C-V measurements.
3. Determine fluences that increase drain current.
4. Use HEMT failure data to determine fluence effects on 2DEG.

Scope

This research is focused on studying the specific effect(s) that electrons with energies between 0.45 - 0.8 MeV have on the electrical characteristics of AlGaN/GaN HEMTs. This study will initially consist of post-irradiation current-voltage (I-V)

measurements of devices irradiated nine months previously. This must be accomplished in order to observe and verify the observed room temperature annealing of electron radiation damage previously reported [21] and develop a familiarization with the equipment and devices. Following the initial characterization of the HEMT devices, temperature dependent capacitance-voltage measurements will be conducted on a different set of devices in order to validate the aforementioned hypothesis. Other possible relevant measurements such as Hall Effect, or deep level transient spectroscopy (DLTS), are not within the scope of this thesis and as such will be left to follow-on work. Throughout the research effort emphasis will be placed on relating the initial I-V and subsequent C-V measurements to the behavior and properties of the 2DEG. The research effort will conclude when there is sufficient evidence to either support or refute the hypothesis through an integration of theory, mathematical modeling, and experimental measurements.

Approach

The overall approach to conducting this research was the use of theory, a mathematical model, and experimental measurements. Theory was developed throughout to provide a basis of understanding of the fundamental principles. Additionally, a mathematical model was used to understand how the channel current of HEMTs functioned. The experimental measurements involved using previously fabricated AlGaN/GaN HEMTs that were fabricated using the GaN baseline 1.0 process used by the Air Force Research Labs (AFRL) Sensors Directorate Aerospace Components and Subsystems Technology Electron Devices Branch (SNDD) [21]. The devices were diced

and packaged, and prepared for irradiation experiments under the direction of Dr. Gary Farlow at the Wright State University (WSU) Van de Graaff (VDG) laboratory.

The experimental approach of this experiment was the individual irradiation of 4 high electron mobility transistors at low temperature by relatively low energy electron irradiation. Prior to irradiation, C-V measurements were taken with the device attached to the experimental setup at low temperature in order pre-characterize the devices in the same environment as the post-irradiation measurements. The irradiation process consisted of grounding the entire apparatus and ensuring that each device was grounded on a cold head to ensure that no spurious charge was allowed to build up on the device and discharge causing damage. A key component to this device isolation was disconnecting the sample from the VDG current integrator during irradiation as failing to do this previously resulted in the destruction of the devices. Immediately following the irradiation process, C-V measurements were again recorded at low temperature with the device attached to the experimental setup. The pre-irradiation and post-irradiation data measurements were compared and analyzed in order to determine the effects of electron irradiation on the AlGaN/GaN transistors.

Assumptions

1. The lifetime of damage is longer than the time required to perform measurements.
2. The capacitance characteristics of the AlGaN/GaN heterojunction are similar to the capacitance of a MOS capacitor / device.
3. The reader possesses a basic understanding of solid-state physics.

Sequence of Presentation

This thesis is divided into six chapters and four supporting appendices. Chapter One introduces the thesis by providing background information important to any reader attempting to obtain a fundamental understanding of the research effort. Chapter Two presents a clear, concise review of current literature that provides detailed background information that stems from previously conducted research as well as justification for this research effort. Chapter Three details the theory behind $Al_{0.24}Ga_{0.76}N$ MODFET operation and the theoretical aspects of capacitance measurements as they relate to MOS devices and heterostructures as well as relevant radiation interaction theory. Chapter Four outlines the important experimental procedures including details of the fabrication process and the irradiation experiments. Chapter Five presents the results of the irradiations and provides relevant discussion. Finally, conclusions and recommendations for further work are presented in Chapter Six.

II. Literature Review

Purpose

In order to determine whether this research is justified and a need exists to conduct electron irradiation experiments on AlGaN/GaN devices, a detailed review of the current literature must be conducted. Although numerous books, papers and other publications have been perused, only highly relevant references are annotated in the following pages to determine whether similar research has already been conducted and to gain insight into the theoretical considerations surrounding this research.

Fundamentals of Gallium Nitride heterostructures

Over the past 30 years the dependence on semiconductor electronics has increased tremendously, as the world has demanded smaller, faster, more powerful, and lower cost electronics. Today, semiconductor devices are essential in almost everything that contains electrical components or systems. The infatuation with rapid, global communication has led to a need for extremely powerful, portable, and inexpensive communications equipment. From the plethora of different semiconductor materials, Gallium Nitride is so far the best suited to fill the requirements for higher power, higher operational frequency and better thermal stability for microwave applications. Communications is also of prime importance to the military as command and control is essential to well-executed operations. The key element in global command and control is the satellite. On earth, the effects of radiation are generally mitigated by the absorbing powers of our atmosphere, however, on earth orbit, there is no natural shield from the detrimental effects of ionizing radiation on electronics. Since Gallium Nitride appears to be the next step in

semiconductor development, it is only a matter of time until these high-speed devices are found in various applications in harsh operating environments.

The major abilities of GaN that have attracted so much attention are that GaN devices can operate in high power, high temperature and high frequency applications. The most spectacular results have been obtained for AlGaN/GaN microwave power HEMTs that yielded over 11 W/mm power at 10 GHz [22]. This is remarkable when compared with the current state-of-the-art semiconductor AlGaAs/GaAs HEMT that has a power density of only 1 W/mm at lower frequencies. This makes their application highly attractive in a world dominated by high speed personal communications as well as microwave uses associated with military needs. Table 1 compares the properties of various semiconductor materials with GaN and clearly shows the similarities and superiority of GaN to other semiconductors.

Material	Bandgap	Molecular and atomic weight	Lattice parameter (Å)	Bandgap (eV)	Melting point (°C)	Thermal conductivity at 300 K ($mW.cm^{-1}.K^{-1}$)
Si	Indirect	28.08	5.430	1.11	1412	1500
GaAs	Direct	144.64	5.653	1.42	1238	540
GaN	Direct	83.73	4.54	3.26	1500	656
AlN	Direct	40.99	4.98	6.28	2400	823
ZnSe	Direct	144.34	5.667	2.67	1500	139
SiC	Indirect	40.1	4.3597	2.2	2800	4000
Diamond	Indirect	12.01	3.5667	5.5	3577	30 000

**Si and GaAs are included for comparison.*

Table 1. Physical properties of wide band gap semiconductors [10].

Importance of Aluminum Gallium Nitride and Gallium Nitride

The results of Chen *et al.* demonstrated the benefits of a silicon carbide (SiC) substrate under an AlGaN/GaN HFETs and emphasized the importance of GaN devices

in high-power microwave applications. In their report, they indicate that they obtained a maximum drain current as high as 1.71 A/mm, a transconductance (g_m) that is more than 200 mS/mm, a drain-gate breakdown voltage exceeding 30 V, and a cutoff frequency (f_t) better than 50 GHz [23].

The variation of the charge carrier velocity as a function of electric field is a fundamental characteristic in determining the magnitude of the current that can be driven through a device [10]. Figure 3 below shows the vast superiority of a wide band gap semiconductor such as AlGaN/GaN over various other types of materials with respect to carrier velocity.

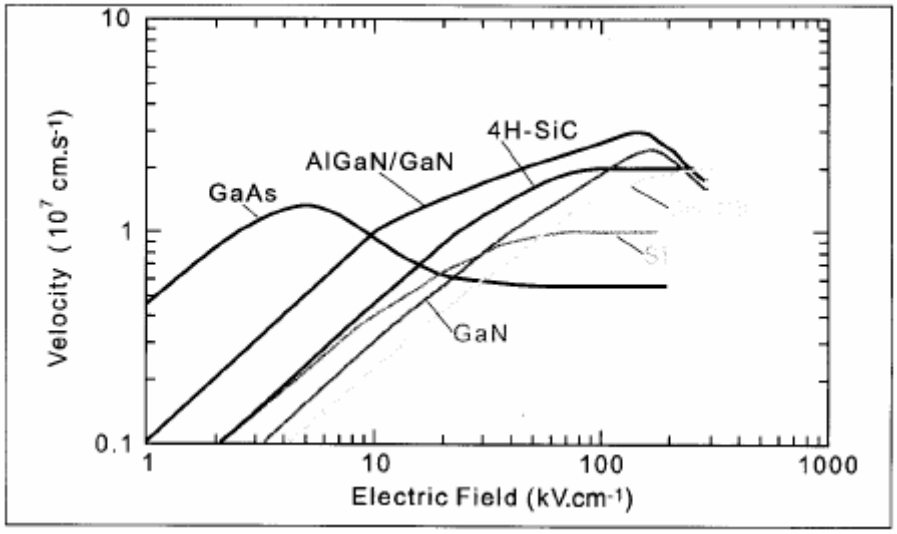

Figure 3. Charge carrier velocity versus electric field for various semiconductors [10].

Table 2 outlines various competitive advantages of devices made from GaN [17].

Need	Enabling Feature	Performance Advantage
High Power/Unit Width	Wide Bandgap, High Field	Compact, Ease of Matching
High Voltage Operation	High Breakdown Field	Eliminate/Reduce Step Down
High Linearity High Frequency	HEMT Topology High Electron Velocity	Optimum Band Allocation Bandwidth μ-wavelength
High Efficiency	High Operating Voltage	Power Saving, Reduced Cooling
Low Noise High Temperature Operation	High Gain, High Velocity Wide Bandgap	High dynamic range receivers Rugged, Reliable, Reduced Cooling
Thermal Management	SiC Substrate	High Power Devices with Reduced Cooling Needs
Technology Leverage	Direct Bandgap Enabler for Lighting	Driving Force for Technology, Low Cost

Table 2. Competitive advantages of GaN devices [17].

Since GaN devices appear to possess a usefulness unsurpassed by other semiconductor devices, continued research is required. The area of radiation exposure is of increasing importance as these new devices begin increased use in environments saturated in radiation. This reason alone justifies the need for research on the radiation effects on gallium nitride devices.

A review of the existing literature contains numerous studies on the effects of radiation on various AlGaN/GaN heterostructures, however, the majority of these research efforts relate to neutron, proton or high energy photon irradiation. Only four studies identified directly focus on electron irradiation of AlGaN or GaN materials [24] [25] [26] [27] and only one [15] on heterostructures devices. This lack of research in the

area of AlGaN / GaN heterostructures leaves little doubt as to the need for increased research emphasis in the area of electron irradiation of AlGaN / GaN heterostructures. Nevertheless, a review of the proton, neutron and limited electron studies provides a wealth of information about radiation effects on AlGaN / GaN heterostructures.

Radiation Effects of Protons on AlGaN / GaN

Ionascut-Nedelcescu *et al.* accomplished an excellent study on the hardness of Gallium Nitride [12]. They irradiated GaN diodes at room temperature with electrons of various energies from 300 to 1400 keV. They report that three different experiments determined that GaN resists damage more than gallium arsenide. In the first experiment the bulk material was studied by photoluminescence. In the second case, the electroluminescence from GaAs and GaN was compared. The third and final experiment studied the resistivity of a two-dimensional electron gas. No displacement of nitrogen atoms was observed, so they concluded that the nitrogen sublattice repairs itself by room temperature annealing [12]. Perhaps the most significant result of their work was the determination of the displacement energy of the gallium atoms in the GaN [12]. They reported that a threshold energy of 440 keV corresponds to a displacement energy of 19 ± 2 eV for gallium [12].

An early study, in 1999, by Wilkins *et al.* [24] looked at ionization and displacement damage irradiation in two-dimensional gas transistors. Their study used monoenergetic 55 MeV protons up to a maximum fluence of 5×10^{10} cm^{-2} in order to simulate the expected proton environment in low earth orbit that might be experienced by the International Space Station with a mission duration of 70-100 years. Apparently, the gamma radiation reduced the transconductance of the device while the proton radiation

increased the transconductance. Later research concludes the opposite for proton radiation; however, at the time they concluded that HEMTs were viable for use in space due to this proton radiation induced enhancement.

Luo *et al.* [11] investigated the device specific effects of high-energy proton irradiation on AlGaN / GaN high-electron mobility transistors (HEMTs). They used 40 MeV protons at fluences that replicated decades of exposure in low-earth orbit. The results demonstrated a decrease in extrinsic transconductance, drain-source current threshold voltage, and gate current. They concluded that the data indicated that protons created deep electron traps that resulted in HEMT channel resistance. The room temperature post irradiation annealing restored approximately 70% of the initial transconductance and drain-source current.

Polyakov *et al.* [29] studied the effects of implantation with 150 keV protons on samples of n-GaN in order to study the nature of point defects and device isolation. They observed a degradation of minority carrier diffusion length. Deep level spectroscopy measurements revealed deep electron traps with activation energies between 0.2 and 0.95 eV and deep hole traps with energies of between 0.25 and 0.9 eV. The results indicated that the 0.75 eV electron traps and/or the 0.6 eV hole traps were probably responsible for lifetime degradation. Excellent recovery of the electrical conductivity of the implanted samples resulted after annealing at temperatures greater than 250°C.

Hu *et al.* [30] studied the degradation of AlGaN/AlN/GaN HEMTs due to 1.8 MeV protons at fluences up to 3×10^{15} cm^{-2}. These devices possessed high radiation tolerance up to 1×10^{14} cm^{-2}, but demonstrated a decreased sheet carrier mobility due to increased carrier scattering and decreased sheet carrier density due to carrier removal at higher

fluences. Overall device degradation was noted to be a decrease in the maximum transconductance, an increase in threshold voltage, and a decrease in the drain saturation current as shown in Figure 4 below.

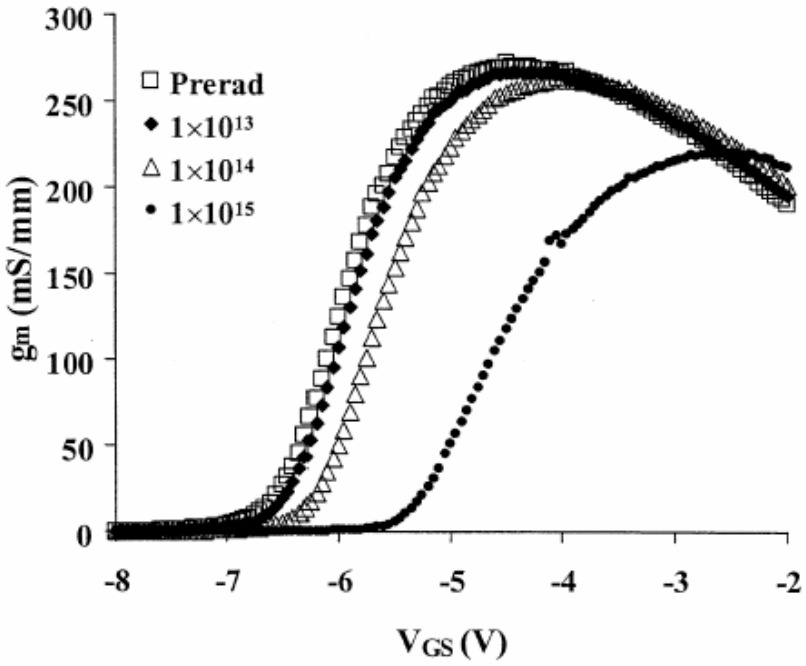

Figure 4. Transconductance versus gate-source voltage for AlGaN/AlN/GaN HEMTs before and after 1.8 MeV proton irradiation with fluences from 1×10^{13} cm^{-2} to 1×10^{15} cm^{-2} [30].

Gaudreau *et al.* [14] investigated the effects of 2-MeV protons on the transport properties of the two-dimensional electron gas at the AlGaN/GaN interface. In a fluence range of 1×10^{13} to 7×10^{15} cm^{-2}, the results of proton irradiation showed a carrier density decrease of a factor of two while the mobility degraded by a factor of a thousand. At a fluence between 3×10^{14} and 3×10^{15} cm^{-2} the two dimensional gas changed phase from a conductor to an insulator which the authors say could be used to establish an upper threshold for radiation damage. They concluded that mobility changes are dependent on the radiation and not sheet charge density. They stated that this indicates

that in a real two-dimensional gas system, if the performance of the system depends mainly on mobility, then the system may function properly only until a critical fluence is reached followed by abrupt failure at higher fluences. Additionally, the authors reconfirm other research that indicated that AlGaN/GaN is at least two orders of magnitude more radiation-resistant than AlGaAs/GaAs.

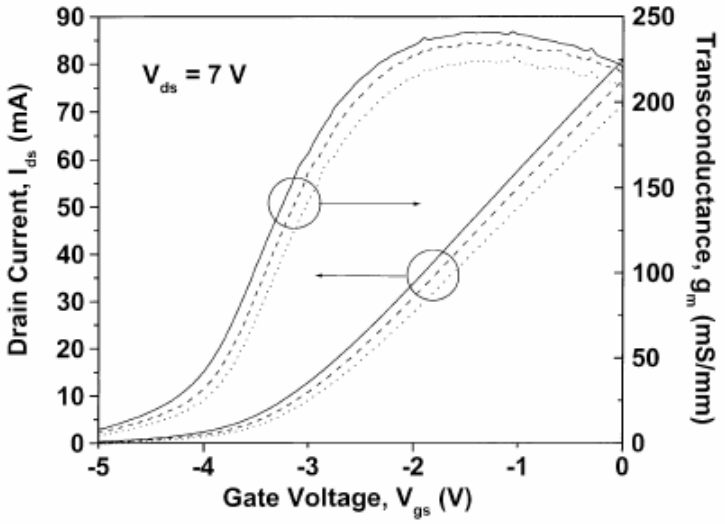

Figure 5. Common-source drain current as a function of gate voltage and transconductance of the same transistor pre-irradiation (solid line), post-10^{12} cm^{-2} fluence (dashed line), and post-5×10^{13} cm^{-2} fluence (dotted line) [13].

In 2002, White *et al.* [13] examined the effects of 1.8 MeV proton irradiated AlGaN/GaN MODFETs. The effects of proton irradiation on the electrical transfer characteristics of the device include: a decrease in the saturation current, drain current and transconductance as shown in Figure 5 [13]. White *et al*. believe that proton radiation forms spatially localized changes in the electronic properties of the AlGaN/GaN heterostructures that reduces the internal electric field as it forms charged defects. The defects created reduce the charge density in the two-dimensional electron gas. This dual reduction, electric field and 2DEG, causes the decrease in the saturation current, drain current and transconductance [13].

Most recently, in 2004, Hu *et al.* [31] investigated the energy dependence of proton-induced degradation in AlGaN/GaN HEMTs. They found that the devices exhibited little degradation when irradiated with 15 MeV, 40 MeV and 105 MeV protons at fluences up to 10^{13} cm^{-2} and the damage recovered after room temperature annealing. Very little degradation was found for proton energies greater than 15 MeV. For a fluence of 10^{13} cm^{-2} 1.8 MeV protons, the drain current decreased by approximately 10% and the maximum transconductance decreased by 6.1% [31]. These results are demonstrated below in Figure 6 and Figure 7.

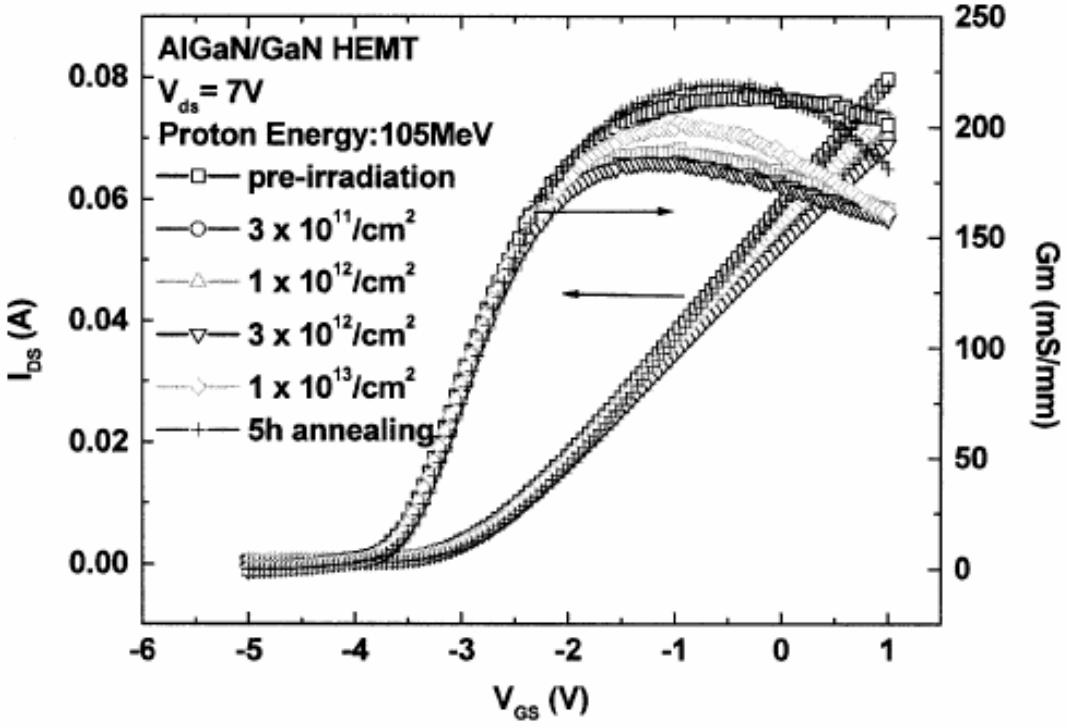

Figure 6. Transfer characteristics for AlGaN/GaN HEMTs before and after 1.8 MeV proton irradiation at various fluences [31].

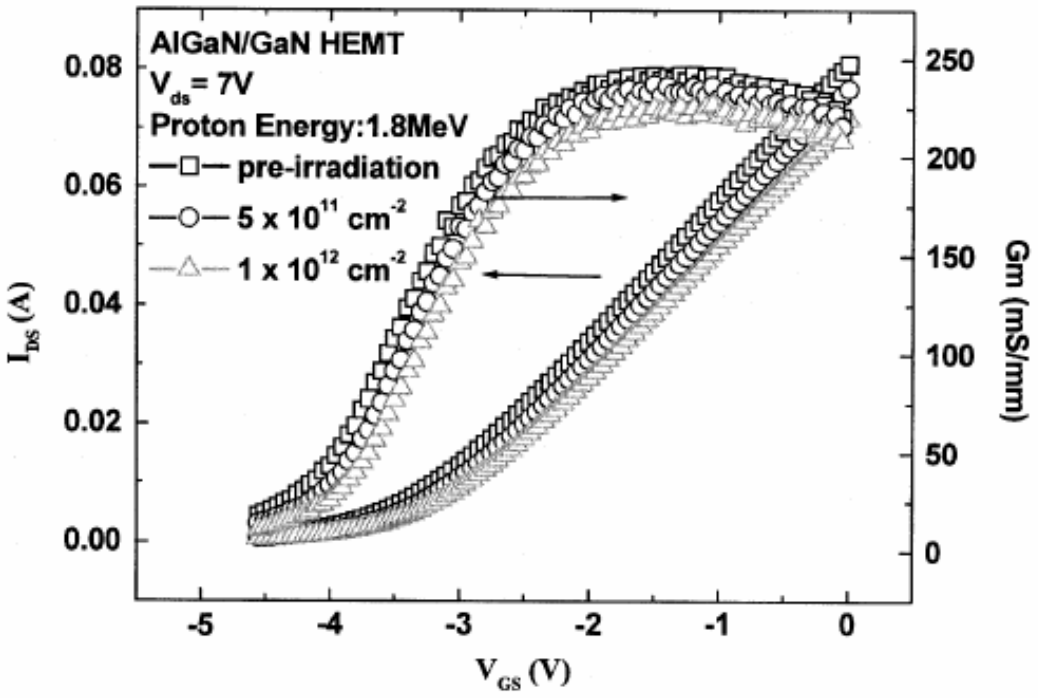

Figure 7. Transfer characteristics for AlGaN/GaN HEMTs before and after 105-MeV proton irradiation at different fluences [31].

Radiation Effects of Electrons in AlGaN / GaN

Fang *et al.* [26] studied deep centers in electron-irradiated n-GaN on sapphire. The electron irradiation created V_N (nitrogen vacancies) related centers with an activation energy of 0.06 eV and a deeper center with E_T = 0.85 eV. Their conclusion indicated that point defects (vacancies and interstitials) in semiconductors are created by high-energy electron irradiation [26].

Goodman, *et al.* [24] studied electron irradiation induced defects in n-GaN and they found that electrons were extremely adept at introducing point defects. They used deep level transient spectroscopy (DLTS) to investigate the electron trap defects during high-energy electron irradiation. Their results indicate that the major electron induced defect is not one defect level but is made up of at least three defect levels [24].

Coskun *et al.* [25] describe an experimental set-up for *in situ* Hall measurements under high-energy electron irradiation for various wide band gap semiconductor materials. They indicate that an associated cryostat allows irradiations to be carried out over a range of temperatures from 95–-300 K. They do not report on specific results, but merely describe the experimental set-up, thus providing useful guidance for follow-on experimental set-ups of the same type [25].

Look *et al.* [32] in 1997 conducted an experiment with high-energy (0.7 to 1 MeV) electron irradiation and GaN on sapphire. The result was the productions of shallow donors as well as deep and shallow acceptors. Their data, coupled with theory, indicated the shallow donor is an N vacancy and the acceptor is a rare appearance of an N interstitial. Their total-energy calculations suggest that both V_N and N_I are not expected to exist in large quantities in *as-grown n*-type material, but appear after irradiation.

In 2003, Look *et al.* [27] conducted electron irradiation experiments on Gallium Nitride. They conducted their experiment at room temperature with 0.42 MeV electrons, a current of 2 $\mu A/cm^2$ and a total fluence of about 3.6×10^{17} cm^{-2}. Look *et al.* base their conclusions on the calculated threshold displacement energies (E_d) by Nord *et al.* Accordingly, the minimum E_d for N displacement is 25 eV and for Ga is 22 eV. Look *et al.* take into consideration an average acceptance angle of 15º to account for thermal motions and possible beam misalignment in order to calculate N and Ga displacement energies of 66 and 38 eV, respectively. From these calculations and factoring in the higher mass of the Gallium, they conclude that the minimum electron energy required for N displacement is 0.32 MeV and for Ga displacement is 0.53 MeV. They conclude that the N production rate should be 0.03 cm^{-1} at the electron energy of 0.42 MeV and will

continuously exceed the Ga production rate up to at least 0.87 MeV. From these facts, they deduced that this level of radiation produces N-sublattice displacements and only the N vacancy is the shallow donor produced by 0.42 MeV electron irradiation [27].

Also in 2003, Sattler [21] showed that various AlGaN /GaN MODFETs were radiation tolerant after receiving various total fluences up to 3.67×10^{15} e^-/cm^2. Additionally, he demonstrated that there were no significant changes between room temperature pre-irradiation and post-irradiation *I-V* measurements. He consistently observed non-fluence dependent increases in both drain and gate current for two different irradiations as shown in Figure 8 and Figure 9 below. He reported that these increases annealed out at room temperatures. He explained that the gate leakage increases were due to the enhancement of trap-assisted tunneling through the AlGaN layer caused by radiation-induced trap creation in the AlGaN.

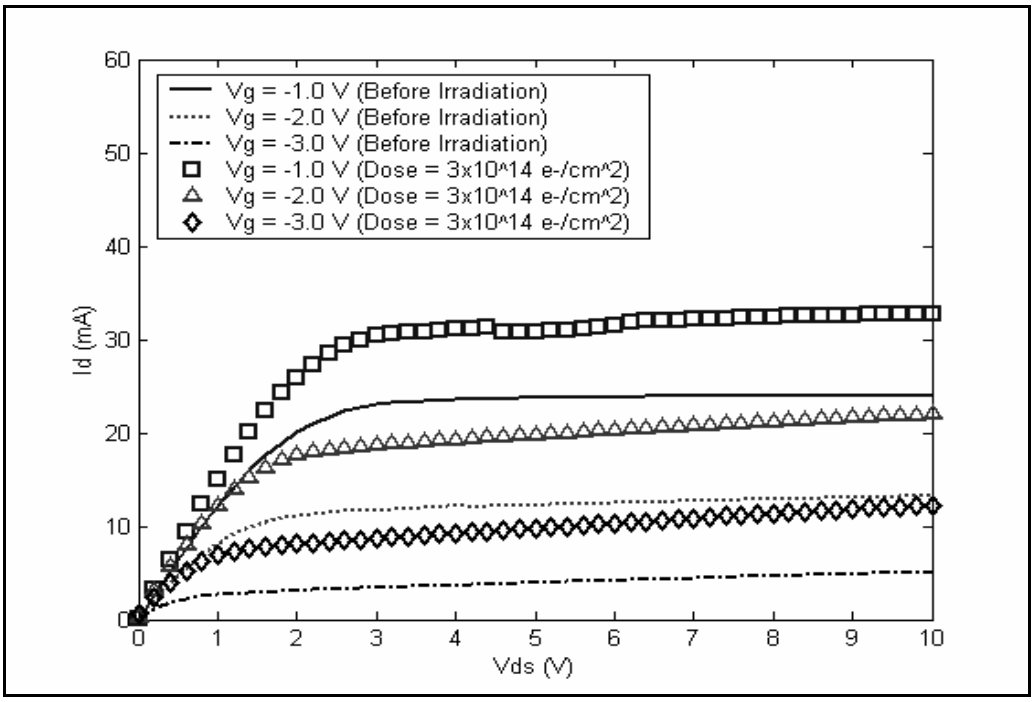

Figure 8. Sample A0409 FatFET First Irradiation: Change in *I-V* Curves at LiN Temperature (0.45 MeV Electrons) [21].

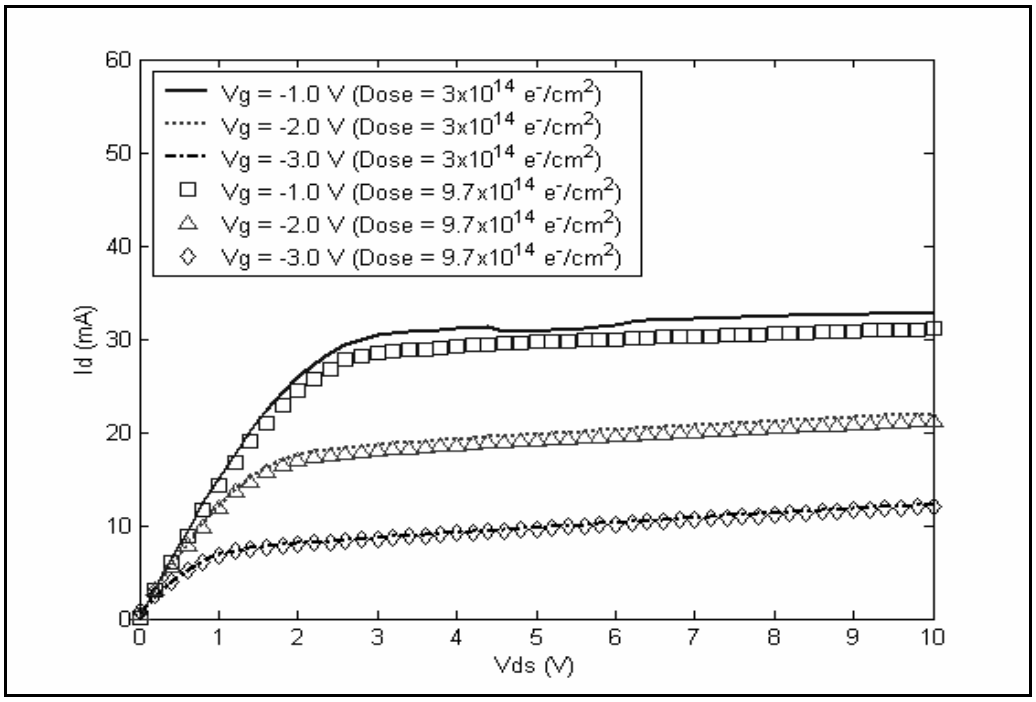

Figure 9. Sample A0409 FatFET Second Irradiation: Change in *I-V* Curves at LiN Temperature (0.45 MeV Electrons) [21].

Sattler [21] stated that the transistor changes are not related to the total fluence but rather to the initial radiation exposure as shown in Figure 9.

Sattler [21] proposed that the drain current increase results from one of two possibilities: (a) the current increase was caused by a direct increase in carrier concentration in the 2DEG; (b) the 2DEG population remained unchanged and the increase was caused by an increase in the electron mean velocity in the 2DEG. His experiment did not record C-V measurements, but suggested that either one of the choices can easily be proven over the other through fluence-dependent C-V measurements and the calculation of the 2DEG carrier concentrations. Table 3 presents the relevant irradiation information for the two FATFET samples that were not

completely destroyed during his experiment and provides a reference starting point for subsequent irradiation levels in follow-on experiments.

Sample	**Energy (MeV)**	**Beam Current (μA)***	**Relative Fluence (e^-/cm^2)**	**Relative Irradiation Time (min)**	**Total Fluence (e^-/cm^2)**	**Total Irradiation Time (min)**
A0408	0.45	0.13	1×10^{14}	7	1×10^{14}	7
A0408	0.45	0.13	2×10^{14}	13	3×10^{14}	20
A0408	0.45	0.13	6×10^{14}	39	9×10^{14}	59
A0409	0.45	0.3	3×10^{14}	8	3×10^{14}	8
A0409	0.45	0.3	6.7×10^{14}	13	9.7×10^{14}	21
A0409	0.45	0.3	9×10^{14}	18	1.87×10^{15}	39
A0409	0.45	0.3	1.8×10^{15}	50	3.67×10^{15}	89

Table 3. Experimental Device Irradiation Values as conducted by Sattler [21].

Capacitance-Voltage Measurements

N. Shaar *et al.* [33] in March 2004, used capacitance-voltage (C-V) measurements to characterize MOS devices and discuss various measurement failures that resulted from using this technique to characterize the devices. Additionally, they provided equations and explanations for determining oxide capacitance (1), the minimum capacitance (2) and the flat-band capacitance (3) as well as the flat-band voltage (4). An interesting discussion and solution to hysteresis problems that resulted during measurement were also provided. They suggested varying the voltage by sweeping from positive to negative and then back to positive again to alleviate the hysteresis problems. Overall, this is an excellent article stressing the foundational factors of capacitance-voltage measurements [33]. The major equations (8), (9), and (11) used to calculate the minimum capacitance and doping concentration from their research are described later in the theory section; however, their experimental results showing the variation of capacitance measurements through a range of gate voltages is plotted in Figure 10.

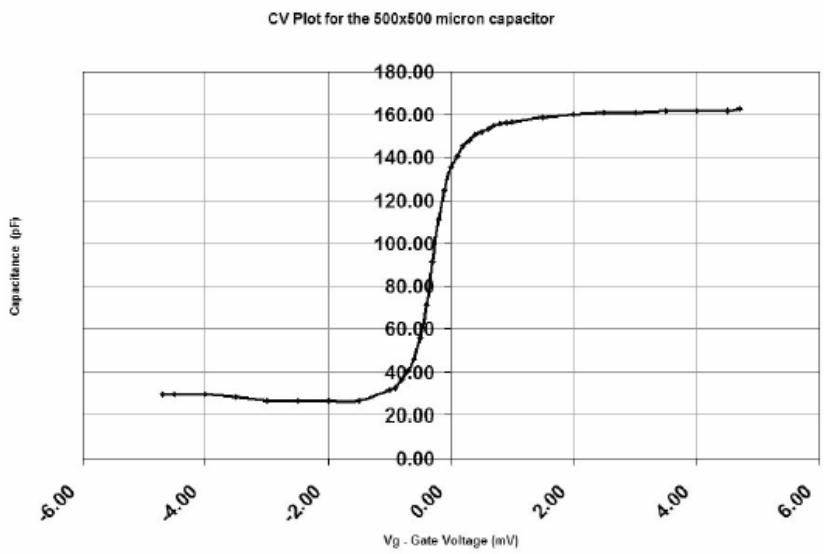

Figure 10. Typical plot of the variation of the capacitance (pF) of a 500 µm x 500 µm capacitor versus gate voltage (V_G) ranging from –4.7 to +4.7 volts [33].

P. Notingher *et al.* [34] in the 2002 Annual Report Conference on Electrical Insulation and Dielectric Phenomena characterized the electric charge in both non-irradiated and irradiated MOS structures using C-V measurements. They offered a broad explanation of the uses of capacitance-voltage measurements at high and low frequencies in order to estimate the amount of trapped charge in the oxide layer, as well as detailed explanations of the accumulation, depletion and inversion regions of a MOS capacitor [34].

Tamotsu Hashizume *et al.* [35] used capacitance-voltage measurements to characterize AlN/GaN MIS structures. The use of high frequency C-V measurements clearly showed deep-depletion behavior at room temperature and allowed for the derivation of the doping density from the slope of the $1/C^2$ plots. Additionally, they determined the low value of interface state density D_{it} of 1×10^{11} cm^{-2} eV^{-1} around E_c –

0.8 eV position. The article also possesses excellent experimental examples of C-V plots that reinforce the textbook C-V plots [35].

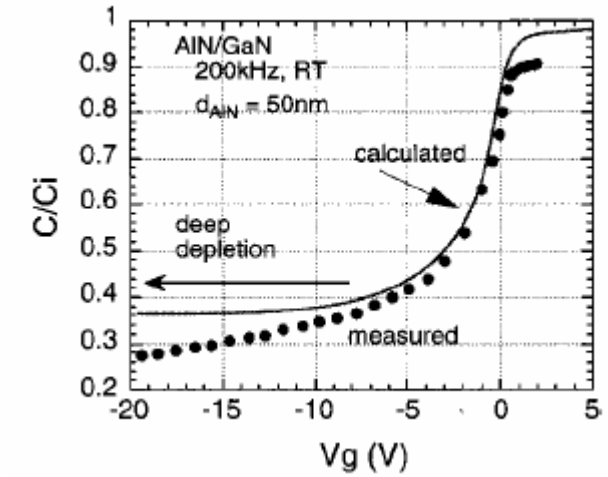

Figure 11. Typical C-V curve measured in darkness at room temperature [35]

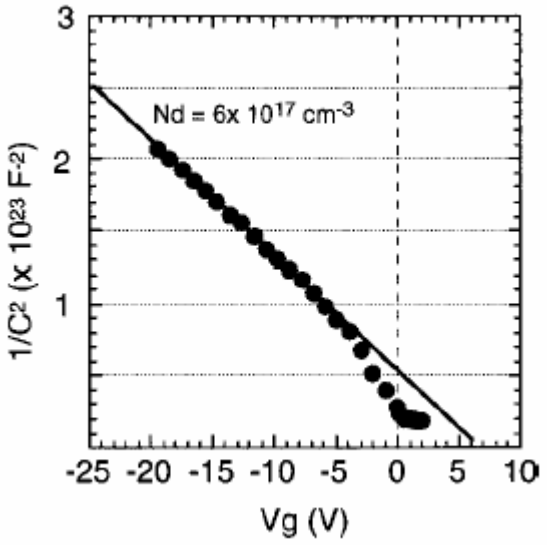

Figure 12. 1/C2 characteristics as a function of bias voltage [35].

Ambacher *et al.* [36] conducted a study on the 2DEG induced by spontaneous and piezoelectric polarization in AlGaN/GaN heterostructures using various methods, but

most notably a C-V profiling technique. They provide an equation (1) that enables the researcher to obtain the carrier concentration from capacitance measurements [36].

$$N_{C-V} = \frac{C^3}{q\varepsilon_o\varepsilon}\frac{dV}{dC}, \quad (1)$$

where V is the voltage applied across the gate, C is the measured differential capacitance per unit area, and ε is the dielectric constant of the material, $\varepsilon_o = 8.854 \times 10^{-14}$ F cm^{-1} and q is the charge on an electron [36]. Using this method on a sample of $Al_{0.24}Ga_{0.76}N$ with a thickness of 20 to 40 nm, they obtained carrier concentrations of 6×10^{12} to 9×10^{12} cm^{-2}. They report that the C-V carrier concentration ($N_{C\text{-}V}$) is equal to the free carrier concentration. Their sample dimensions are compatible with the dimensions of the samples used in this research and are excellent for comparing calculation results using equation (5) with data obtained from the FATFET [36].

Pavol Pisecny *et al.* [37] use the quasistatic C-V method to determine interface trap density (D_{it}) in MOS structures irradiated by 305 MeV Kr+ and 710 MeV Bi+ ions at various fluences. This paper provides an excellent description of low frequency measurements highlighting the main advantage of the low frequency C-V method in determining the distribution of D_{it} across the entire width of the bandgap. Paramount to this research is their comment on the radiation changes as observed through C-V measurements. They report that the radiation changes the D_{it} and this change can be observed through the slope of the C-V curves in the depletion and weak inversion regions. Additionally, they report that the flat-band voltage shifts to a higher negative value as the fluence increases. From their experimental data, they conclude that an increase in fluence and ion mass induces an increase in D_{it}. Their final conclusion is that

the irradiated MOS devices maintain the basic capacitance behavior even after high-energy irradiation [37].

E. F. da Silva *et al.* [38] use high-frequency C-V measurements to study interface defects in n-type MOS capacitors after X-ray irradiation. This paper provides representative C-V curves before irradiation and after various levels of radiation. The curves clearly show a parallel negative voltage shift indicating generation of positive interface oxide charge. Although not specifically the same, the devices used in this experiment produce similar plots and the curve by da Silva provides an example of a possible result after irradiation. The interface traps stretch out the C-V curve as compared to the pre-radiation plot [38] as shown in the example plot Figure 13.

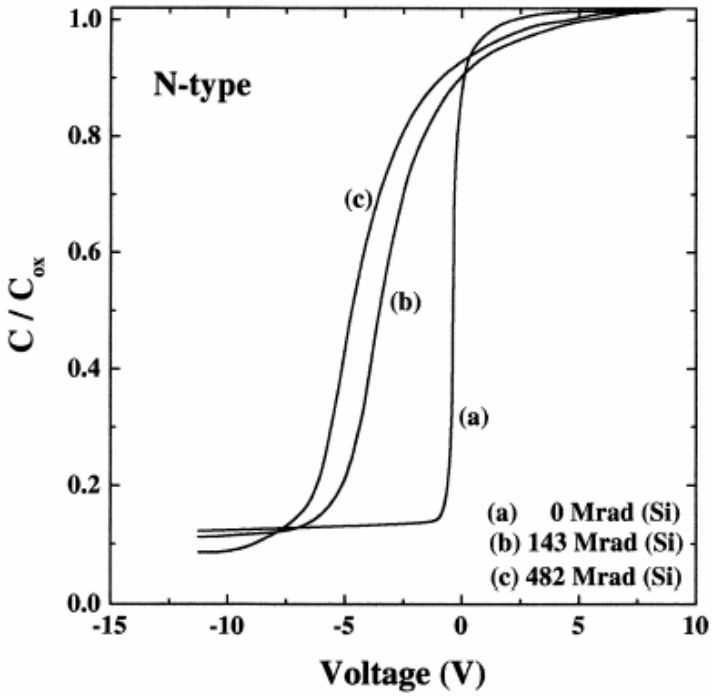

Figure 13. High frequency capacitance-voltage curves for a n-type MOS capacitor measure: (a) before irradiation; (b) after 143 Mrad (Si) irradiation; and (c) after 482 Mrad (Si) irradiation [38].

B. J Gordon [39] provided textbook basics on C-V measurements in "C-V plotting: myths and methods." He provided solutions to common pitfalls and directions that make conducting C-V measurements second nature. He detailed step-by-step instructions for correct application of the voltage sweep direction as well as comprehensive descriptions of the accumulation, depletion and inversion regions. Overall, this is an excellent source for initiating C-V measurements.

As can clearly be seen, there are numerous studies on capacitance-voltage in various types of MOS capacitors which function in a similar manner to HEMTs; however, no specific reports could be found detailing C-V measurements on HEMTs.

Research Justification

Since gallium nitride devices are projected to play important roles in sensors and satellite based systems where they might be subject to intense effects of radiation, it can be concluded from a study of the current literature that continued study and experimental procedures on the effects of radiation on AlGaN/GaN HEMTs is justified. The literature is conspicuously absent of in-depth research concerning the irradiation of GaN heterostructures especially with respect to capacitance-voltage measurements; therefore this research investigated the effects of radiation on GaN heterostructures through capacitance measurements.

III. Theory

CV Measurements

The capacitance-voltage (C-V) measurement technique conducted at frequencies above 10 kHz is a widely used method for measuring the charge present in Metal Oxide Semiconductor (MOS) devices. This technique allows for determining the amount of charge held within the oxide layer making up the insulator portion of the device. In the high frequency case, the modulation frequency is high enough that the minority carriers are too slow to respond to the voltage modulation, whereas in the low-frequency case the frequency applied is low enough that the minority carriers respond sufficiently to the voltage modulation. The almost universally accepted high-frequency measurement is 1 MHz and is the frequency used in this experiment to obtain high-frequency measurements needed to observe the inversion region.

The normalized textbook capacitance-voltage curve below clearly shows the characteristic accumulation, depletion and inversion regions.

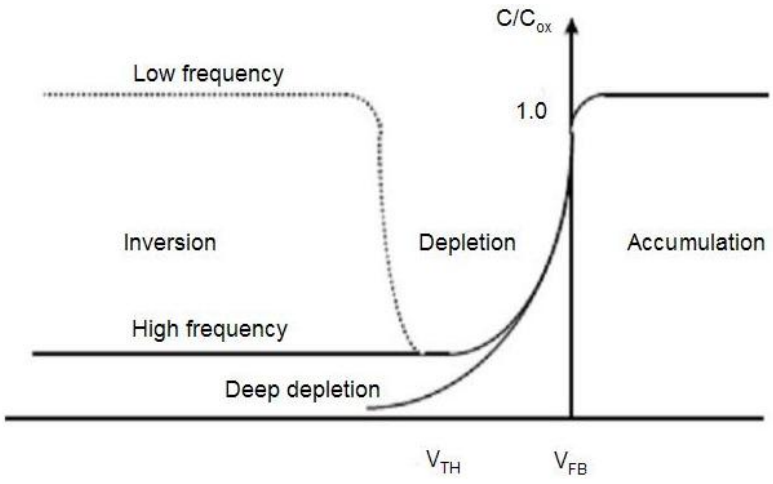

Figure 14. Textbook example of a Capacitance-Voltage Curve [38].

A typical MOS device is shown in the diagram below. The GaN and $Al_xGa_{1-x}N$ devices as shown in Figure 2 and used in this experiment are similar in structure to a typical MOS device that functions like a parallel plate capacitor. The device structure depicted below can be treated as a series of two capacitors: the capacitance of the oxide material (SiO_2) and the capacitance of the silicon (Si).

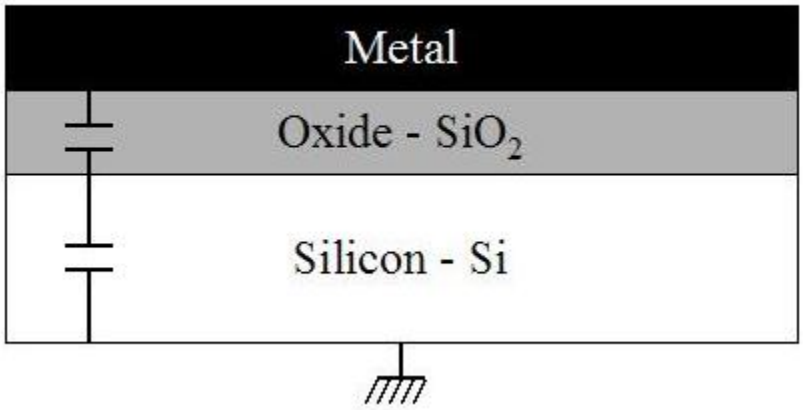

Figure 15. Diagram of a typical MOS structure [34].

The capacitance of the oxide is independent of any applied gate voltage and is found by

$$C_{OX} = \frac{\varepsilon_o \varepsilon_{ox} A}{d_{ox}}, \quad (2)$$

where ε_o is the permittivity of free space, ε_{ox} is the dielectric constant of the oxide, A is the surface area of the gate and d_{ox} is the thickness of the oxide layer [34]. A space charge (W) layer is formed in the depletion region when a gate bias (V_G) is applied which allows the Si layer capacitance to be determined as discussed in following paragraphs.

The C-V measurement method obtains measurements of capacitance by applying a high or low frequency sinusoidal voltage of a few millivolts superimposed over the bias voltage. In this way, the capacitance is measured for various values of the bias voltage,

V_G or gate voltage. The Keithley 590 C-V Analyzer used in this experiment uses this method to measure the capacitance. A theoretical output plot from a *n*-type MOS capacitor and the *n*-type device used in this experiment is shown in the figure below.

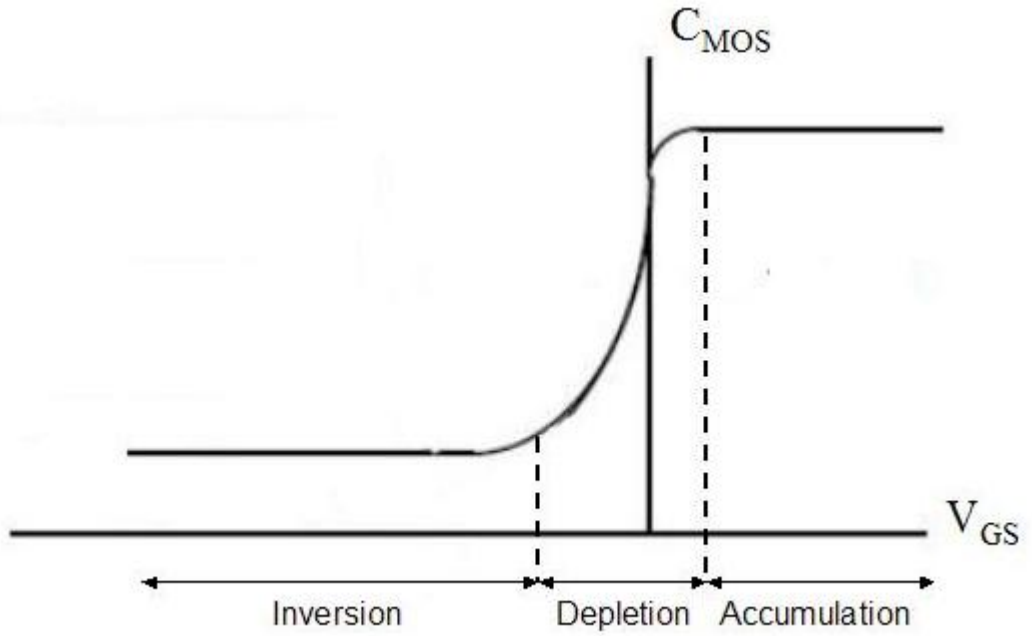

Figure 16. Shape of Capacitance-Voltage curves for ideal and real MOS capacitors with *n*-type Si substrate [34].

There are three modes of operation for a MOS device: accumulation, depletion, and inversion. Each of these will be discussed in detail below.

For an ideal *n*-type HEMT, just like an ideal MOS, accumulation occurs when a positive gate bias ($V_G > 0$) is applied and the positive charge of the gate attracts electrons (majority carriers) from the substrate, thus accumulating these majority carriers. The GaN behaves as a conductor and its capacitance is very high with respect to the AlGaN capacitance and therefore the overall capacitance is equal to the capacitance in the AlGaN [34].

$$C_{device} = C_{AlGaN} \quad (3)$$

As stated above, the C_{device} is similar to C_{ox} and is therefore equal to:

$$C_{device} = \frac{\varepsilon_o \varepsilon_{AlGaN} A}{d_{AlGaN}} . \quad (4)$$

When a large positive voltage ($V_G > 0$) is applied to the gate, strong accumulation is obtained and an extremely high density of majority carriers stacks up at the GaN surface (Figure 17a). These electrons effectively block the interior of the GaN from changes in the electric field due to the effects of the gate voltage modulation by the applied frequency. At this point, since there is no depletion layer (W) in the GaN all of the field lines terminate at the surface of the GaN and the GaN acts to short circuit the AC signal. Thus, in accumulation the overall device behaves like a parallel-plate capacitor with the AlGaN acting like the dielectric spacer and the equivalent of an 'oxide capacitance', C_{AlGaN}. This corresponds to the maximum capacitance of the device [34].

When a negative bias is applied ($V_G < 0$), the negative charge on the gate pushes the electrons of the GaN away (Figure 17b). A positive charge builds up in the device due to the depletion of the semiconductor originating at the GaN-AlGaN interface. The depletion layer width continues to increase as the gate voltage decreases. The capacitance of the device drops as V_G decreases and is then [34]:

$$\frac{1}{C_{device}} = \frac{1}{C_{AlGaN}} + \frac{1}{C_W} . \quad (5)$$

Finally, as the potential across the device continues to decrease further ($V_G << 0$), another charge emerges at the AlGaN/GaN interface due to an accumulation of minority carriers (holes). This accumulation of holes forms an inversion layer (Figure 17c). As the gate voltage continues to decrease, the depletion width hardly increases any more since

the charge due to the holes increases as the gate voltage increases. The depletion width, W, reaches a maximum in this mode and as a result the capacitance is a minimum. This value is then [34]:

$$C_{Min} = \frac{\varepsilon_o \varepsilon_{GaN} A}{W_{Max}} \quad (6)$$

Or alternatively written,

$$C_{Min} = \frac{C_{OX} C_{SC}}{C_{OX} + C_{SC}} \quad \text{or} \quad C_{Min} = \frac{C_{AlGaN} C_{GaN}}{C_{AlGaN} + C_{GaN}} \quad (7)$$

Where C_{SC} is the capacitance of the semiconductor.

A real device behaves somewhat differently due to fixed and mobile charges in the AlGaN layer and charge in surface states. The result of these additional charges is a stretching of the characteristics or a shift either to the right or left along the V_G axis as in Figure 25.

A fixed charge in the 'oxide' layer shifts the measured curve along the V_G axis. A positive fixed charge at the interface between the AlGaN and GaN shifts the flat-band voltage by an amount that is equal to the charge divided by the oxide capacitance.

$$\Delta V_{FB} = \frac{Q_{FC}}{C_{OX}} \quad (8)$$

This shift changes linearly as the position of the fixed charge varies from the gate in the oxide. The shift is a maximum when the fixed charge is located at the AlGaN / GaN interface and zero when the fixed charge is located at the gate contact and AlGaN interface [33].

A mobile charge also causes a flat-band voltage shift to occur and is also described by equation (8) the same as that for a fixed charge. The fixed charge and the mobile charge measured curves will differ since a positive gate voltage causes mobile charges to

move away from the gate, whereas a negative gate voltage will attract the mobile charges toward the gate. An excellent method for recognizing the mobile charge is through the hysteresis in the high frequency capacitance curve after sweeping the gate voltage forward and backward. This will be explained in a later next section.

From the inversion region, the minimum capacitance is found and can be used to calculate the doping concentration of the GaN using the following equations [33]:

$$C_{Min} = \left[\frac{1}{C_{AlGan}} + \left(\sqrt{\frac{q \varepsilon_o \varepsilon_{GaN} N_D}{4 \phi}} \right)^{-1} \right]^{-1} \quad (9)$$

where, $\phi = \frac{kT}{q} \ln\left(\frac{N_D}{n_i}\right)$, and also by use of equation (1) [36],

$$N_{C-V} = \frac{C^3}{q \varepsilon_o \varepsilon} \frac{dV}{dC} . \quad (10)$$

Similarly, once the doping concentration is found, the flat-band capacitance can be determined using [33]:

$$C_{FB} = \left[\frac{1}{C_{AlGan}} + \sqrt{\frac{kT}{q \varepsilon_o \varepsilon_{GaN} N_D}} \right]^{-1} . \quad (11)$$

Additionally, the depletion depth can be determined as well from the capacitance:

$$W_d = \frac{\varepsilon A}{C} . \quad (12)$$

The previous discussion related to a metal-oxide semiconductor, which is assumed to possess similar capacitance characteristics as a heterostructure. However, the actual energy bands for a heterostructure are not the same as those of a MOS device as depicted in Figure 17. These differences are discussed next.

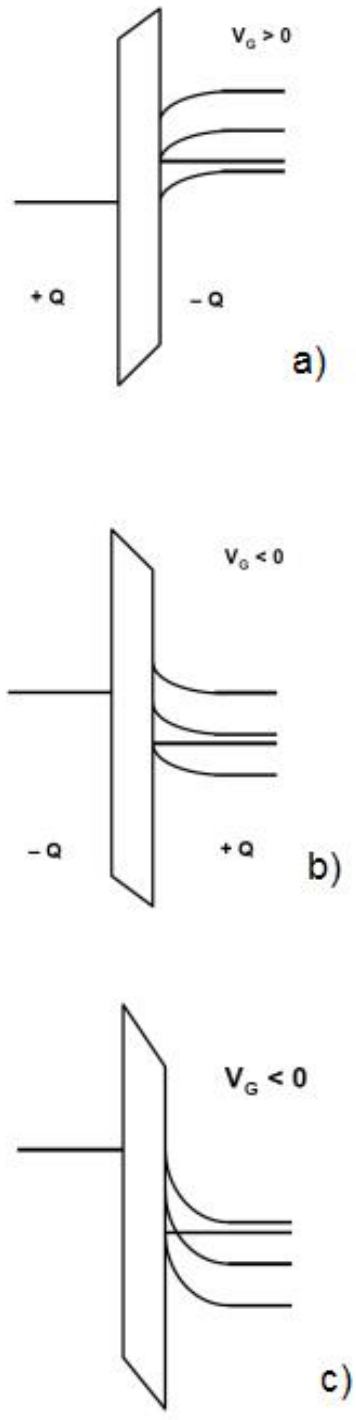

Figure 17. Band bending diagrams for a Metal Oxide Semiconductor under various applied biases a) accumulation, b) depletion, c) inversion [40].

Heterostructure Energy Band Diagrams

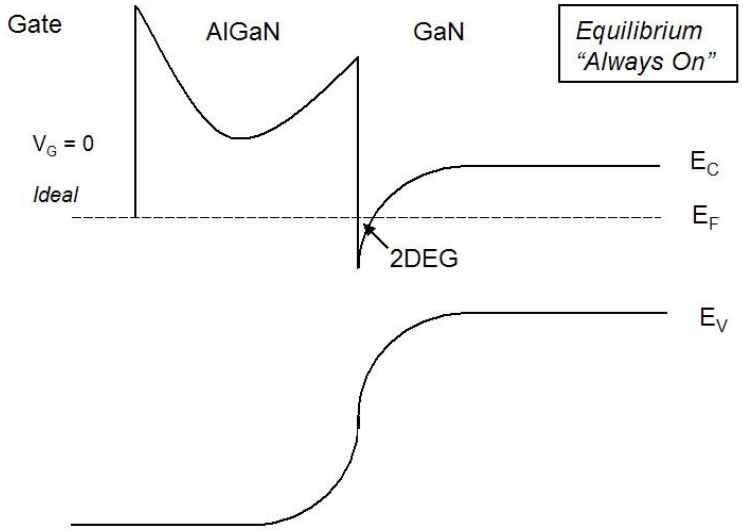

Figure 18. Schematic diagram of the energy bands and the quantum well in an AlGaN/GaN MODFET with gate bias of $V_G = 0$. E_C, E_V and E_F are conduction band, valence band and the Fermi level, respectively. The vertical axis is a measure of energy, qV, and the horizontal axis represents the various heterostructure layers.

Although MODFETs have been assumed to behave similar to MOSFETs, the reality of device operation is quite different. A MOSFET creates a p- or n-channel through an applied gate voltage, whereas a MODFET inherently possesses a high electron mobility channel due to heterostructure properties and the resulting formation a two-dimensional electron gas (Figure 18).

The band diagram in Figure 18 is a schematic band diagram of a heterostructure in equilibrium. The device is 'always on' due to the formation of a 2DEG in the quantum well as a result of the intrinsic electric field in the AlGaN directed toward the GaN.

Figure 19, 20 and 21 illustrate the band diagrams for accumulation, depletion and inversion, for an ideal heterostructure, and can be compared to energy band diagrams for

an n-type MOS device in Figure 17. In the accumulation region, an applied gate voltage greater than zero draws charge carriers from the GaN and populates the 2DEG. The conduction band drops below the Fermi level and creates a triangular quantum well containing the 2DEG. For an ideal MODFET, an applied bias of $V_G = 0$ indicates that the device is in equilibrium and always on due to the 2DEG. In depletion, the applied gate voltage is less than zero that has the effect of decreasing the 2DEG in the quantum well. Essentially, an applied bias less than zero starts to turn the device off by collapsing the well. The larger the negative applied bias, the more the well collapses as the Fermi level drops toward the valence band. When the conduction band just touches the Fermi level, the device has attained maximum depletion. As the applied gate bias continues to become increasingly negative, the Fermi level continues to drop away from the conduction band and the device enters inversion. The gate bias where this occurs is the threshold voltage.

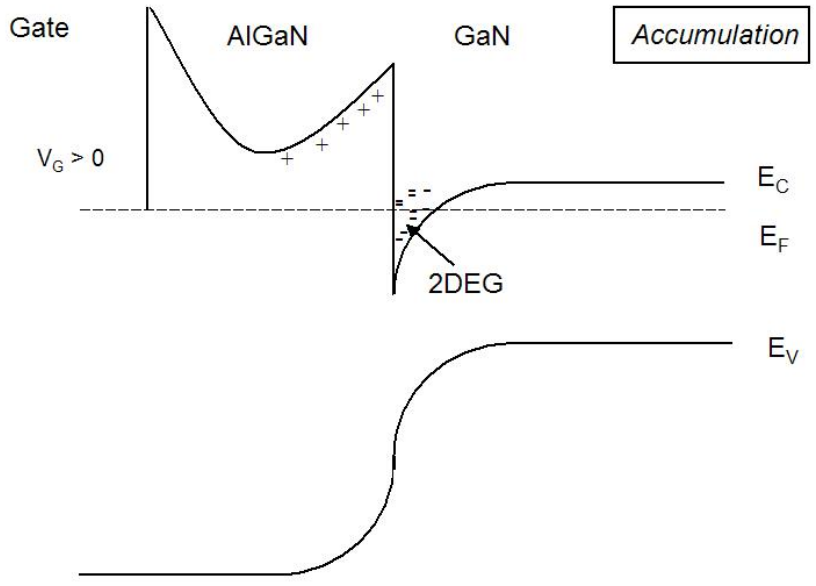

Figure 19. Band diagram of AlGaN/GaN MODFET in accumulation due to an applied gate bias of $V_G > 0$.

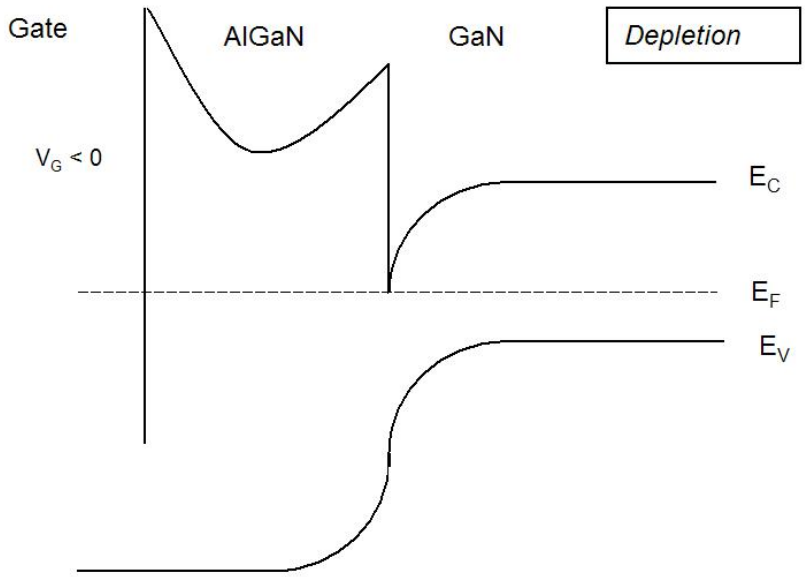

Figure 20. Band diagram of AlGaN/GaN MODFET in depletion due to an applied gate bias of $V_G < 0$.

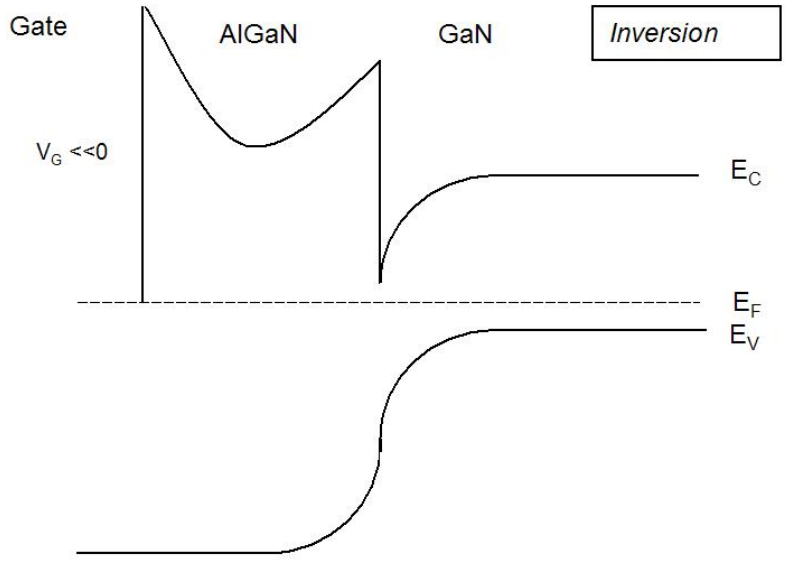

Figure 21. Band diagram of AlGaN/GaN MODFET in inversion due to an applied gate bias of $V_G << 0$.

Performing CV Measurements

In order to obtain accurate CV measurements, the measurements must be taken ensuring that the data is only recorded at equilibrium conditions and that the signals are measured in the correct sequence in order to compensate for stray capacitance. The Keithley Model 590 provides an integral setting that compensates for stray capacitance.

A method used to verify that the measurement equipment records true capacitance is by using calibration capacitors. These are precisely known capacitance sources that are connected to the CV analyzer in place of a test device. Specifically, the known capacitances used in this experiment were two Keithley devices of 479.08 pF and 1815.1 pF at 1 MHz and 22.3 °C (part number 5900-301-7 and 5900-301-8, respectively.) The capacitance measurements of the experimental setup in Figure 32 were accurately verified using the calibration capacitors and found to be within 1-3% of the known value.

The most important measurement requirement is the recording of data under equilibrium conditions. Each voltage step must allow the 'capacitor' to become fully charged before a measurement is taken. This fully charged condition is known as the equilibrium condition. The way in which the Keithley 590 accomplishes this is after initially applying the voltage there is a hold time before measuring the capacitance and after each subsequent voltage step there is a delay before recording the next capacitance. This hold and delay helps eliminate hysteresis curves for capacitance measurements taken in different directions (i.e. from -8V to 0V or from 0V to -8V). For this experiment, the Keithley 590 CV analyzer measurements produced negligible hysteresis curves as shown in Figure 22. The blue data points show the measurements taken from -8 V to 0 V

while the purple data points show measurements taken from 0 V to -8 V with no noticeable deviation.

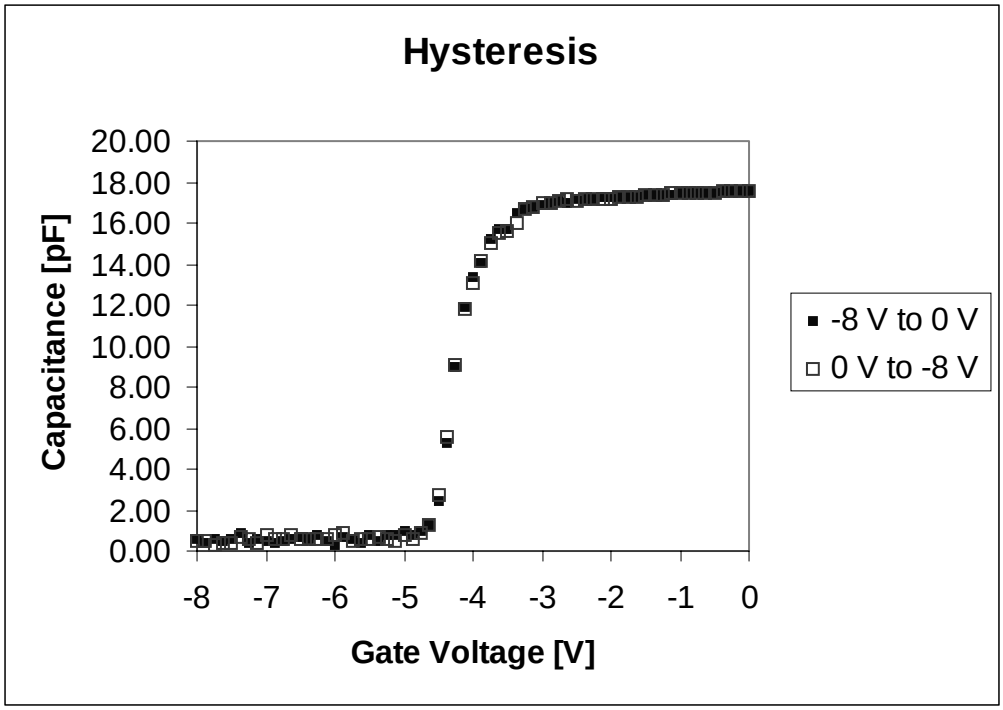

Figure 22. Plot showing the sweep direction (start voltage of –8V (solid square) and 0V (open square)) and the statistically insignificant effects of hysteresis on the measurements.

The preferred measurement sequence is from the inversion to accumulation since it is faster and more controllable that sweeping from accumulation to inversion. In this experiment, all subsequent measurements were taken from inversion to accumulation through an applied gate voltage range of -6 V to 0.5 V. This measurement technique is in accordance with the procedures as outlined in [39] except that the experimental setup did not incorporate a light in the beam tube to stimulate carriers in the device. Step two was not performed. Figure 23 is characteristic of the n-type devices used in this research.

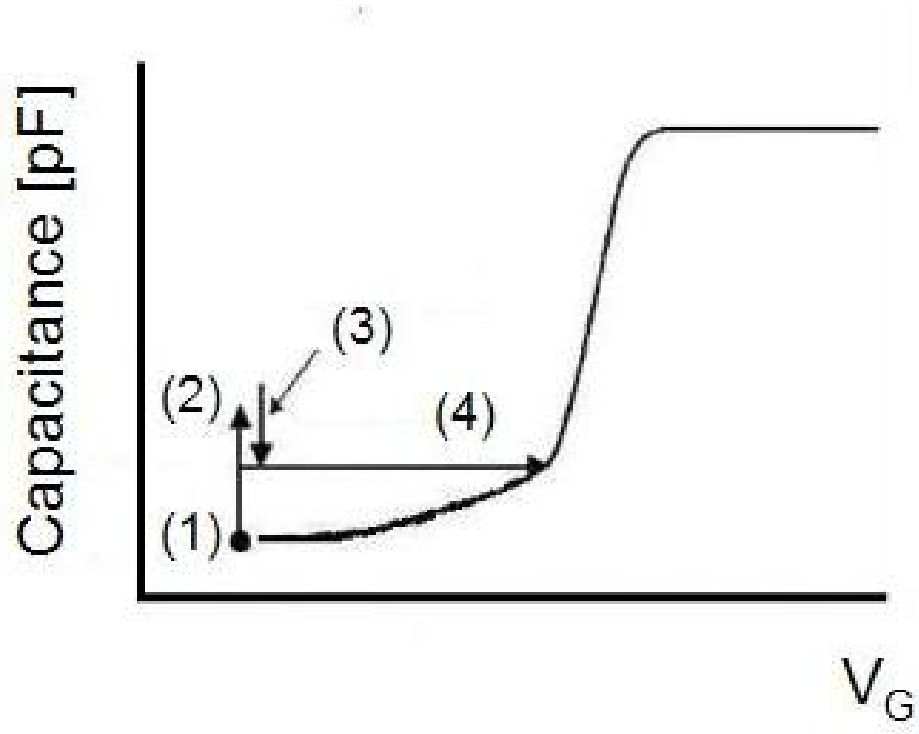

Figure 23. Illustration of the standard C-V measurement procedures: (1) Apply Bias, (2) Light On, (3) Light Off Stabilization, (4) Bias Sweep [39].

Additionally, before any measurement sweeps start and prior to recording data, all lights should be turned off in order to take all measurements in total darkness since the GaN heterostructures under investigation are extremely light sensitive. For this experiment, this was only a consideration during bench testing measurements and not during the irradiation process when the transistors were in the beam tube of the Van de Graaff machine.

Radiation Interaction in GaN

There are two principal effects of ionizing radiation on Gallium Nitride. These two effects are the introduction of permanent and transient defects in the material. Permanent are the defects of total dose and transient defects are dependent upon the dose rate. With

respect to the AlGaN / GaN HEMTs both of these play a role in transistor operation following irradiation and have an equal chance of occurring simultaneously [18].

The permanent defects manifest themselves as displacement damage as a result of elastic collisions with the lattice atoms as well as populate or depopulate traps. The rate of displacement damage is a function of the atomic binding energy and the energy transfer due to the collision [18]. In the wurtzite crystal structure of GaN, the nitrogen atoms (N) are bound much more tightly than the gallium atoms (Ga); however, the mass of the gallium is five times as massive as the nitrogen atom. The energy deposited by an elastic collision is extremely dependent upon the atom's mass, which means much more energy is transferred to the atom with the least mass.

As stated by Greene [18], Nord *et al*. has previously calculated the various displacement energies for the atoms in gallium nitride. The minimum energy required to displace a gallium atom from the lattice is 22 ± 1eV while the minimum energy needed to displace a nitrogen atom from the lattice is 25 ± 1eV. This minimum is calculated over all angles, while the average energy required for displacement from the lattice is 45 ± 1eV and 109 ± 2eV for Ga and N, respectively. On the other hand, the maximum amount of energy that can be transferred to an atom through coulomb scattering by an energetic electron is

$$E_{trans}^{\max} = 2\,\frac{\left(E_{e^-} + 2\,m_{e^-}\,c^2\right)}{m_{atom}\,c^2}\,E_{e^-} \qquad (13)$$

The table below shows the maximum energy available to lattice atoms due to irradiation by electrons of various energies as used in this research. These have been calculated using equation 13.

Incident Electron Energy (MeV)	Maximum Energy Transferred to Nitrogen Atom (eV)	Maximum Energy Transferred to Ga Atom (eV)
0.45	20.27	100.86
0.7	36.87	183.45
0.8	44.58	221.45
1.2	81.53	405.73

Table 4. Maximum electron energy transferred to lattice atoms [18].

Using Table 4 above and Figure 24 below, nitrogen point defects will occur above incoming electron energies of 0.3 MeV while gallium point defects start appearing around electron energies in excess of 0.5 MeV. Once incoming electron energy reaches 1 MeV both defects will occur in the sublattice [18]. Additionally, according to Green, the expected types of radiation-induced damage will most likely be V_N, I_N and related V_{GA} and I_{GA} [36]. The above data is corroborated by the work of Look *et al.* with 0.42 MeV electrons and the conclusion that the minimum displacement energy for nitrogen is 0.32 MeV and for gallium is 0.53 MeV [27].

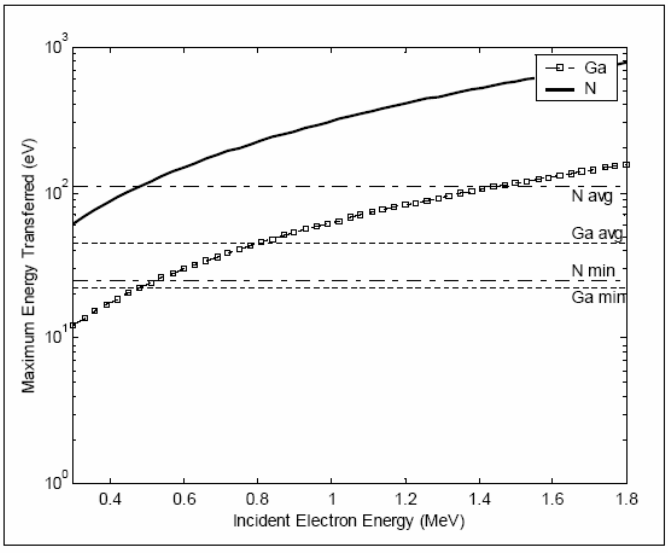

Figure 24. Maximum energy transfer for gallium and nitrogen as a function of the incident energy. The average and minimum displacement energy for both gallium and nitrogen are shown as horizontal lines [18].

Expected Radiation Effects on C-V Curves

The current literature provides minimal information on the radiation effects on the capacitance measurements of GaN heterostructures. However, there is ample research documenting the radiation effects on the capacitance characteristics of MOS devices. In order to proceed in this research effort, GaN heterostructures and MOS devices are assumed to possess similar capacitance characteristics. The discussion that follows relates the characteristics of MOS devices to GaN heterostructures.

Radiation changes interface trap density, D_{it}, that can be observed on the slope of C-V curves in depletion and weak inversion region. Also, the flat-band voltage V_{FB} shifts to a higher negative value with increasing fluence. An increase in fluence creates a growth of D_{it}. Nevertheless, irradiated MOS structures retain their basic capacitance behavior even after high-energy radiation [30] as shown the high frequency capacitance-voltage curve of Figure 13 [38].

Numerous experimental results indicate that interface traps build up over time during irradiation in Silicon MOS devices, but more experimental results are required before this can be conclusively stated for GaN. This incremental build up can occur in a few seconds to thousands of seconds at room temperature. Figure 25 below illustrates the time dependent build up of interface traps through normalized high-frequency C-V curves of a MOS capacitor before irradiation and at various time intervals from 0.04 seconds to 400 seconds after irradiation [3].

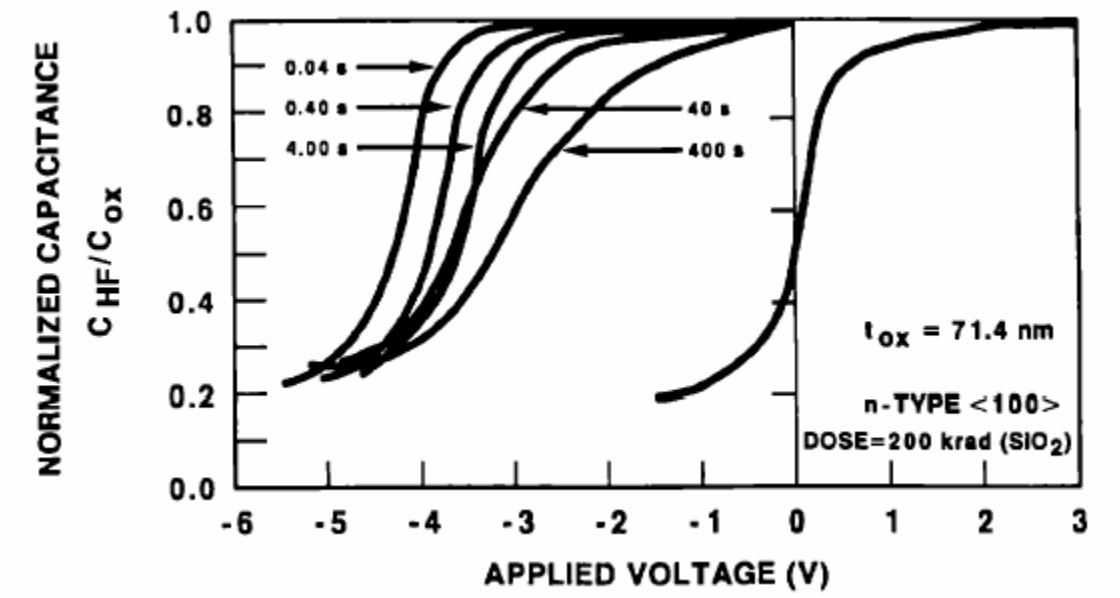

Figure 25. Normalized 1-MHz C_{HF}-V curves of an MOS capacitor at several times following pulsed electron beam irradiation [3].

There is no change in shape to the curve immediately following irradiation at 0.04 seconds. The curve is simply shifted in the negative direction along the applied voltage axis. From 0.4 seconds to 4 seconds the curves show a shift back in the positive direction with only slight changes in shape. This return toward the positive direction is due to the annealing of trapped holes in the insulator. Of interest, between 4 seconds and 40 seconds the curves begin to stretch along the applied voltage axis. This stretching increases at the 400 seconds mark with a noticeable slope change. The changing slope over time is due to the delayed build up of radiation-induced interface traps [3].

Figure 26 shows the doping dependence of a MOS-capacitor measured at high frequency resulting in the measured C-V curves. In the case of an *n*-type device, the effect of increasing the doping concentration from 10^{14} cm^{-3} to 10^{16} cm^{-3} is a vertical shift in the capacitance in the inversion region of the curve. This shift occurs due to an increase in charge carriers due to an increase in donors that increases the charge in the

inversion region and results in an increase in measured capacitance. This shift can be explained by the following equation:

$$C_{Min} = \frac{C_{AlGaN} C_{GaN}}{C_{AlGaN} + C_{GaN}} \tag{14}$$

where

$$C_{GaN} = \frac{\varepsilon_{GaN}}{x_d} \tag{15}$$

$$C_{Min} = \frac{C_{AlGaN} \frac{\varepsilon_{GaN}}{x_d}}{C_{AlGaN} + \frac{\varepsilon_{GaN}}{x_d}} \tag{16}$$

$$C_{Min} = \frac{C_{AlGaN}}{\frac{x_d}{\varepsilon_{GaN}}(C_{AlGaN}) + 1} \quad . \tag{17}$$

From

$$x_d = \sqrt{\frac{2\varepsilon_{GaN}\phi_s}{qN_d}} \, , \tag{18}$$

the proportionality of x_d to N_d is,

$$x_d \propto \frac{1}{N_d^{1/2}} \, . \tag{19}$$

Thus, when N_d increases, x_d decreases and the overall capacitance increases as shown in Figure 26 with each subsequent curve moving up the capacitance-axis.

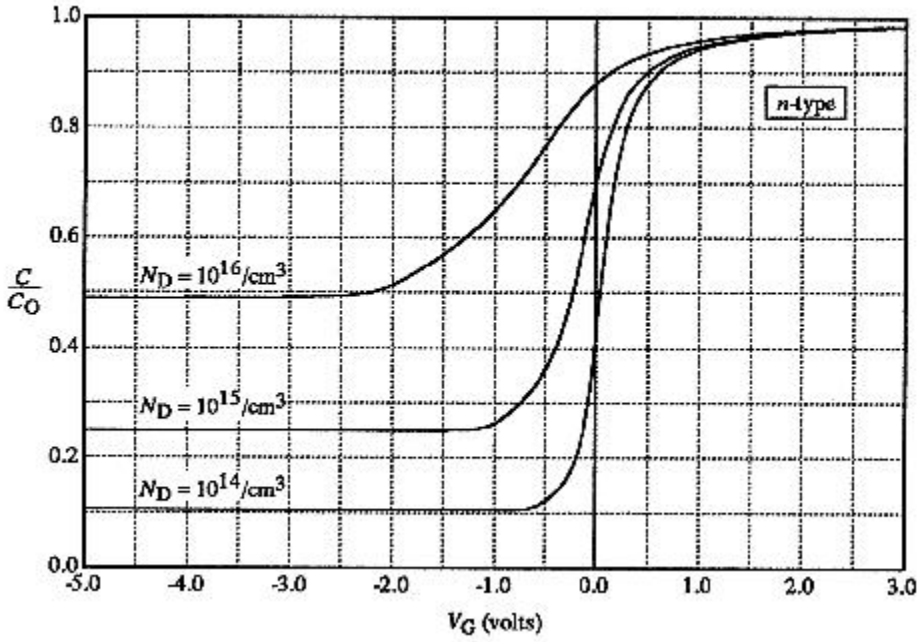

Figure 26. Doping dependence of MOS-capacitor high frequency C-V characteristics [41].

The expectation in any experimental results is that when this same vertical shift is observed after irradiation by means of a comparison of the before and after irradiation curves, then the electron irradiation will have caused an increase in the donor concentration in the GaN. This increase will likely be due to displacement damage in the GaN resulting in an active Nitrogen vacancy that is a donor. This influx of extra electrons should be the cause of the increase in drain current as reported by Sattler [21] due to an increase in the sheet charge density of the 2DEG.

The drain current model proposed by Morkoç *et al.* yields an equation for the source-to-drain current which clearly shows the dependence of the IDS current on four variables [42].

$$I_{DS} = -qWv(x)n_s(x) \tag{20}$$

where q is the charge on an electron, W is the gate width, v(x) is the electron mean velocity and $n_s(x)$ is the carrier concentration. Both the charge of an electron and the gate width are constants which means that any change in the drain current is caused by either a change in the 2DEG carrier concentration or a change in the electron mean velocity in the channel. C-V measurements cannot determine the electron mean velocity, but they can and will be used to calculate carrier concentration.

Ambacher *et al.* [36] use equation (21) and the capacitance from the C-V profiling technique to yield the carrier concentration in the inversion region. The sample parameters used by Ambacher *et al.* are close to the parameters of the samples used in this research and calculations using equation (21) yield similar carrier concentrations for data obtained on FATFETs used in this report when compared with Ambacher *et al*.

$$N_{C-V} = \frac{C^3}{q\,\varepsilon_o\,\varepsilon}\,\frac{dV}{dC} \tag{21}$$

Equation (21) will be used in conjunction with the post-irradiation results similar to Figure 26 to determine mathematically, as well as graphically, whether the carrier concentration increases or decreases due to electron irradiation; thus, satisfying the condition of the thesis hypothesis. These calculations are included in Appendix C.

IV. Experimental Procedures

Transistor Background

The GaN heterostructures used in this research are from wafer sections manufactured by Cree using the metal-organic vapor-phase epitaxy (MOVPE) process with a substrate of SiC layered with GaN and $Al_xGa_{1-x}N$. The transistor dimensions are shown in Figure 30 and are as follows: the substrate is 413 μm thick; the GaN layer over the substrate is a nominal thickness of 2 μm while the $Al_xGa_{1-x}N$ layer over the GaN is 25 nm. The $Al_xGa_{1-x}N$ is composed of a 27% mole fraction of AlN and 73% mole fraction of GaN that results in a layer of $Al_xGa_{1-x}N$ that is $Al_{0.27}Ga_{0.73}N$. According to the specifications provided by Cree the room temperature carrier concentration is 1.3×10^{13} cm^{-2} while the mobility is measured as1300 $cm^2/V\cdot s$

The actual fabrication of the transistor was accomplished at the Air Force Research Laboratories (AFRL) Sensors Directorate Aerospace Components and Subsystems Technology Electron Devices Branch (SNDD). Sattler [21] provides an in-depth description of the original fabrication, dicing and packaging process in a previous work. Sattler's previous research utilized all previously fabricated, diced and packaged devices. In order to replicate the conditions of previous work as closely as possible, new devices were diced and packaged from the remaining portions of the previously used wafer. Although there are three wafer sections (JSO1A, JSO1B, and JSO1C) remaining from the original disk manufactured by Cree only transistors from Wafer JSO1A were used in this research. Wafer JSO1A consisted of approximately 40 chips containing transistors of various types and is shown Figure 27 prior to dicing and packaging.

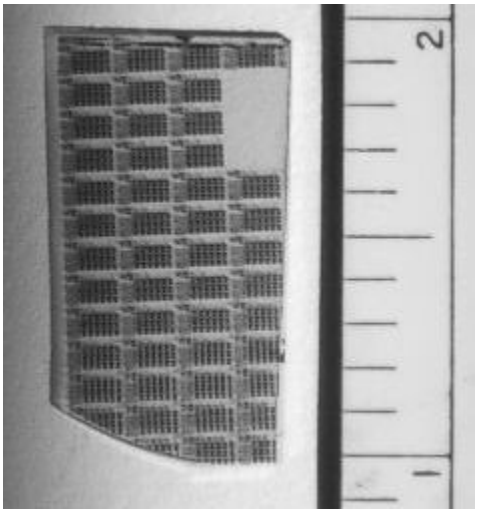

Figure 27. Wafer section JSO1A containing approximately 40 individual chips. Scale to the right is inches for comparison only.

The transistor used in this research is located in the upper right corner of the chip and is called a FATFET to differentiate it from the other 'thin' transistors on the chip in Figure 28. The name FATFET has gained acceptance due to the fact that the transistor gate is 50 μm in length, which is much larger than a gate length of approximately 1.2 μm for all other transistors on the chip. Figure 28 shows the location of the FATFET on the chip as well as the contact connections labeled G, S, and D for gate, source and drain, respectively. Figure 29 shows the special orientation of the gate, source and drain contacts on the device. The vertical line AB corresponds to the cross section diagram in Figure 30 that emphasizes the layered structure and composition of the device.

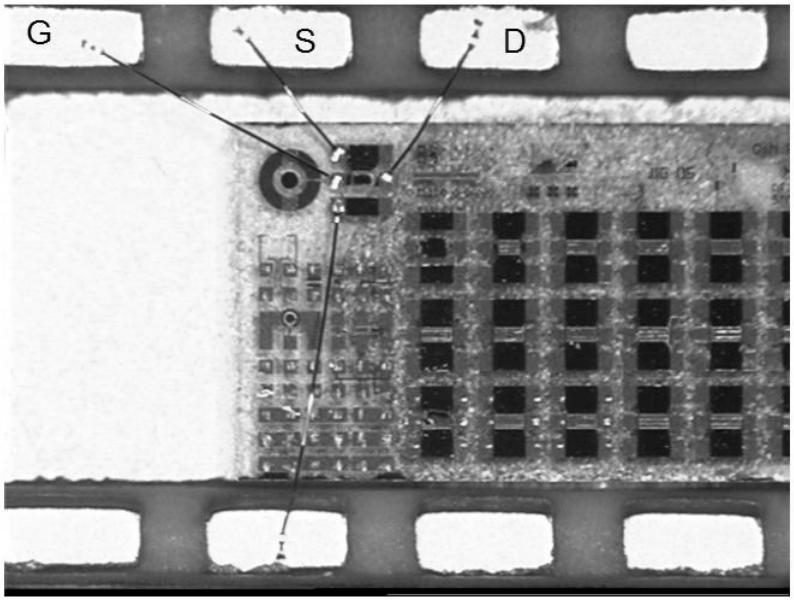

Figure 28. Close-up of individual chip showing FATFET location in upper left of the image to the right of the CV ring. Contacts labeled G, S and D. Photo taken by Larry Callaghan of AFRL/SN.

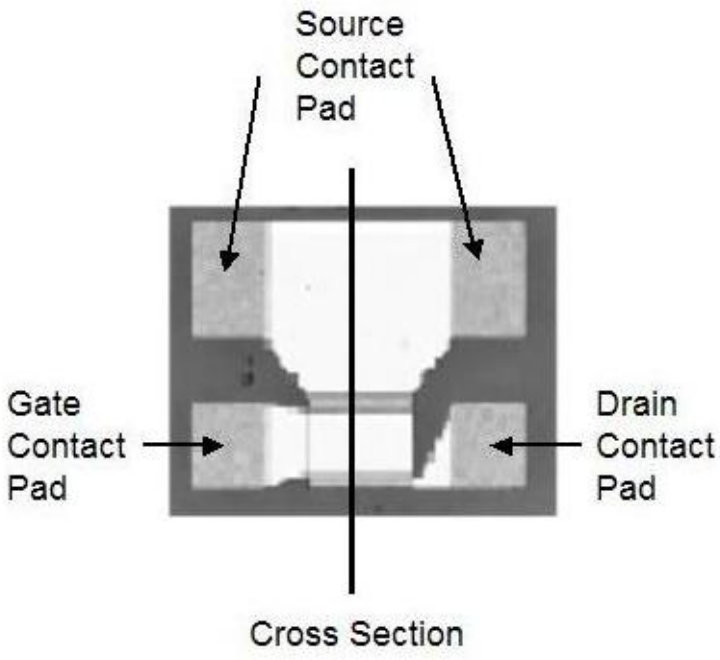

Figure 29. Individual FATFET spatial layout.

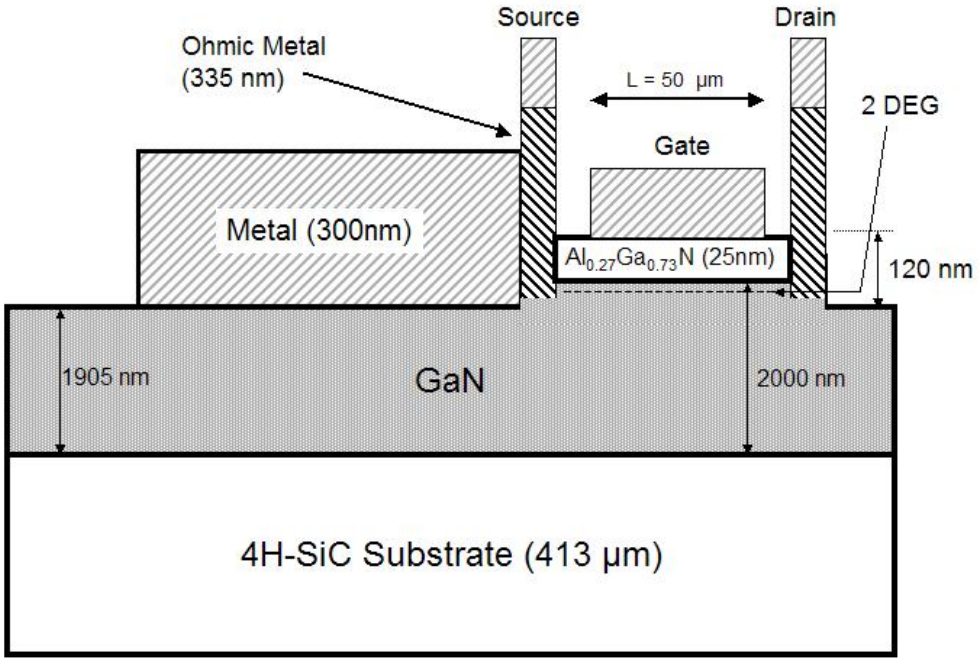

Figure 30. Cross section of FATFET along AB in Figure 13.

Once the desired wafer was chosen for use in the experiment, Mr. Larry Callaghan of AFRL/SN was employed to dice and package all of the chips on JSO1A. He accomplished this feat within two days and produced 40 diced and packaged devices like the one in Figure 31. This packaging process involved bonding the chip to the package and then wire bonding the FATFET to the package pins. In this case, the first three pins were used to attach the gate, source and drain from left to right Figure 28. The package was left open to allow the electron radiation clear access to the transistors so that attenuation of electrons by the package was not a factor.

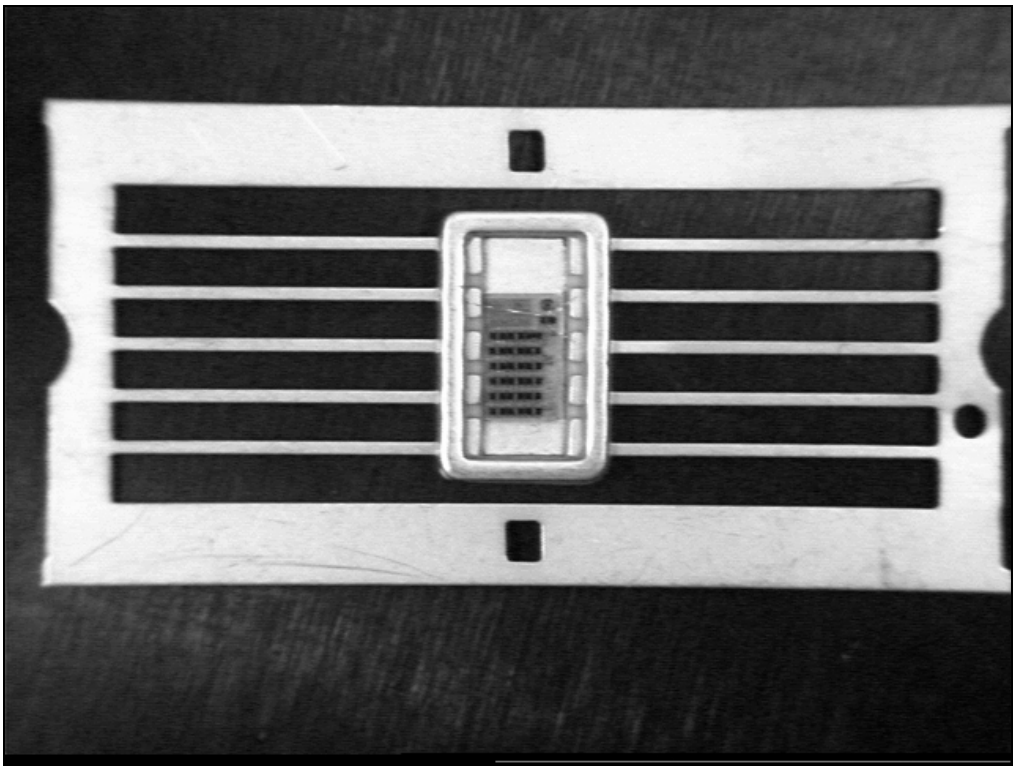

Figure 31. Diced and packaged chip from wafer section JSO1A. Photo taken by Larry Callaghan of AFRL/SN.

Pre-Irradiation Characterization

After packaging was completed, the transistors were tested using two different methods. One method used two Keithley 237 High Voltage Source Measurement Units (SMUs) in order to obtain the I-V characteristics. These measurements determined the transistor action and the gate leakage in order to choose transistors that possessed similar operating parameters with respect to current output and leakage current. Another method used a Keithley 590 CV Analyzer in order to obtain the capacitance and conductance data to produce CV curves. Both methods utilized a National Instruments General Purpose Interface Bus (GPIB), and a laptop running either an IV characteristics Microsoft Visual

Basic program [21] or a CV characteristics Microsoft Visual Basic program depending on the measurements required (Appendix A – Visual Basic Data Acquisition Program).

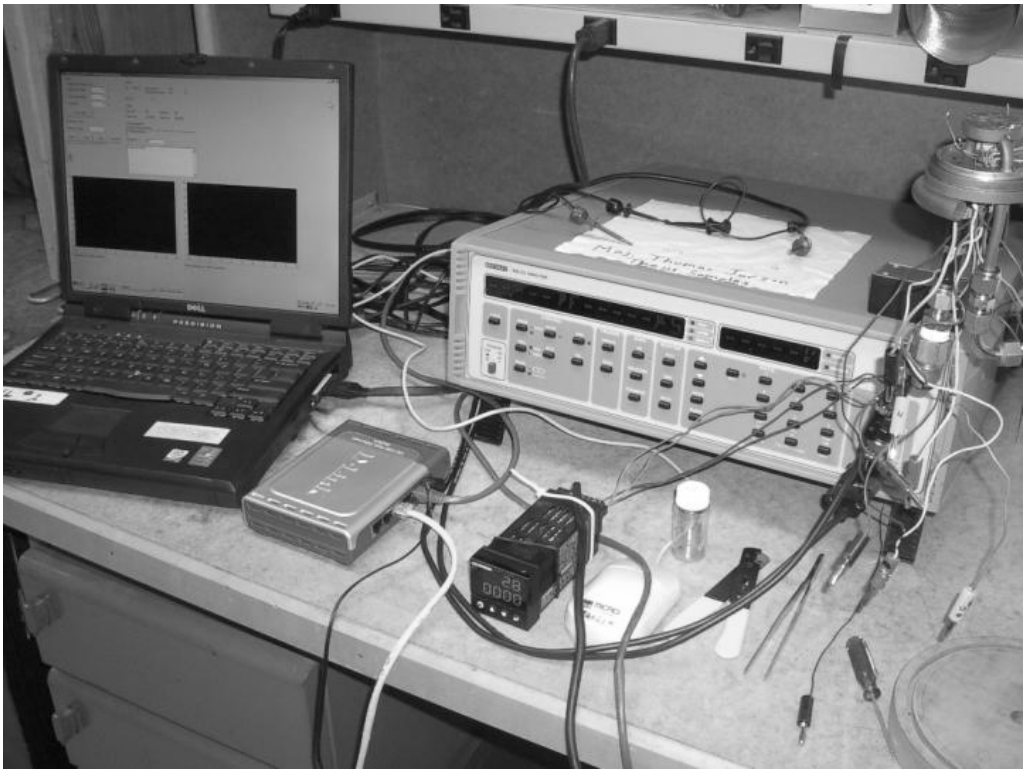

Figure 32. Building 470 laboratory Experimental Setup for Pre-Irradiation C-V Characterization

Following the initial tests, the devices were retested using the experimental setup that would be used to execute the irradiation experiment. The only addition to the apparatus used was a cold head sample mount assembly as shown in Figure 33 that was machined for previous work [21] by the AFIT model shop. The cold head is required in this experiment for several reasons: 1) it maintains the devices at low temperatures (~80K) during irradiation thereby 'freezing in' any defects created during irradiation, and 2) it allows electrical operation and measurement of samples following irradiation without removing the sample from vacuum and low temperature, as well as concurrent temperature monitoring using a Resistive Temperature Device (RTD) implanted in the

cold head. In the first method the transistor *I-V* curves were measured in a range of 0 V < V_D < 10 V with gate voltages of V_G = 0, -1 V, -2 V, -3 V, and -4 V; the sample was always grounded during measurement. An important point is that the range of gate voltages over which these transistors can operate is approximately -6 V < V_G < 0.5 V. For V_G < -6 V the transistors enter cutoff (no 2DEG exists) and for V_G > 0.5 V the transistors cease to function properly causing the associated *I-V* curves to experience large distortions [21].

All devices were initially tested at room temperature and then at ~80K for both the I-V characteristics and the C-V characteristics. The plot in Figure 34 provides a comparison of the C-V curves at room temperature (~22 C) and ~80K. Each curve in Figure 34 is the average of 7 measurements of all nine-device averages that are themselves averages of 7 measurements for each device. The pre-characterization curves for room temperature and 80K for the devices used in this research are located in Appendix B.

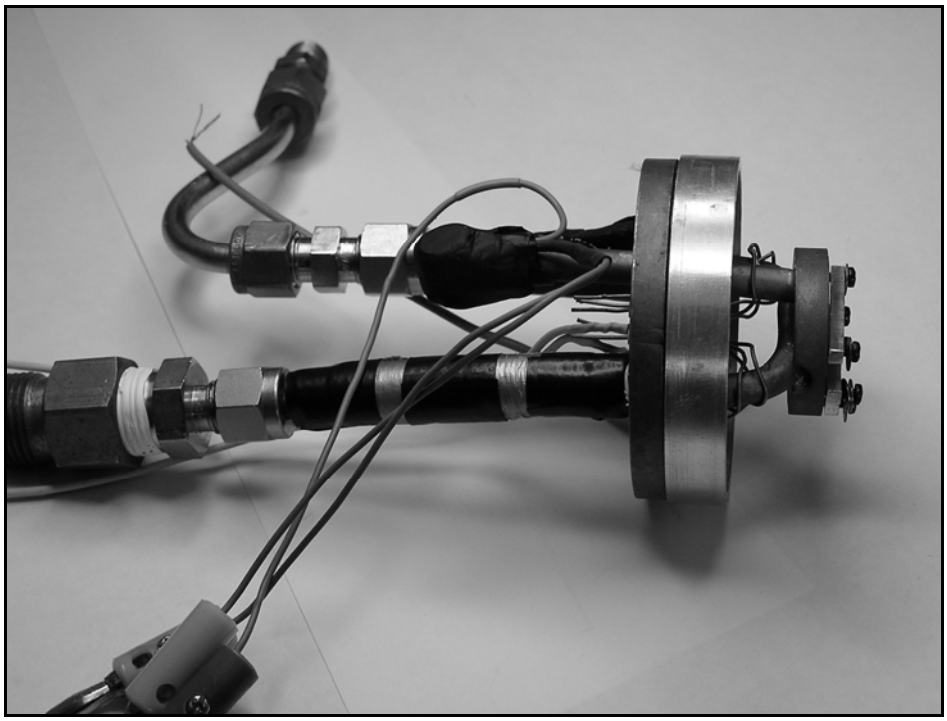

Figure 33. Cold Head and Sample Mounting Assembly [18].

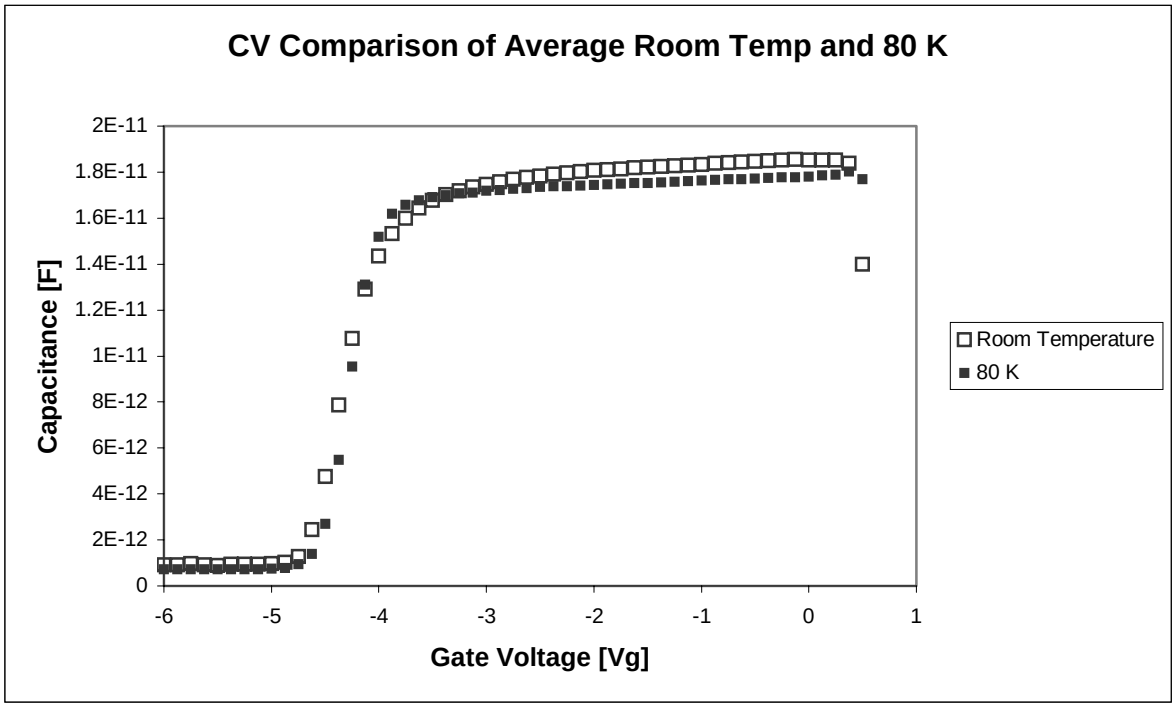

Figure 34. Comparison of capacitance-voltage measurements for nine devices averaged over seven cycles and measured at 300K and 80K.

Once the initial pre-characterizations were complete, the devices were mounted on the cold head and tested to determine any additional capacitance induced by the cold head and the feed-through wires. As expected, the wires and the cold head added to the overall capacitance measured by the CV analyzer. A test device, A0411, similar to those used in the irradiation experiments was used to determine this additional capacitance. Three distinct tests were run: 1) measurement of the device alone, not attached to the cold head but grounded, 2) measurement attached to the cold head ungrounded and 3) measurement attached to the cold head and grounded. Figure 35 indicates the comparative capacitances of the three different measurement systems. Due to the extra capacitance inherent in the cold head and wires, it was imperative that during the experiment the devices were characterized at low temperature (~80K) while the cold head was attached to the beam tube of the VDG just prior to irradiation. This added additional time to the measurements; however, this ensured that the base line measurements reflected any additional capacitance due to the measurement system materials. For device A0411, the additional capacitance at room temperature was an average of 6.63615×10^{-13} Farads which is 10% of a picofarad measurement and not negligible.

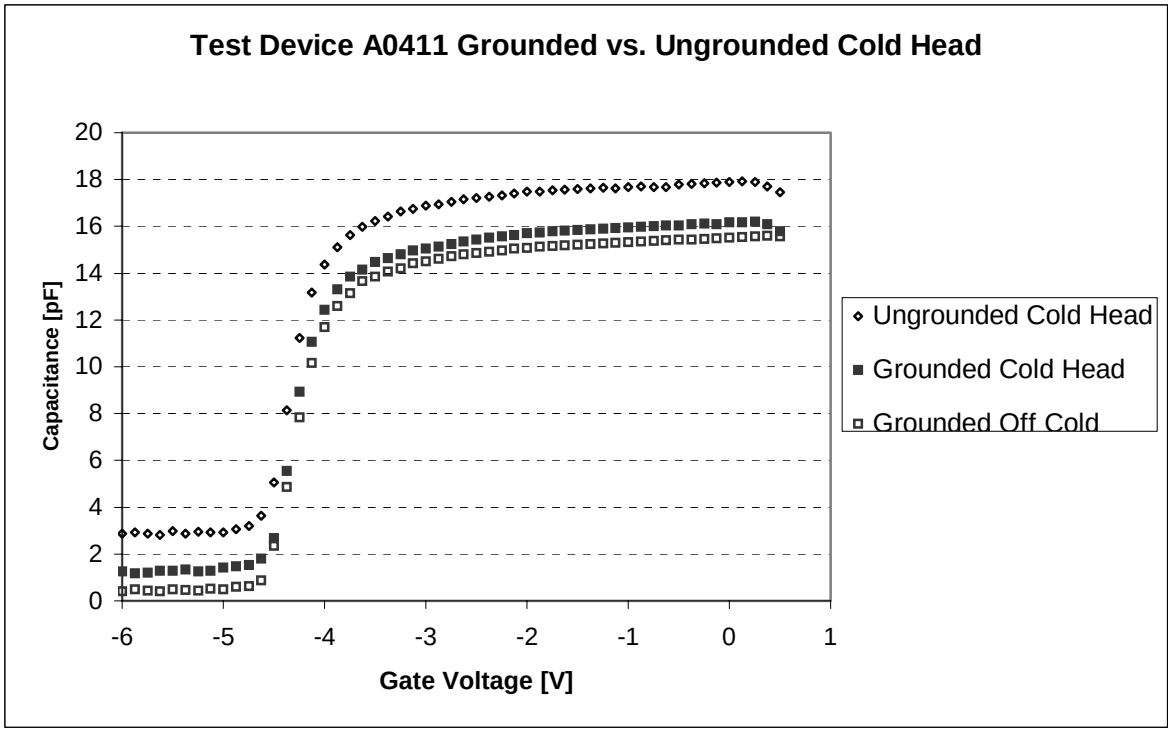

Figure 35. Graphical representation of the impact of grounding the devices and the intrinsic (additional) capacitance added by the cold head mounting system.

Irradiation Experiments

Irradiation experiments were conducted at Wright State University under the equipment supervision of Dr. Gary Farlow who operated the electron Van de Graaff electron accelerator (Figure 36).

The Wright State University Van De Graaff generator produces low- to mid-energy electrons in a range from 400 keV to about 1.8 MeV with beam currents at and below 30 μA. The aperture area of the electron beam is 3.3 cm^2 and this beam passes through an aluminum tube that must be evacuated to at least as 9 x 10^{-6} torr. Within this tube a relatively uniform beam of energetic electrons can be created. From specifications provided in previous work, the temporal current deviation is estimated at ±3%, while the temporal energy deviation is estimated at ±5% [21]. Additionally, Dr. Farlow estimates

that the spatial beam uniformity is ±2-3% as noted on a piece of irradiated plastic with a 2 cm by 2 cm discolored square etched by the electron beam [21]. The beam current was used to control the fluence rate and was set between a range of 0.13 μA and 6.0 μA. The total fluence is determined using a current integrator that measures the beam current imparted onto the cold head. The most important component of the machine is the cryogenically cooled vacuum cap at the end of the evacuated aluminum tube that holds the device mounting assembly and electrical connections for temperature and electrical measurements. Henceforth, this cap will simply be referred to as the cold head. Due to added impressed currents from the electron beam causing transistor burnout in the affected regions, true *in-situ* measurements could not be performed; however, all experimental measurements were conducted at low temperature (~80K) under as low a vacuum as possible within equipment capabilities. Ultimately, this was on average about 5×10^{-6} torr.

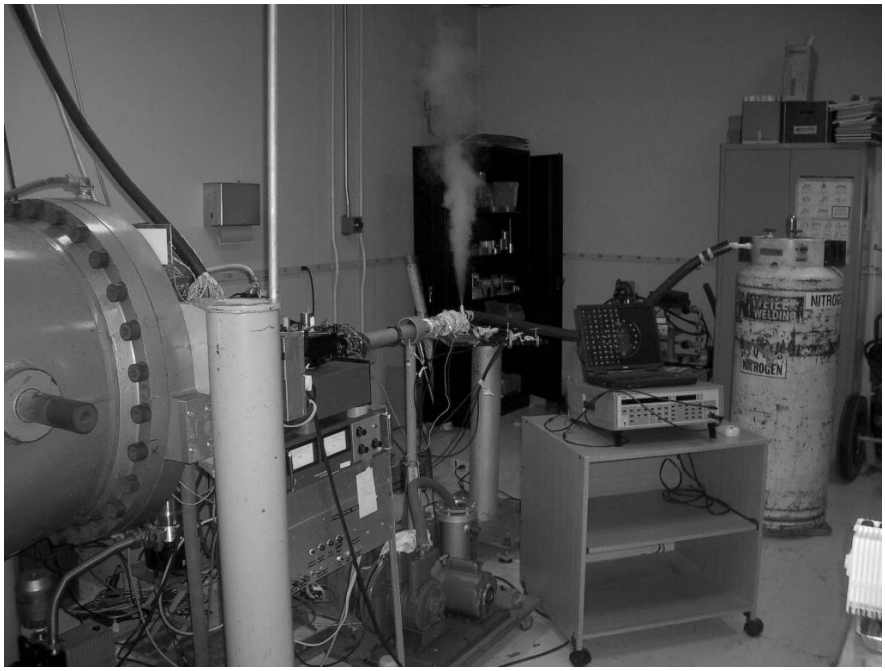

Figure 36. Van de Graaff facility at Wright State University.

Due to the operating parameters of the Van de Graaff generator, the energy range of electrons used in this experiment was 0.45 MeV to 0.85 MeV and a fluence range of 10^{12} e^-/cm^2 to 10^{15} e^-/cm^2 based on beam current. This, however, fits in well with the initial premise that these devices, as components of satellites, could experience an electron fluence up to 3×10^6 $e^-/cm^2/min$ or an annual fluence of 9.46×10^{13} e^-/cm^2 while on earth orbit.

The first irradiation experiment was conducted on the 12th of January 2005 due to more than 10 weeks of maintenance on the VDG.

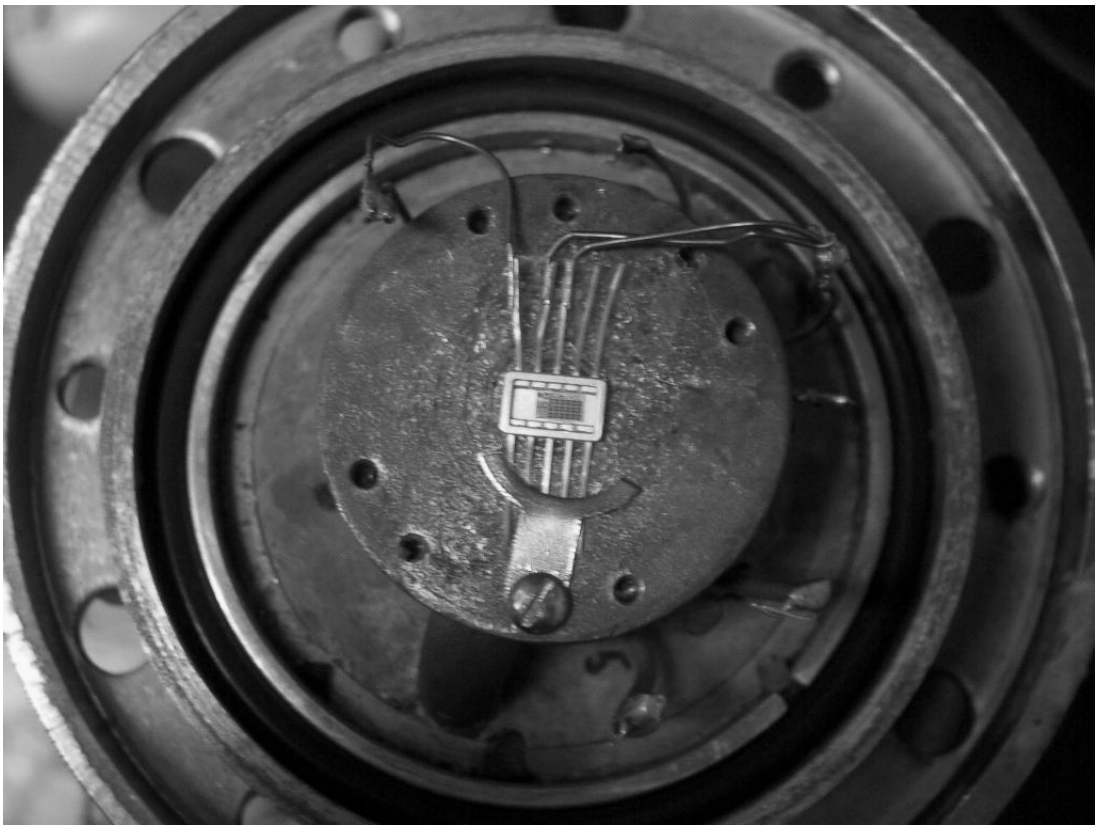

Figure 37. Sample device attached to cold head by clamp and contact leads soldiered to cold head feed-through lines.

All experiments began by mounting the device to the cold head, attaching the cold head to the aluminum beam tube on the VDG and lowering the temperature of the device

with liquid nitrogen. The sample was mounted to the cold head by clamping the five unattached contacts on the device as shown in Figure 37. The extraneous leads were clamped to the cold head to ensure that a secure conductive path for any beam-deposited charge could escape by way of the VDG current integrator, and thus reduce the chance of device damage due to charge buildup. Additionally, the device was centered on the face of the cold head to ensure that a uniform electron beam interacted with the transistor (The electron beam is scanned to ⅓ intensity). Conductive grease was used to ensure a good thermal connection with the cold head to assist in maintaining the device at a low temperature. The grease also served as an electrical insulator between the cold head and the metal packaging, nevertheless, this insulating effect is somewhat reduced at low temperature and exposure to the electron radiation.

After the physical mounting of the device was accomplished, the three leads (gate, source and drain) were soldered to the electrical feed-through lines on the cold head. The gate was attached to one line while the source and drain were attached together to another as in Figure 38. Once the device was cooled to ~80K, the sample was pre-characterized while attached to the VDG in order to establish a pre-irradiation baseline. During the measurement phase of the experiment, the Keithley 590 CV Analyzer was wheeled in on a cart and positioned approximately ½ m from the cold head in order to reduce the chance of measuring extraneous capacitance inherent in long cables.

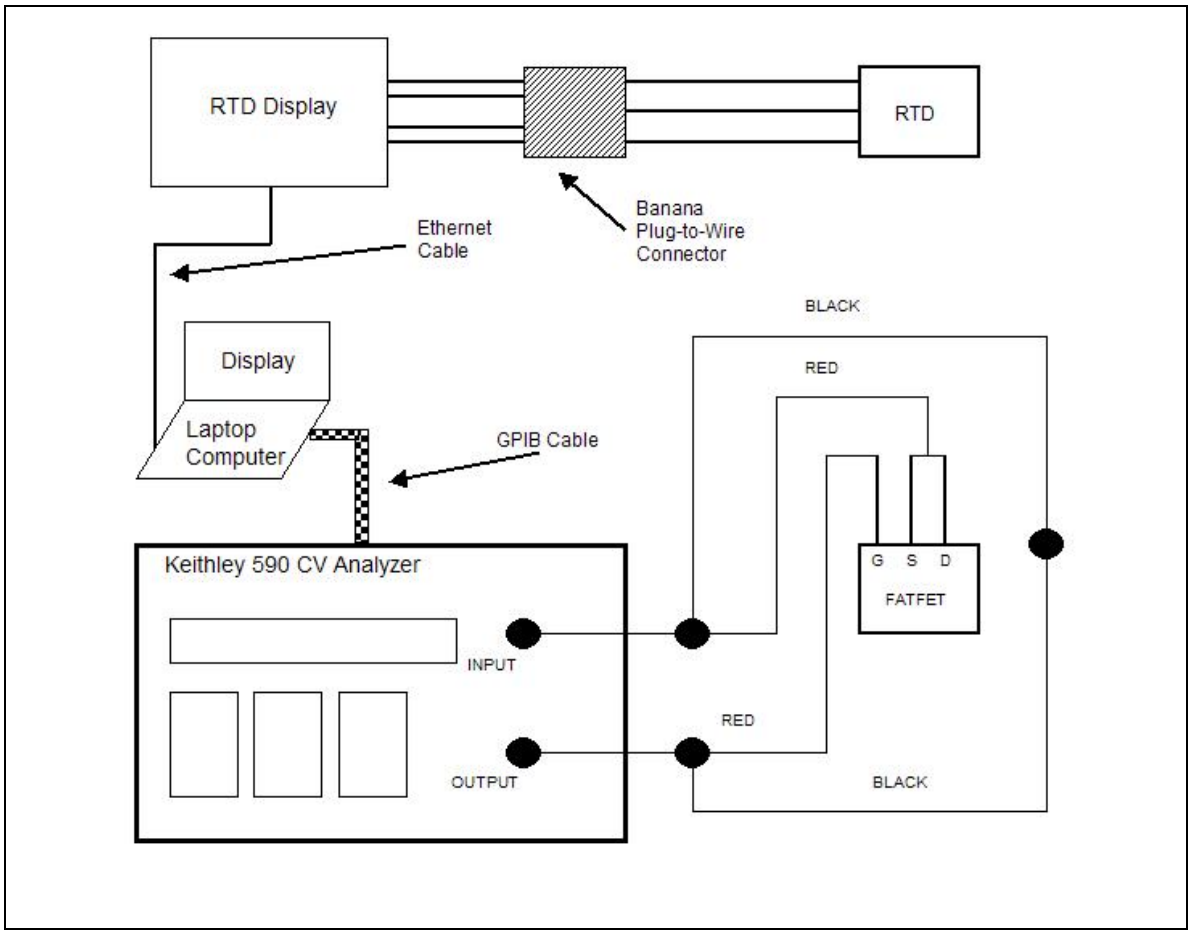

Figure 38. Schematic of the Experimental Setup at the Wright State University Van de Graaff Facility

A major concern resulting from condensation on the electrical connections was the possibility of an electrical short occurring between the numerous electrical lines on the cold head. Isolating the lines by sealing them with paper towel strips and masking tape kept this from occurring. This ultimately was not a problem as the water condensed onto the tape and paper towels as shown in Figure 39.

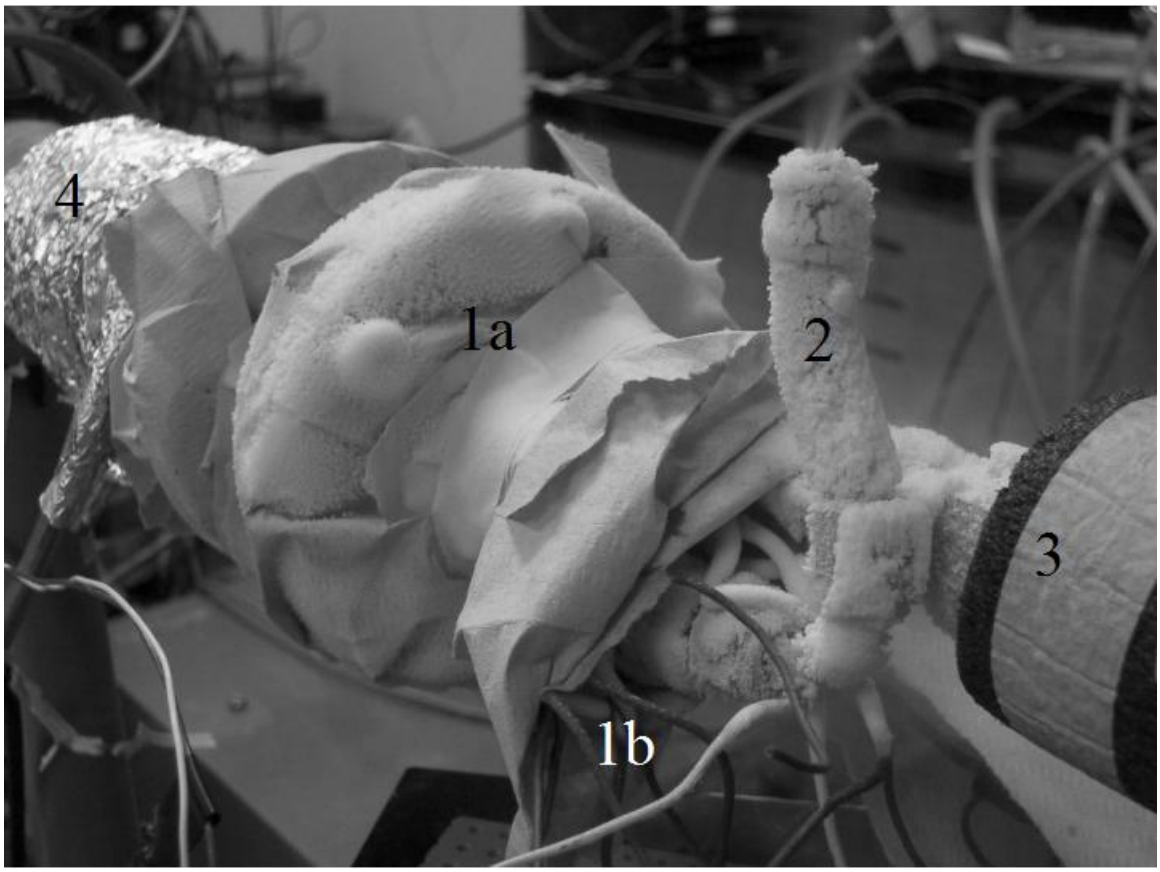

Figure 39. Insulation of cold head by sealing with masking tape and paper towels. 1a) Cold head, 1b) Feed through lines, 2) Liquid nitrogen exit port, 3) Liquid nitrogen input, and 4) VDG beam tube.

A time consuming portion of the procedure was the evacuation of the beam tube. Prior to the irradiation of a sample, the beam tube was reduced to a vacuum level of at least 9×10^{-6} torr. Once the beam tube was evacuated and the temperature lowered to around 80K, the pre-irradiation baseline measurements were made. Due to lessons learned from previous research [21], actual *in-situ* measurements were not attempted as these measurements resulted in the destruction of samples. Rather, the following procedure was used. The device was turned off and grounded completely to the cold head and current integrator of the VDG. After the low temperature irradiation at the specified

electron energy and fluence, the VDG was turned off and the measurement apparatus was moved into the irradiation room, connected to the leads of the cold head and powered up. Prior to recording any measurements, the current integrator was disconnected and the cold head ground was connected to the ground on the Keithley 590 in order to provide a sufficient current path for any excess electrons deposited by the beam onto the cold head.

The initial irradiation plan called for using a sample to test the experimental setup and record data using electrons with an energy of 0.45 MeV at an initial fluence of 1.0×10^{14} e^-/cm^2. However, due to an initial calculation error identified at the start of the second day of irradiation all initial irradiations were with 3.3 times as many electrons as initially desired. This error helps explain some of the observed results of A19.

After irradiating the first sample A19 to an actual total fluence of 3.3×10^{14} e^-/cm^2, *A19-1*, while the device was left in the off mode (the coax lines running to the Keithley 590 were left connected but the 590 was turned off), the VDG was turned off and the current integrator disconnected from the cold head metal. The cold head metal was then shorted to the Keithley system ground and CV measurements were taken. Upon examining the CV data, the device did not function according to design parameters. Due to the recent maintenance on the VDG, the current output of the device was higher than anticipated at about 100 μA or a current density of 6.024 μA/ cm^2 when only 1 μA or a current density of 0.06024 μA/ cm^2 was desired. The extreme current load damaged the device and resulted in the Keithley 590 measuring 9.9×10^{30} F during three attempts to obtain usable capacitance data. Even after warming the cold head to room temperature and disconnecting the cold head from the beam tube, capacitance measurements of A19

resulted in unusable data and an uncharacteristic CV curve. At this point, the cold head was removed, and another device, A16, mounted.

The experiment continued with device A16 using the same procedure mentioned in the previous paragraph. After irradiating the next sample to a fluence of 3.3×10^{14} e^-/cm^2, *A16-1*, while the device was left in the off mode, the VDG was turned off and the current integrator disconnected from the cold head. The cold head ground was then shorted to the Keithley system ground and CV measurements were taken. Initially during a portion of the first measurement cycle, the Keithley measured a capacitance of 9.9×10^{30} F and then began recording capacitance values in the picofarad range. At this point, seven cycles were recorded at the fluence rate of 3.3×10^{14} e^-/cm^2. The experiment continued by disconnecting the measurement equipment, turning the VDG on, and irradiating the sample to 6.6×10^{14} e^-/cm^2, *A16-2*, or a fluence two times the initial fluence, yielding a total fluence of 9.9×10^{14} e^-/cm^2 corresponding to three times the initial fluence. This pattern was selected in order to increase the fluence in a logarithmic manner. Following irradiation, the VDG was turned off, the current integrator disconnected, and the cold head shorted to the ground on the Keithley 590. Again, during measurement, the Keithley 590 measured a capacitance of 9.9×10^{30} F across a gate voltage range of –6V to 0.5V and did not recover as in the previous measurement by recording measurements in the picofarad range. Three attempts were made to obtain usable capacitance readings while at 80K and attached to the beam tube of the VDG. Nevertheless, no usable readings were obtained. However, after warming the cold head to room temperature and disconnecting the cold head from the beam tube, capacitance measurements of A16 resulted in usable data and a characteristic CV curve.

Table 5 summarizes information about the samples, irradiation sequence number, irradiation energy used, beam current, fluence and total fluence specifics relating to the irradiation experiment of device A19 and A16.

Sample & Seq. #	Energy (MeV)	Beam Current (μA)	Relative Fluence (e^-/cm^2)	Relative Irradiation Time (min)	Total Fluence (e^-/cm^2)	Total Irradiation Time (min)
A19-1	0.45	100+	3.3×10^{14}	2.2	3.3×10^{14}	2.2
A16-1	0.45	1.0	3.3×10^{14}	2.2	3.3×10^{14}	2.2
A16-2	0.45	1.0	6.6×10^{14}	4.4	9.9×10^{14}	6.6

Table 5. A19 and A16 Irradiation Experiment Summary (12 January 2005).

The experiment continued on January 13th with device A1 using the same procedure mentioned previously. Since the sample on the previous day failed to yield usable data after a total fluence of 9.9×10^{14} e^-/cm^2, the consensus was that the fluence should be reduce an order of magnitude and the irradiation cycle attempted again. The new irradiation plan was to irradiate samples in a logarithmic manner increasing from 1.0×10^{13} e^-/cm^2 to 1.0×10^{15} e^-/cm^2 in order to create a fluence continuum between sample A1 and the previous results of sample A16. However, during a post irradiation calibration of the beam spot size the actual fluences used in the irradiation of samples A1 and A2 were about a third lower than thought. The actual beam spot size was 16.6 cm^2.

Incident Electron Energy (MeV)	Planned Fluence (e^-/cm^2)	Actual Fluence (e^-/cm^2)
0.45 and 0.8	1×10^{13}	3.5×10^{12}
0.45 and 0.8	2.3×10^{13}	7.9×10^{12}
0.45 and 0.8	6.7×10^{13}	2.3×10^{13}
0.45 and 0.8	23×10^{13}	7.9×10^{13}

Table 6. This table compares the corresponding corrected irradiation fluences calculated after the spot size measurements of 20 January.

Using the corrected fluences of Table 6, sample A1 was initially irradiated at an actual fluence of 3.5×10^{12} e^-/cm^2, *A1-1*, while the device was left in the off mode, the VDG was turned off and the current integrator disconnected from the cold head. The cold head ground was then shorted to the Keithley system ground and CV measurements were taken. An initial short measurement cycle from –1V to 0V was used to attempt to flush out any excess stored charge since the first few readings of the previous device initially measured extremely high capacitance levels of 9.9×10^{30} F. This procedure worked and the seven cycle measurements recorded usable capacitance data. The experiment continued by disconnecting the measurement equipment, turning the VDG on, and irradiating the sample to 7.9×10^{12} e^-/cm^2, *A1-2*, or a fluence approximately two and a quarter times the initial fluence, yielding a total fluence of 1.14×10^{13} e^-/cm^2 corresponding to a little more than three and a quarter times the initial fluence. A third irradiation of the sample to 2.3×10^{13} e^-/cm^2, *A1-3*, or a fluence six and a half times the initial fluence, yielding a total fluence of 3.44×10^{13} e^-/cm^2 which corresponds to ten times the initial fluence. The fourth and final irradiation of 7.9×10^{13} e^-/cm^2, *A1-4*, or twenty-two times the initial fluence ultimately made the total fluence of sample A1 roughly equivalent to that received by A16. Thus establishing a fluence continuum from 1.0×10^{12} e^-/cm^2 to 1.0×10^{15} e^-/cm^2. Measurements were also taken immediately after warming the cold head to room temperature and disconnecting the cold head from the beam tube.

Table 7 summarizes the pertinent information about the sample, irradiation sequence number, irradiation energy used, beam current, fluence and total fluence specifics relating to the irradiation experiment of A1.

Sample & Seq. #	Energy (MeV)	Beam Current (μA)	Relative Fluence (e^-/cm^2)	Relative Irradiation Time (min)	Total Fluence (e^-/cm^2)	Total Irradiation Time (min)
A1-1	0.45	0.15	3.5×10^{12}	3	3.5×10^{12}	3
A1-2	0.45	0.10	7.9×10^{12}	7	1.14×10^{12}	10
A1-3	0.45	0.13	2.3×10^{13}	10.2	3.44×10^{13}	20.2
A1-4	0.45	0.13	7.9×10^{13}	35.1	1.13×10^{14}	55.3

Table 7. A1 Irradiation Experiment Summary (13 January 2005).

The final irradiation iteration on January 14th also followed the previously described procedure but involved electrons with energy of 0.8 MeV. A different energy level was used in order to determine if higher energy electrons would create any observable changes or alternate effects as compared to lower energy electrons.

A2 was used as the experimental sample during the final irradiations since it possessed similar device parameters compared to A1. Again, the procedure followed was the same as the previous day; however, sample A2 was initially subjected to 0.8 MeV electrons and a fluence of 3.5×10^{12} e^-/cm^2, *A2-1*. After a short irradiation, data measurements were made resulting in usable numbers. The experiment continued by disconnecting the measurement equipment, turning the VDG on, and irradiating the sample to 7.9×10^{12} e^-/cm^2, *A2-2*, or a fluence approximately two and a quarter times the initial fluence, yielding a total fluence of 1.14×10^{12} e^-/cm^2 corresponding to a little more than three and a quarter times the initial fluence. After the second irradiation, data measurements were made again resulting in usable data. A third irradiation of the sample to 2.3×10^{13} e^-/cm^2, *A2-3*, or a fluence six and a half times the initial fluence, yielding a total fluence of 1.0×10^{14} e^-/cm^2 also corresponding to ten times the initial fluence. After the third irradiation however, temperature control was lost during data collection due to a loss of pressure inside the liquid nitrogen tank. The tank started out full at the beginning

of the experiment and the gas pressure decreased during the experiment to a level that did not provide enough pressure to maintain the cold head at 80K. Measurements were made while the sample warmed to room temperature.

An extra tank with high pressure and very little liquid nitrogen was attached in series to the full tank in order to use the pressure to drive the full tank. This worked well for about 30 minutes, but during the attempted fourth irradiation the temperature dropped below 130K and continued to fall. At this point the experiment ended due to lack of temperature control of the sample mount.

Table 8 summarizes the sample, irradiation sequence number, irradiation energy used, beam current, fluence and total fluence specifics relating to the irradiation experiment of A2.

Sample & Seq. #	Energy (MeV)	Beam Current (μA)	Relative Fluence (e^-/cm^2)	Relative Irradiation Time (min)	Total Fluence (e^-/cm^2)	Total Irradiation Time (min)
A2-1	0.8	0.15	3.5×10^{12}	0.5	3.5×10^{12}	0.5
A2-2	0.8	0.30	7.9×10^{12}	1.2	1.14×10^{12}	1.7
A2-3	0.8	0.45	2.3×10^{13}	3.4	3.44×10^{13}	5.1

Table 8. A2 Irradiation Experiment Summary (14 January 2005).

Data collection at the WSU VDG facility terminated at 1400 hours on 14 January 2005. Anneal effect measurements continued at intervals of 24, 36, 48, 60, 72 and 84 hours at low and room temperatures.

V. Experimental Results

Irradiation Experiment: Sample A19

The first irradiation sequence, *A19-1*, was not successful in producing any usable post-irradiation C-V data at low temperature. The fact that measuring usable data was not likely was immediately recognized during irradiation since the beam current was 100 μA when calculations indicated that it should have been around 1 μA. Prior to taking data the device was identified as having failed and the subsequent attempt to measure capacitance corroborated this belief. The capacitance measured while at low temperature sent the Keithley 590 into compliance measurement indicating that the capacitance was extremely large.

Data obtained immediately after irradiation at room temperature resulted in a capacitance measurement, but not a recognizable characteristic C-V curve. Figure 40 below indicates an increase in capacitance in the low gate voltage region corresponding to the inversion region in a characteristic C-V curve followed by a drop in capacitance in the accumulation region. During and immediately after irradiation, device A19 failed to operate as designed.

Subsequent room temperature annealing for 60 hours and measurements at 80K and room temperature failed to exhibit any recovery in the device at all. This failure to recover is attributed to the damage caused by the extremely high initial beam current.

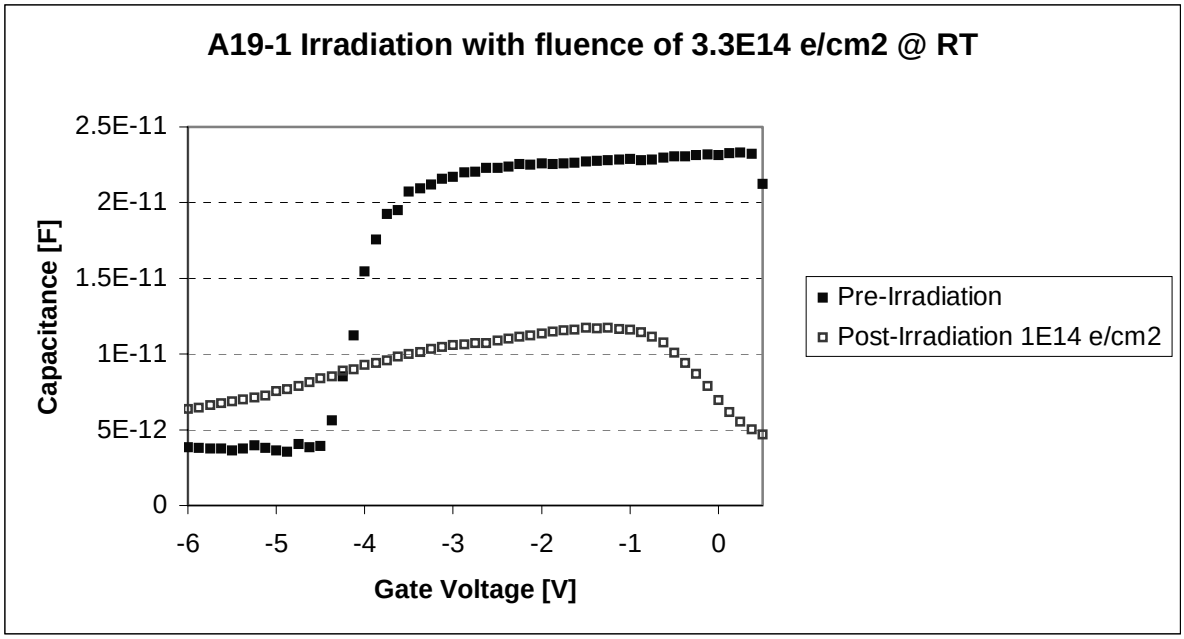

Figure 40. Pre- and Post-Irradiation capacitance-voltage measurements of A19 recorded at room temperature.

Irradiation Experiments: Sample A16

The second device, A16, produced results closer to expectation. Figure 41 shows the change in capacitance as a result of irradiation by 0.45 MeV electrons and a fluence of 3.3×10^{14} e^-/cm^2 in irradiation *A16-1*. The effects of this fluence are clearly seen as shift of the flat-band and threshold voltages to the negative indicating an increase in interface trapped charge. Also, a slight decrease in the capacitance is indicated in the depletion region corresponding to the GaN, while there is no apparent increase or decrease in the capacitance in the accumulation region relating to the AlGaN.

After the second irradiation, *A16-2*, at a total fluence of 9.9×10^{14} e^-/cm^2, the capacitance measurements recorded at 80K were extremely high (9.9×10^{30} F) and ultimately were unusable data. However in Figure 42, room temperature data recorded immediately after irradiation, resulted in a characteristic C-V curve indicating a slight

decrease in capacitance between the pre-irradiation and post-irradiation curve, and a recovery in device operation after a short room temperature anneal of approximately 5 minutes. The fact that the device failed to exhibit a characteristic C-V curve at low temperature is not surprising since device A0408 was initially reported as having failed after receiving a similar fluence [21] at a beam current that was an order of magnitude less than that experienced by *A16-2*.

After 60 hours of room temperature annealing Figure 41 shows and overall decrease in capacitance in all regions and a shift positive when compared with both pre- and post-irradiation data. After a total of 84 hours of room temperature annealing, the curve almost mirrors the initial pre-irradiation curve except for the slight negative threshold voltage shift.

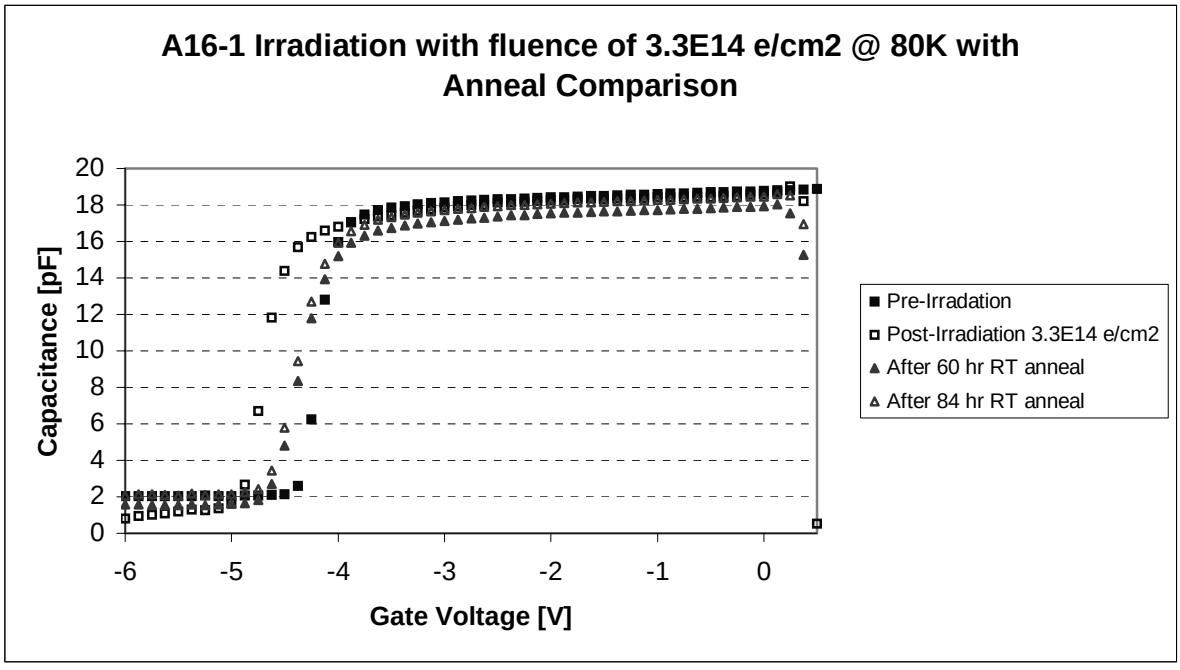

Figure 41. A16 Pre- and Post-Irradiation capacitance-voltage measurements recorded at low temperature (~80K) plotted with 60- & 84-hour room temperature anneal curves.

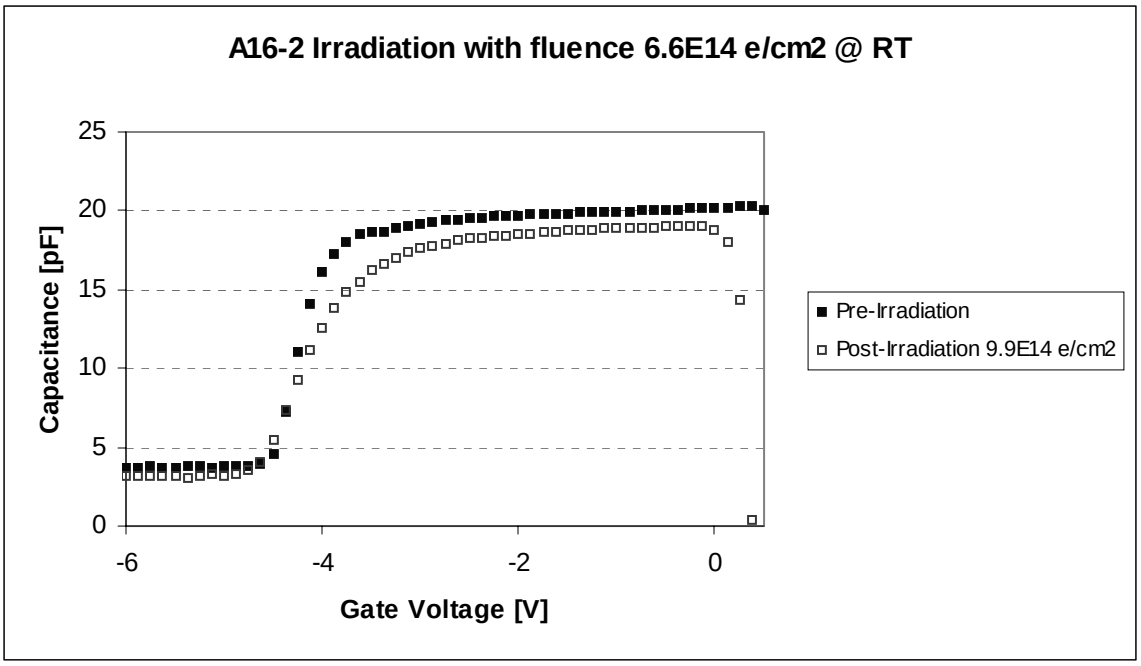

Figure 42. A16 Pre- and Post-Irradiation capacitance-voltage measurements at room temperature.

Irradiation Experiments: Sample A1

The third sample, A1, produced capacitance measurements exactly as expected during irradiation *A1-1*. Figure 43 below clearly shows an increase in the capacitance in the inversion region of the curve as well as in the accumulation region of the curve after experiencing a fluence of 3.5×10^{12} e^-/cm^2. The increase in capacitance in the inversion region yields an increase in the carrier concentration as presented in Figure 44. These concentrations were calculated using equation (21). Additionally, the curve shifts more negative and the threshold voltage decreases from a pre-irradiation –4.3V to a post-irradiation V_{TH} of –5.0V. This shift in threshold voltage is also an expected result.

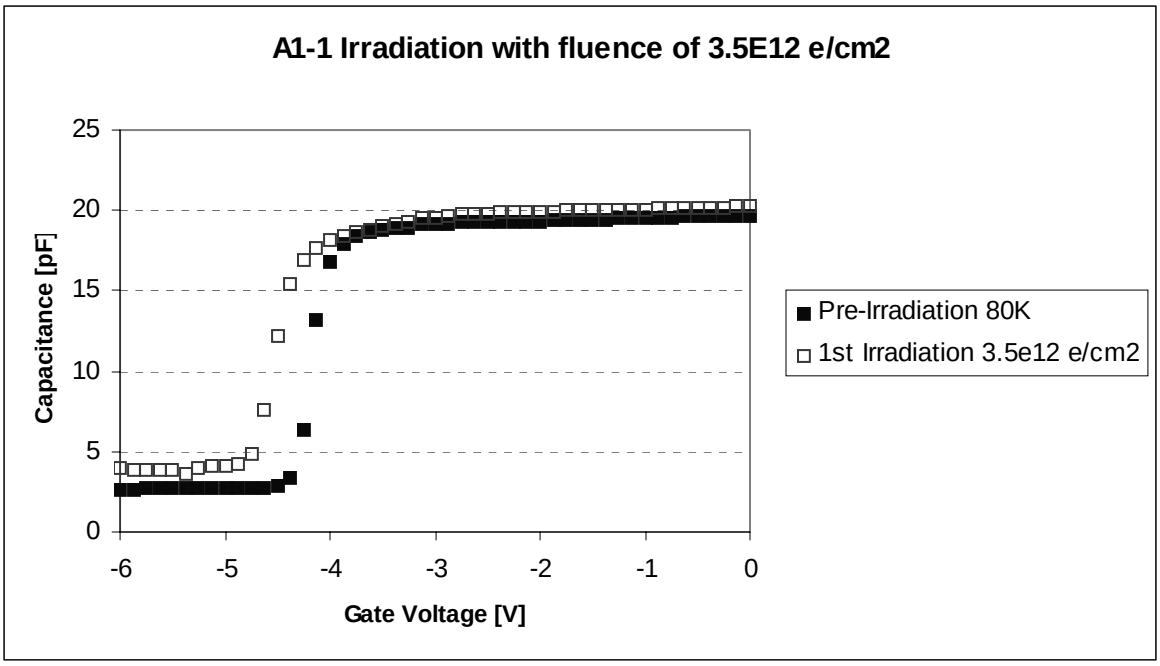

Figure 43. Pre- and Post-Irradiation capacitance-voltage measurements of device A1 recorded at low temperature (~80K) after a fluence of 3.5×10^{12} e/cm^2 with 0.45 MeV electrons.

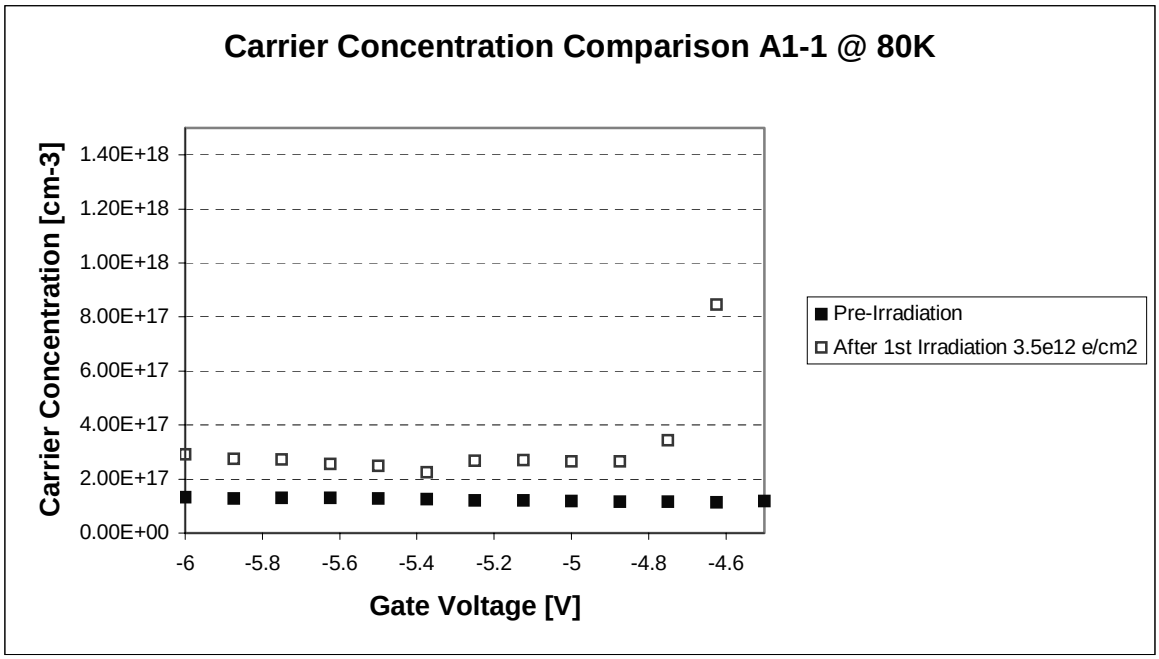

Figure 44. Pre- and Post-Irradiation carrier concentrations of device A1 recorded at low temperature (~80K) after a fluence of 3.5×10^{12} e/cm^2 with 0.45 MeV electrons.

The second data set, *A1-2*, measured after an additional fluence of 7.9×10^{12} e^-/cm^2 and a total fluence of 1.14×10^{12} e^-/cm^2 resulted in C-V curves for A1 that appeared to be very non-characteristic when plotted with characteristic curves. However, on a smaller scale the curves possess similar characteristics of the usual C-V curve, but there is a larger inversion region and very little if any accumulation region. During measurement, the capacitance did not converge around a specific value as all previous seven cycle measurements had before. The tendency was a slight creep of increasing capacitance during each subsequent cycle measurement. Figure 45 below graphically demonstrates the change in capacitance during cycle measurement.

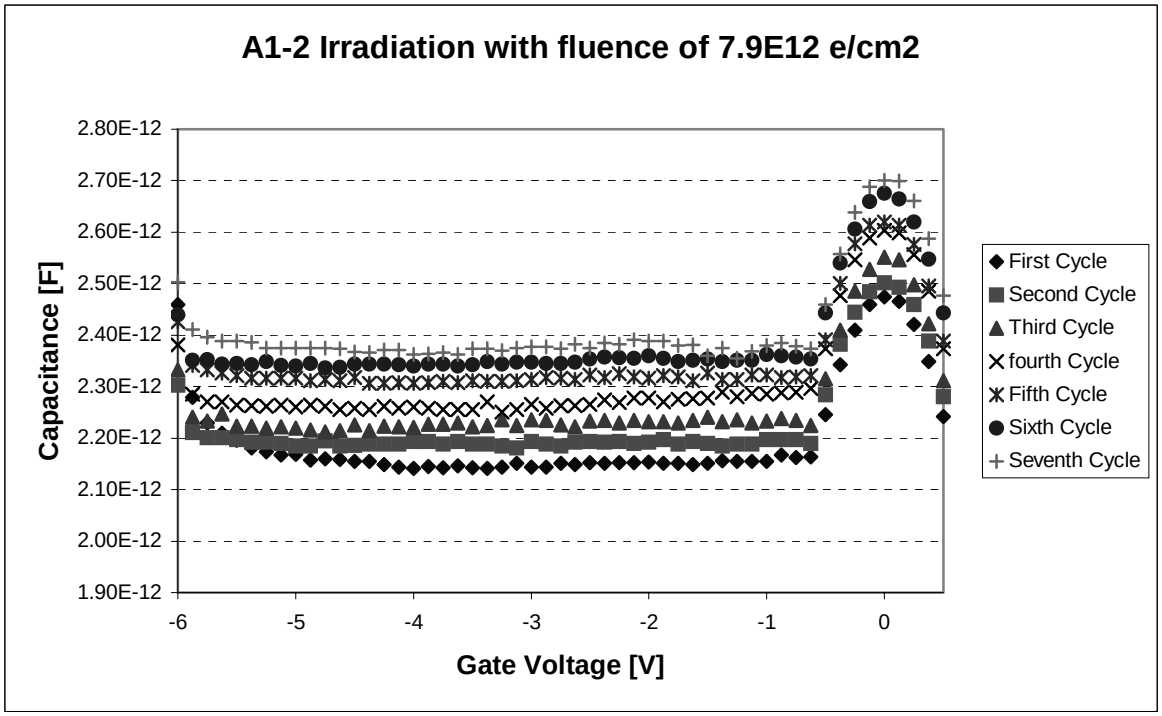

Figure 45. A1 Post-Irradiation capacitance-voltage measurements at low temperature (~80K) after a fluence of 7.9×10^{12} e/cm^2 with 0.45 MeV electrons.

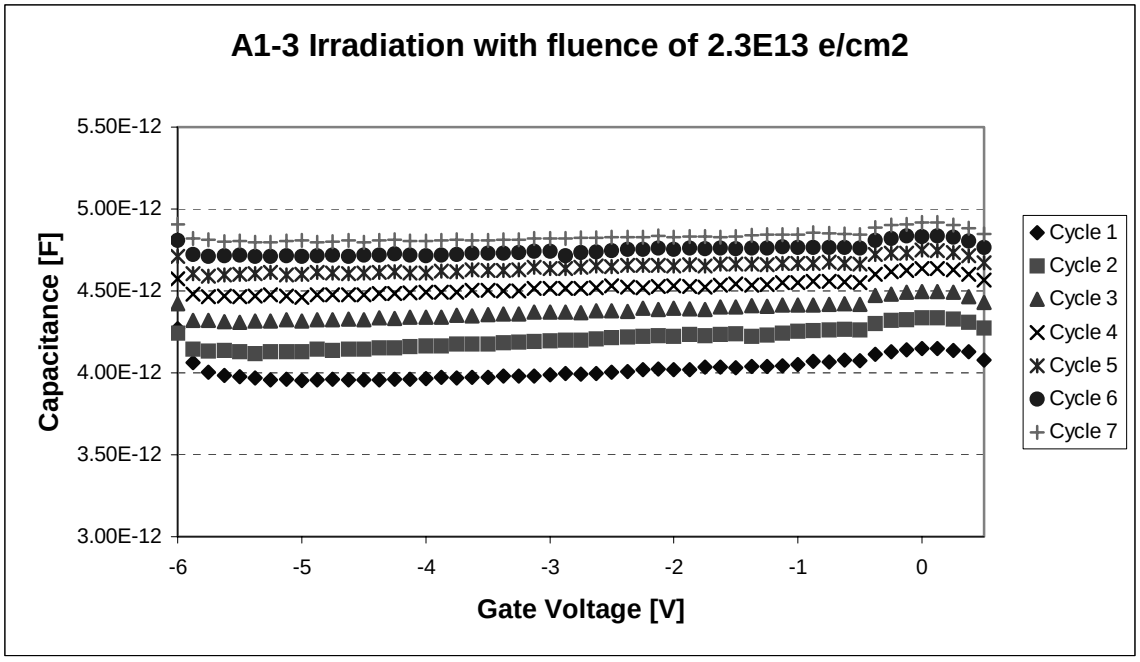

Figure 46. A1 Post-Irradiation capacitance-voltage measurements at low temperature (~80K) after a fluence of 2.3×10^{13} e/cm^2 with 0.45 MeV electrons.

The third data set, *A1-3*, measured after an additional fluence of 2.3×10^{13} e^-/cm^2 culminating in a total fluence of 3.44×10^{13} e^-/cm^2 appeared very similar to data obtained after the second irradiation. However, the capacitance measured was about twice that measured previously. Additionally, the increase around 0V in the second set is much less pronounced than in the third set producing a much more uniform curve as observed in Figure 46.

The fourth irradiation, *A1-4*, at a fluence of 7.9×10^{13} e^-/cm^2 resulted in a capacitance measurement that exceeded the Keithley 590 CV capabilities resulting in unusable numbers around 9.9×10^{30} F.

Figure 47 below compares all three irradiation iterations (*A1-1*, *A1-2*, and *A1-3*) that resulted in usable data and except for *A1-2* there is a definite increase in capacitance in the inversion region of the curve. *A1-2* and *A1-3* appear to indicate that the entire

device is operating as though it were in inversion from the gate through the GaN as there is no characteristic depletion or accumulation region.

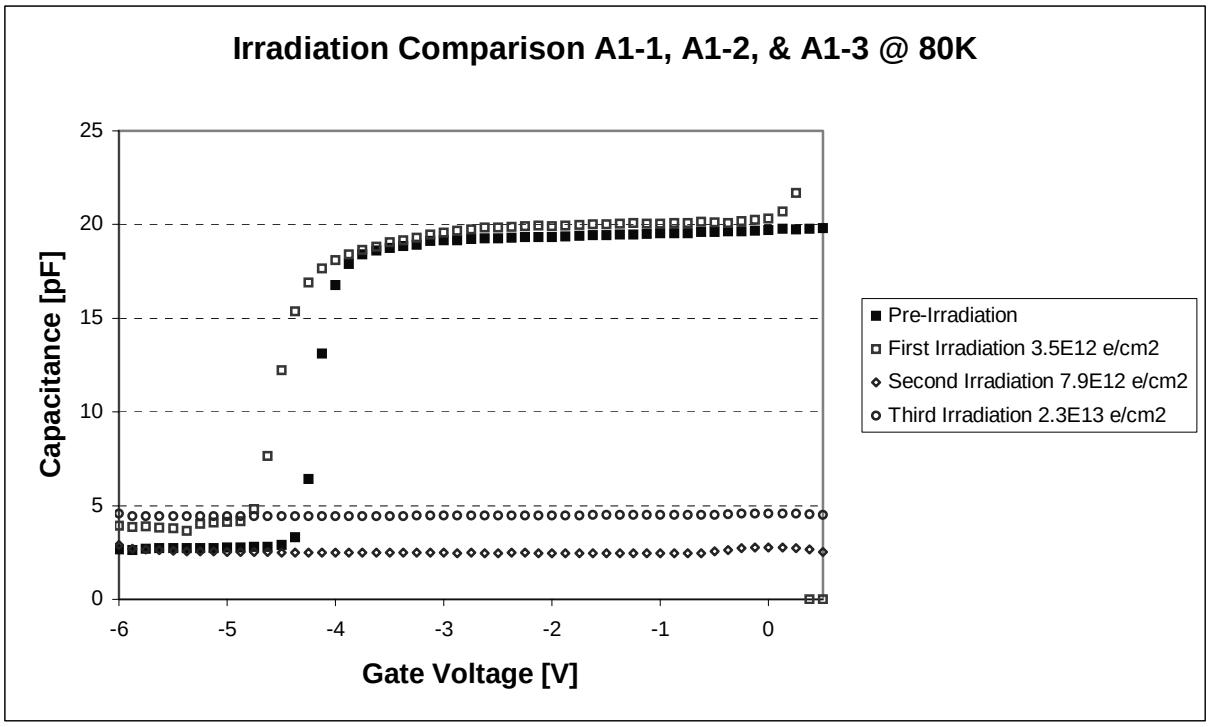

Figure 47. Comparison of Sample A1 Pre-Irradiation C-V data with subsequent irradiation C-V data at fluence levels of 3.5×10^{12} e/cm^2, 7.9×10^{12} e/cm^2 and 2.3×10^{13} e/cm^2 with 0.45 MeV electrons.

Using the data in Figure 47, the carrier concentrations for all irradiation iterations of sample A1 were calculated using equation (21). Figure 48 shows an increase in carrier concentration as a result of irradiation as the general trend. The second irradiation, *A1-2*, appears out of order and somewhat anomalous; however, the third irradiation, *A1-3*, indicates an increase in capacitance over all previous curves with respect to the inversion region.

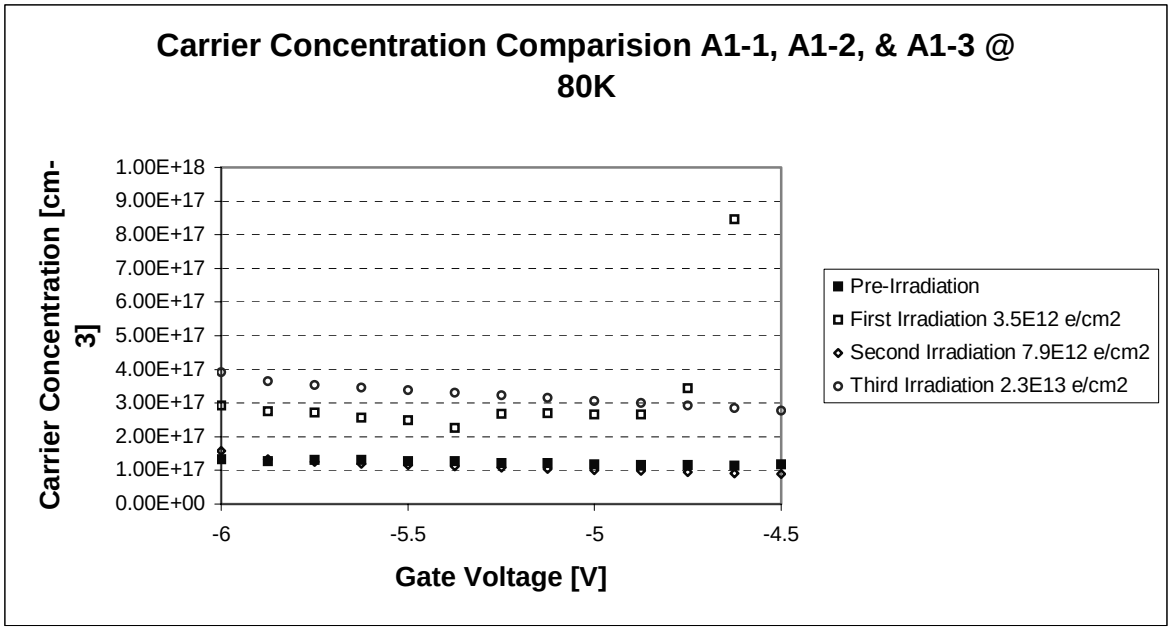

Figure 48. A1 Pre- and Post-Irradiation carrier concentrations at low temperature (~80K) after irradiation at fluence levels of 3.5×10^{12} e/cm^2, 7.9×10^{12} e/cm^2 and 2.3×10^{13} e/cm^2 with 0.45 MeV electrons.

The room temperature measurements recorded immediately after irradiation, again resulted in a characteristic C-V curve as they did for *A16-2*. Figure 49 shows that there is a clear increase in capacitance between the pre-irradiation and post-irradiation curve in the inversion region and a decrease in capacitance in the accumulation region. The measurement after a thirty-six-hour room temperature anneal also clearly shows an increase in capacitance over pre-irradiation values and post-irradiation levels. Although the post-irradiation capacitance in the accumulation region is less than that measured pre-irradiation, the measurements after a thirty-six hour anneal have increased with respect to the measurements recorded immediately after irradiation at room temperature. Charge appears to be increasing over time in the accumulation region as the device remains at room temperature.

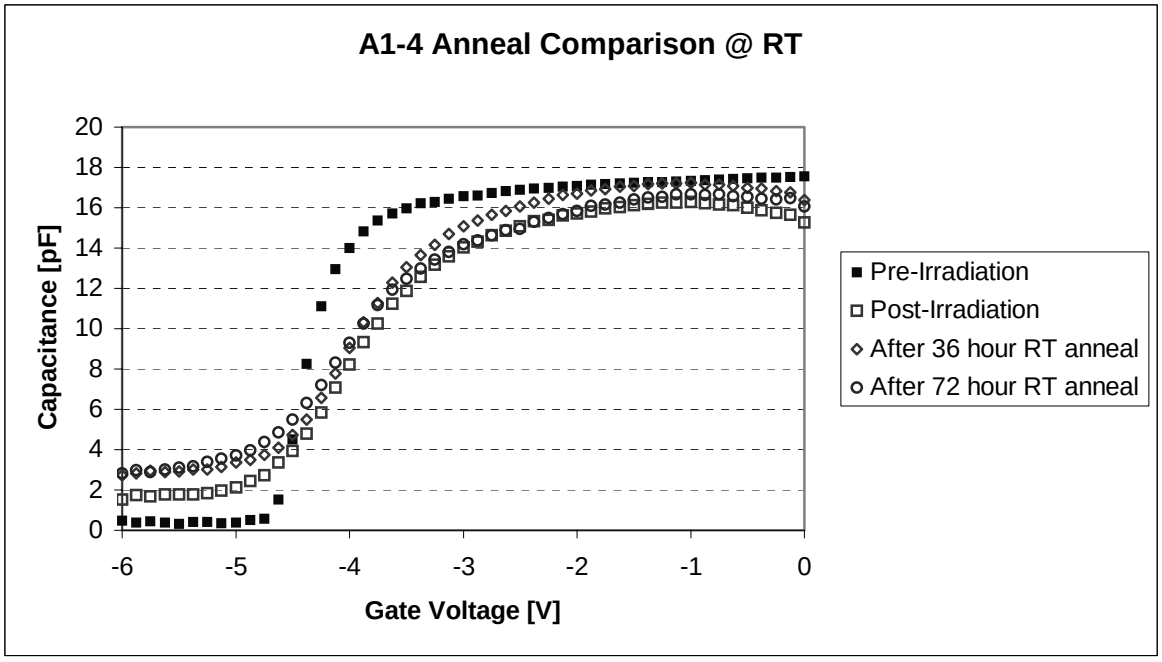

Figure 49. A1 Pre- and Post-Irradiation capacitance-voltage measurements at room temperature after a total fluence of 1.13×10^{14} e/cm^2 and compared with the 36 and 72-hour room temperature anneal curve.

After 48 hours of room temperature annealing, Figure 50 shows that the capacitance level in the inversion region has returned to pre-irradiation levels, while the curve has dropped below pre-irradiation levels in the accumulation region. There is also a slight decrease in slope in depletion indicating trapped interface charge. There are definite permanent changes due to irradiation that anneal somewhat but not completely.

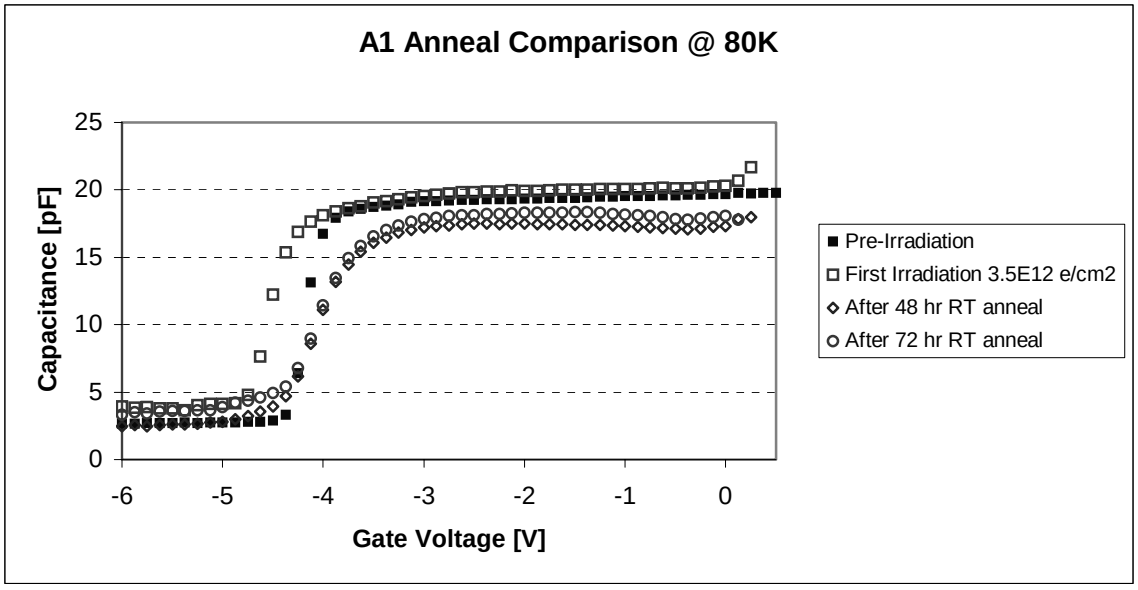

Figure 50. A1 Pre- and Post-Irradiation capacitance-voltage measurements at low temperature after a total fluence of 1.13×10^{14} e/cm^2 compared with the 48 and 72-hour room temperature anneal curves.

In Figure 51 the carrier concentration is plotted using information from the inversion region in the curves in Figure 50 and yields a 2-3 times increase in carrier concentration when measured at room temperature.

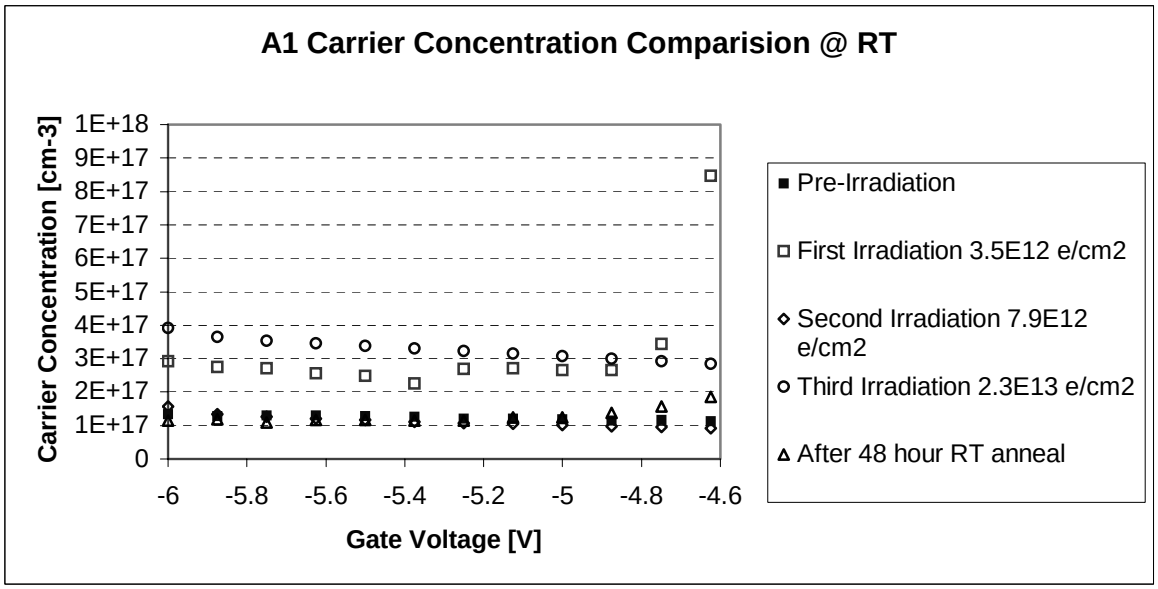

Figure 51. A1 Pre- and Post-Irradiation carrier concentrations at room temperature with carrier concentration of 48-hour room temperature anneal data.

Irradiation Experiments: Sample A2

Sample A2 produced capacitance in total contrast to any recorded previously either at room or low temperature, and whether or not the device had been irradiated. Iteration *A2-1* irradiated sample A2 with 0.8 MeV electrons and a fluence of 3.5×10^{12} e^-/cm^2. The procedure followed was the same as in the previous iterations and measurements were recorded in the same manner at low temperature. However, during the initial sweep of -1V to 0V that had previously been used to clear extraneous charge from initial measurements of other devices, the Keithley 590 recorded capacitance values within the measurement capabilities of the analyzer immediately. The interesting part about the capacitance measurements of *A2-1* was that instead of positive capacitance in the pF range, this time the capacitance measured was in the negative pF range. While continuing to take measurements, a rapid check of the lead connections ensured that the device was properly connected and not grounded to any extraneous connection around the beam tube. Figure 52 clearly shows a negative capacitance measurement after *A2-1* and Figure 53 shows the first measurement compared with the pre-irradiation data highlighting the negative capacitance measurements. These negative values for capacitance indicate that the analyzer is measuring the capacitance of something with an opposite charge to that measured in the previous heterostructures.

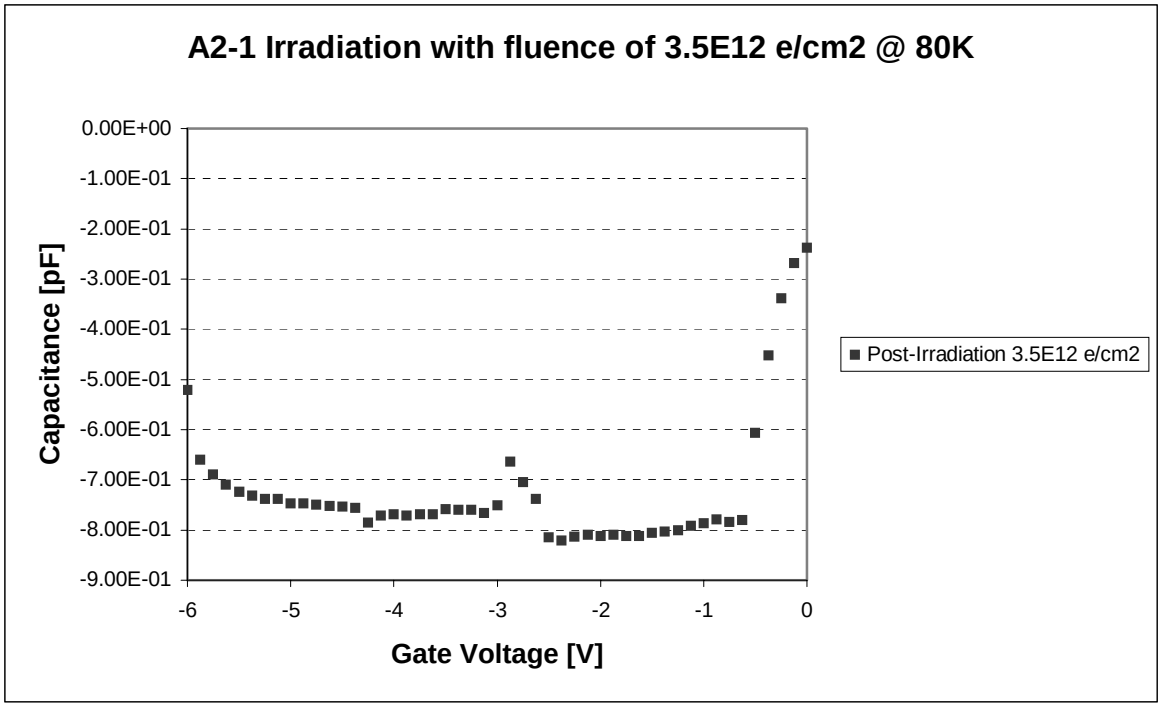

Figure 52. A2 Post-Irradiation capacitance-voltage measurements at low temperature (~80K) after a fluence of 3.5×10^{12} e/cm^2 with 0.8 MeV electrons.

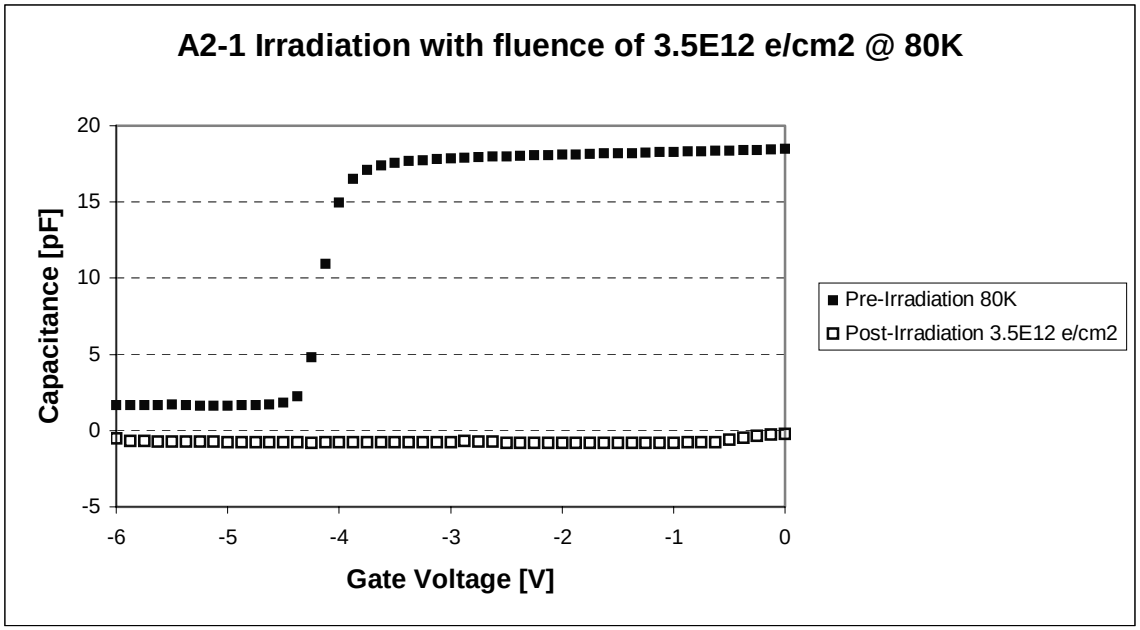

Figure 53. A2 Pre- and Post-Irradiation capacitance-voltage measurements at low temperature (~80K) after a fluence of 3.5×10^{12} e/cm^2 with 0.8 MeV electrons.

The second seven-cycle measurement, *A2-2*, produced the same negative capacitance effect although the values were slightly more positive than the first measurements.

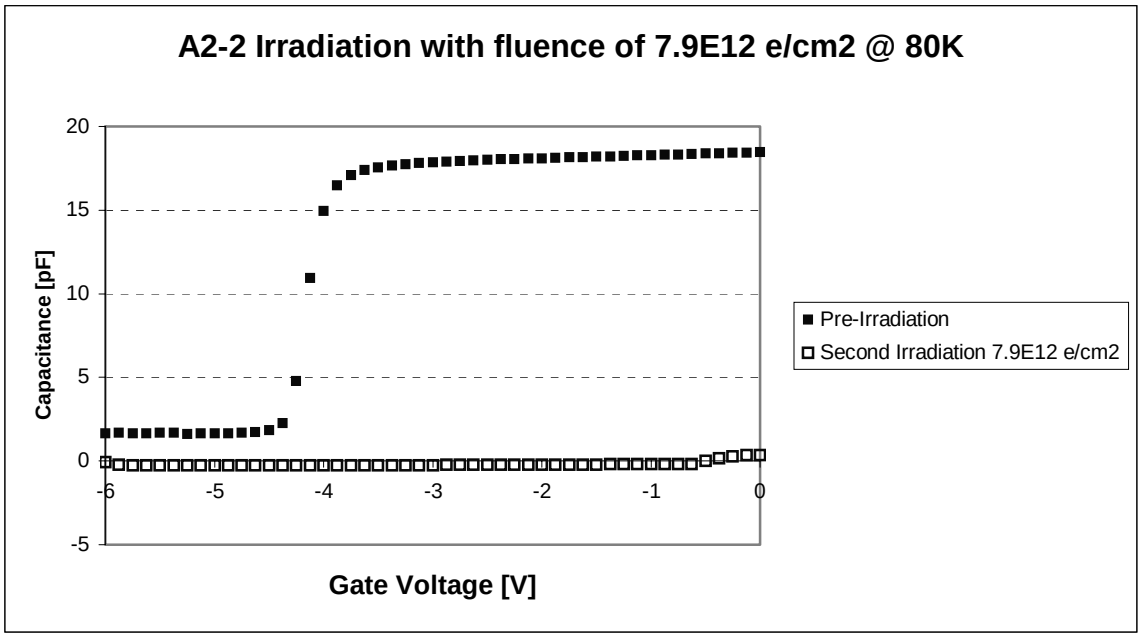

Figure 54. A2 Pre- and Post-Irradiation capacitance-voltage measurements at low temperature (~80K) after a fluence of 7.9×10^{12} e/cm^2 with 0.8 MeV electrons.

The third measurement set, *A2-3*, depicted in Figure 55 was interrupted by a loss of temperature control; however, during the slow rise in temperature from 80K to 192K capacitance measurements continued. The measurements showed a general trend of increasing negative capacitance in each subsequent cycle as the temperature increased. Figure 56 highlights the change between pre-irradiation capacitance levels and the capacitance after the third irradiation, *A2-3*, at 2.3×10^{13} e^-/cm^2. Although, the loss in temperature control makes the interpretation and comparison of the third set of data with previous sets difficult and inconclusive in isolation (Figure 57), the important fact is that the capacitance of the third set was negative just as the previous two data sets were

(Figure 58). The negative capacitance indicates that charges of opposite polarity are measured due to electron irradiation by electrons with incident energy of 0.8 MeVs.

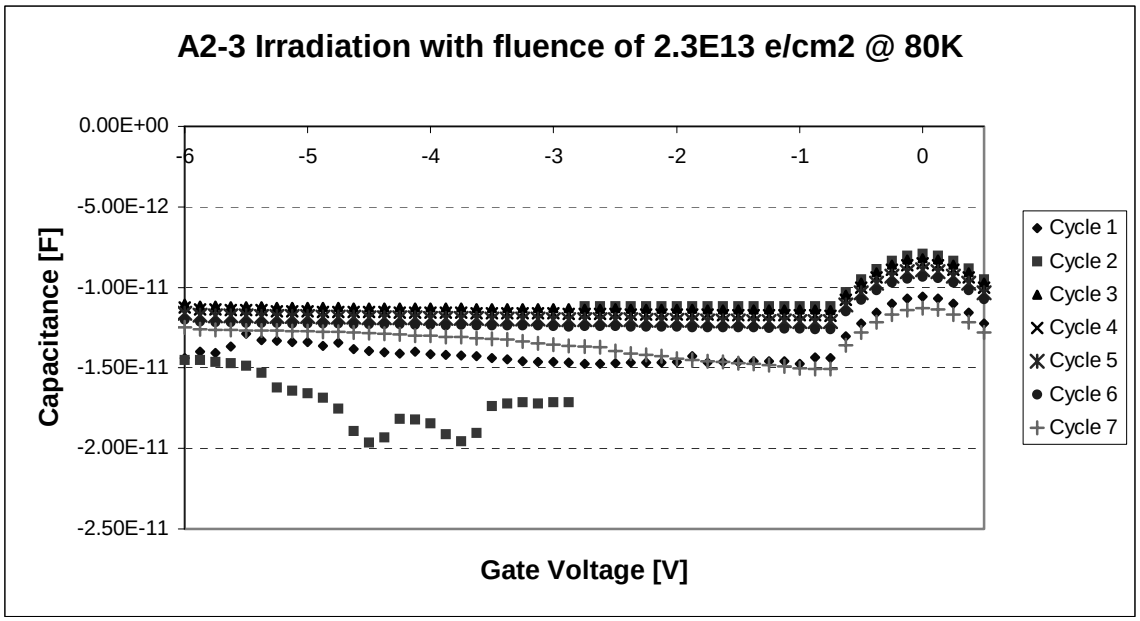

Figure 55. A2 Post-Irradiation capacitance-voltage at low temperature (~80K) after a fluence of 2.3×10^{13} e/cm^2 with 0.8 MeV electrons.

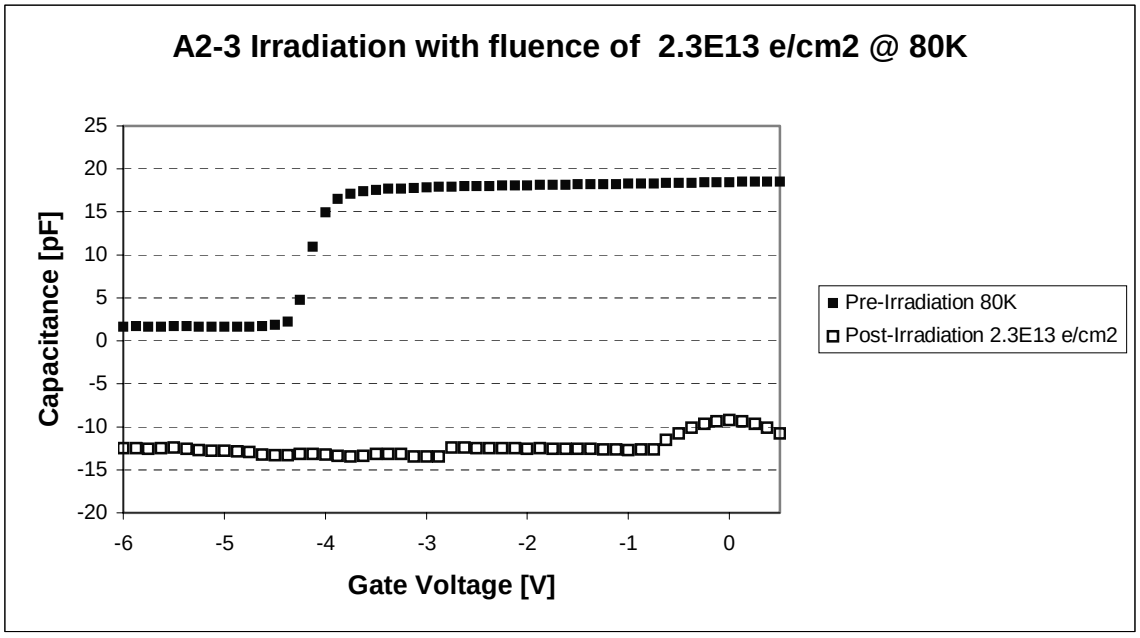

Figure 56. A2 Pre- and Post-Irradiation capacitance-voltage measurements at low temperature (~80K) after a fluence of 2.3×10^{13} e/cm^2 with 0.8 MeV electrons.

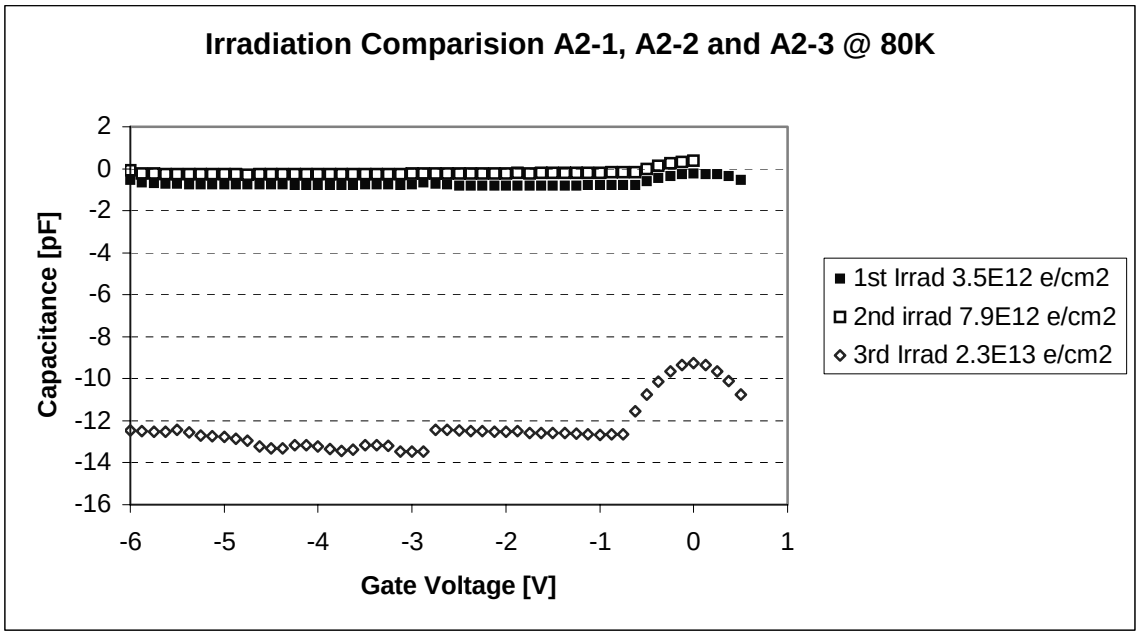

Figure 57. Comparison of irradiation C-V data at fluence levels of 3.5×10^{12} e/cm^2, 7.9×10^{12} e/cm^2 and 2.3×10^{13} e/cm^2 with 0.8 MeV electrons.

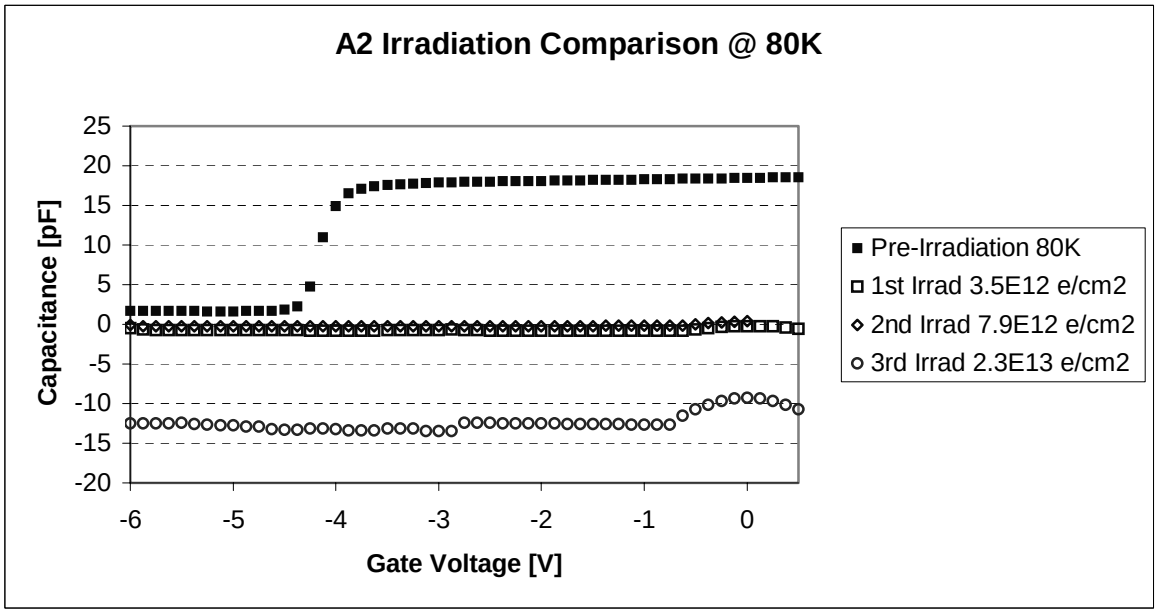

Figure 58. Comparison of Pre-Irradiation C-V data with subsequent irradiation C-V data at fluence levels of 3.5×10^{12} e/cm^2, 7.9×10^{12} e/cm^2 and 2.3×10^{13} e/cm^2 with 0.8 MeV electrons showing negative increase in capacitance.

The room temperature measurements for device A2 recorded immediately after irradiation, *A2-3*, again resulted in a characteristic C-V curve (Figure 59) as did *A16*-2 and *A1*-4; however, the capacitance measurements continued to increase negatively as the anneal process progresses. There is a slight decrease in capacitance between the pre-irradiation and 24 hour anneal curve in the inversion region and a slight increase in capacitance in the accumulation region with an apparent no change in depletion.

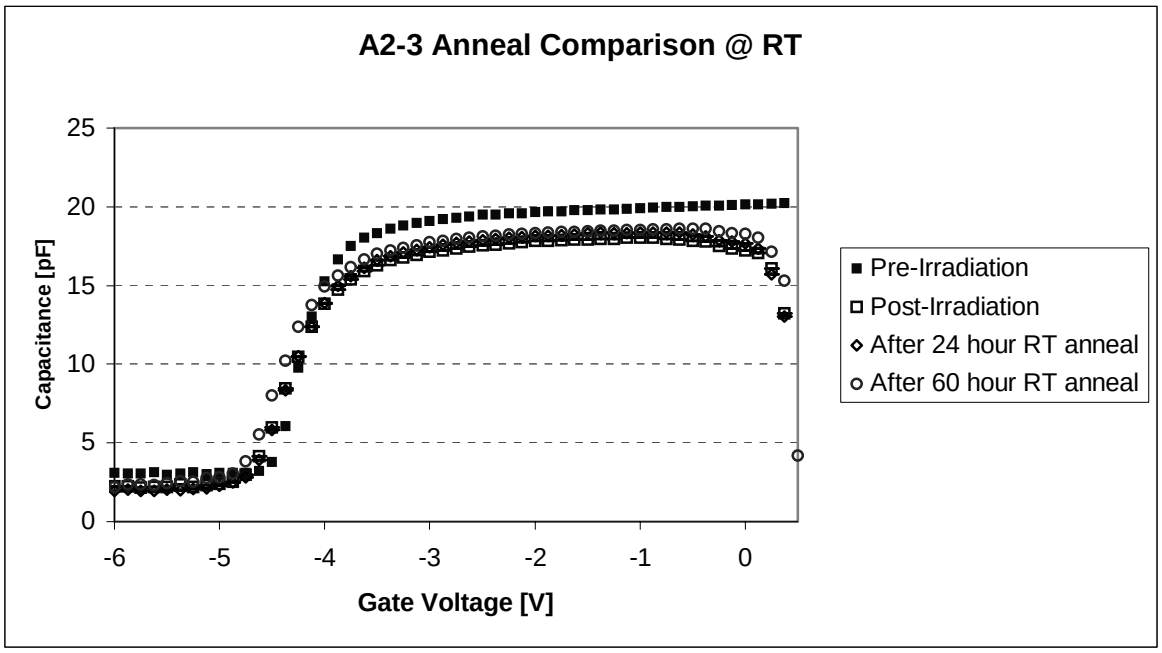

Figure 59. A2 Pre- and Post-Irradiation capacitance-voltage measurements at room temperature after a total fluence of 1.14×10^{14} e/cm^2 and compared with the 24 & 60 hour room temperature anneal curves.

The 36 and 60 hour anneal measurements at 80K revealed a characteristic C-V curve in Figure 60 with positive capacitance values indicating that the major damage due to 0.8 MeV electrons annealed after exposure to room temperature. Both anneal curves show a shift in the negative direction with a more negative threshold voltage of –5V compared to a pre-irradiation V_{TH} of –4.3V. There is also a recovery toward the pre-

irradiation curve in all regions in both anneal curves except for the threshold voltage shift. In this manner, the damage due to a fluence of 1.14×10^{14} e^-/cm^2 is permanent.

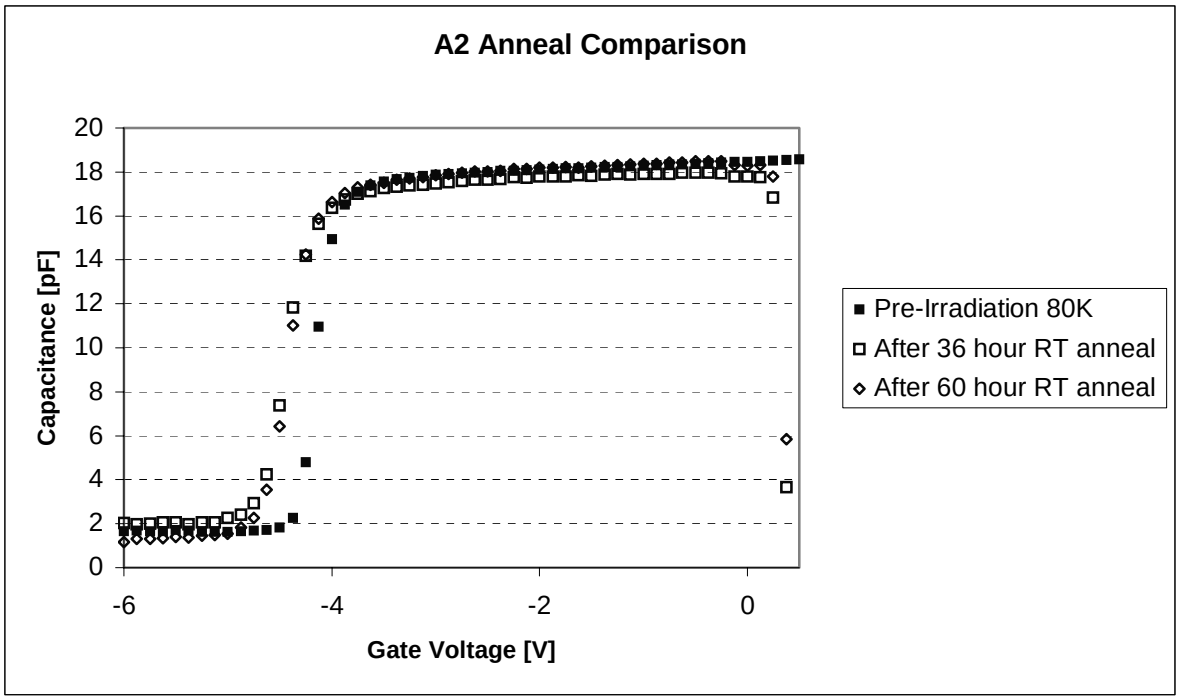

Figure 60. A2 Pre-Irradiation capacitance-voltage measurement at low temperature after a total fluence of 1.14×10^{14} e/cm^2 compared with the 36 and 60 hour room temperature anneal curves.

Previously Irradiated Samples: A0408 and A0409

During the eight-week maintenance period of the WSU VDG irradiation of samples was not possible. In light of this, the two surviving samples (A0408 and A0409) irradiated on 28 January 2004 by [21] have been analyzed with respect to the effects of low energy electron irradiation as well as room temperature annealing effects after 9 months in order to attempt to explain the observations in previous research [21].

The 9 new samples were pre-characterized and measured by the Keithley 590 C-V analyzer in order to produce capacitance versus gate voltage curves for analysis. Each

transistor was measured for capacitance at low temperature (80K) with an applied gate voltage from –6 V to 0.5 V in increments of 0.125 V. This interval comprised one cycle. A total of seven cycles were taken for each device.

Figure 61 shows the pre- and post-irradiation C-V curves for Sample A0408. This sample was given a total fluence of 9×10^{14} e^-/cm^2 after three separate irradiations, and clearly shows an increase in capacitance in the inversion region and a slight if not negligible increase in capacitance in the accumulation region. Using equation (21), the carrier concentration was calculated for A0408 both pre- and post-irradiation. The results of these calculations are presented in Table 9 and show that the carrier concentration increased approximately two orders of magnitude after a total fluence of 9×10^{14} e^-/cm^2. Figure 62 graphically shows the carrier concentration increase after total fluence. A two orders of magnitude increase is clearly evident in the inversion region.

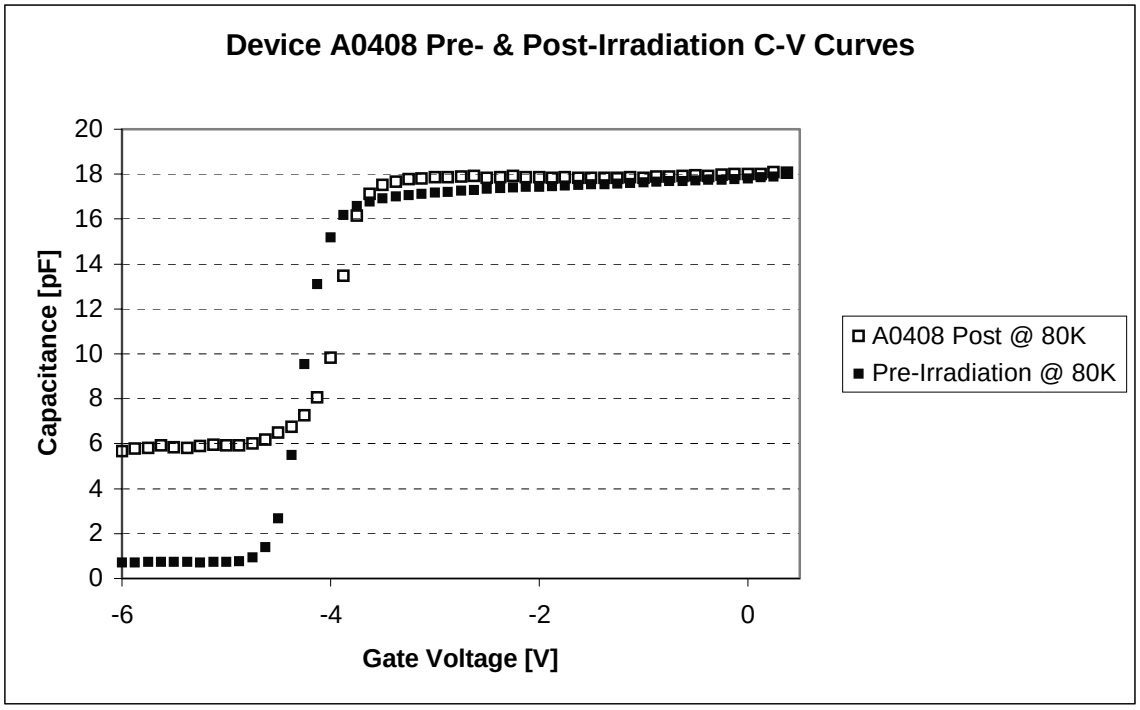

Figure 61. Sample A0408 Pre- and Post-Irradiation C-V curve (0.45 MeV electrons)

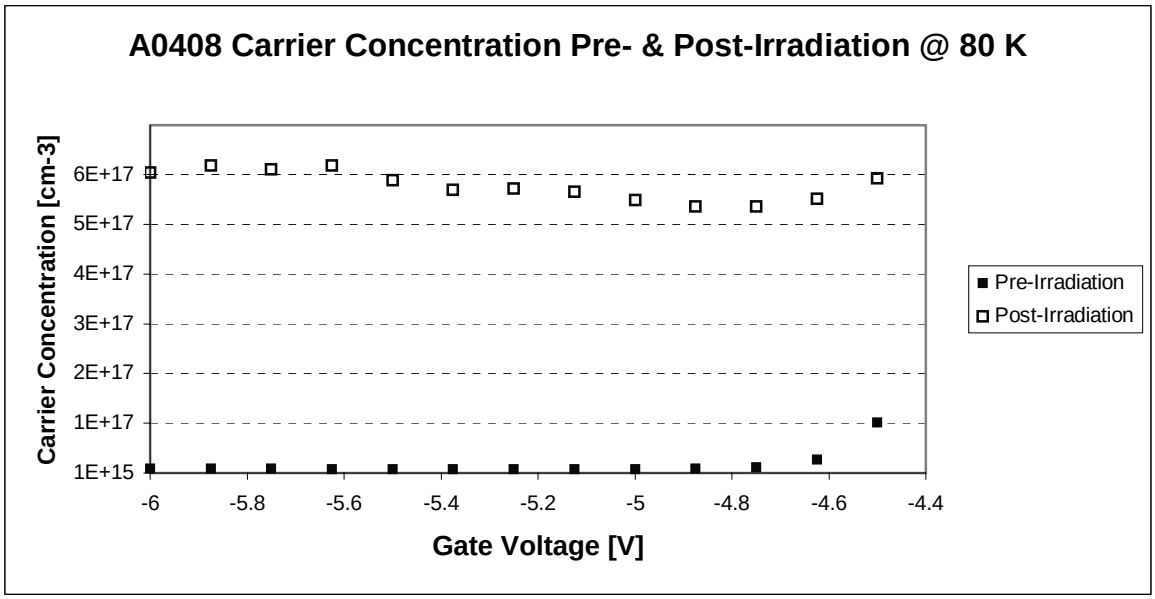

Figure 62. Sample A0408 Pre- and Post-Irradiation Carrier Concentration

Figure 62 shows the pre- and post-irradiation C-V curves for Sample A0409. This sample was given a total fluence of 3.67×10^{15} e^-/cm^2 after a total of four irradiations, and clearly shows a large increase in capacitance in the inversion region and a smaller increase in capacitance in the accumulation region. Using equation (21), the carrier concentration was calculated for A0409 both pre- and post-irradiation. The results of these calculations are presented in Table 9 and show that the carrier concentration increased three orders of magnitude after a total fluence of 3.67×10^{15} e^-/cm^2. Figure 64 graphically shows the carrier concentration increase after total fluence. A three orders of magnitude increase is clearly evident in the inversion region. The slope of the post-irradiation curve in the depletion region is also flatter than the pre-irradiation curve indicating trapped charge at the interface.

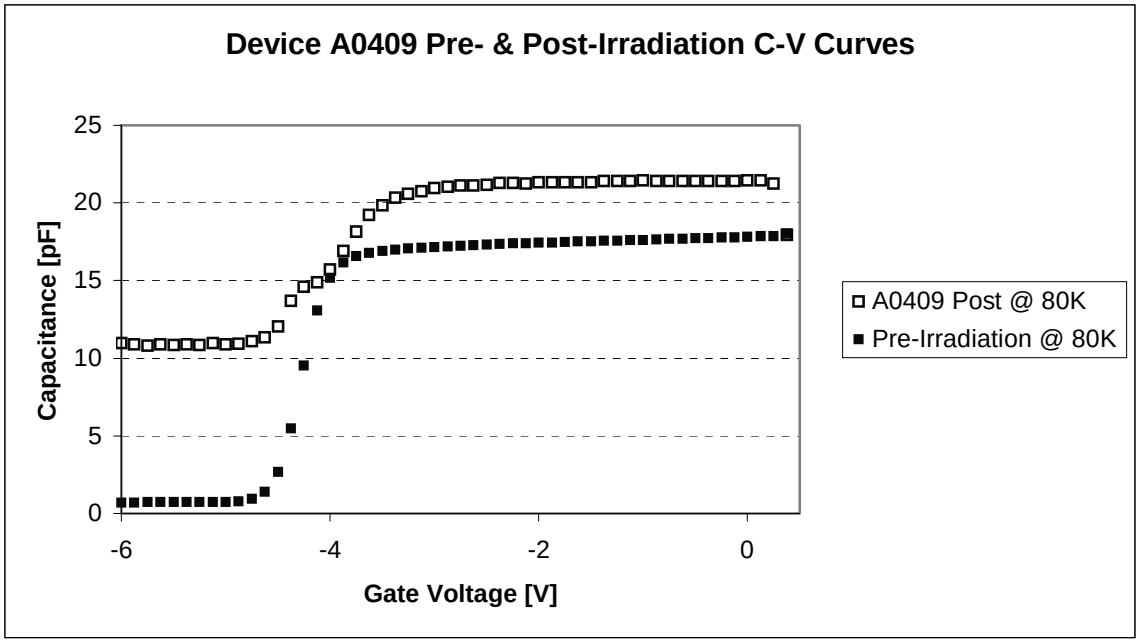

Figure 63. Sample A0409 Pre- and Post-Irradiation C-V curve (0.45 MeV electrons)

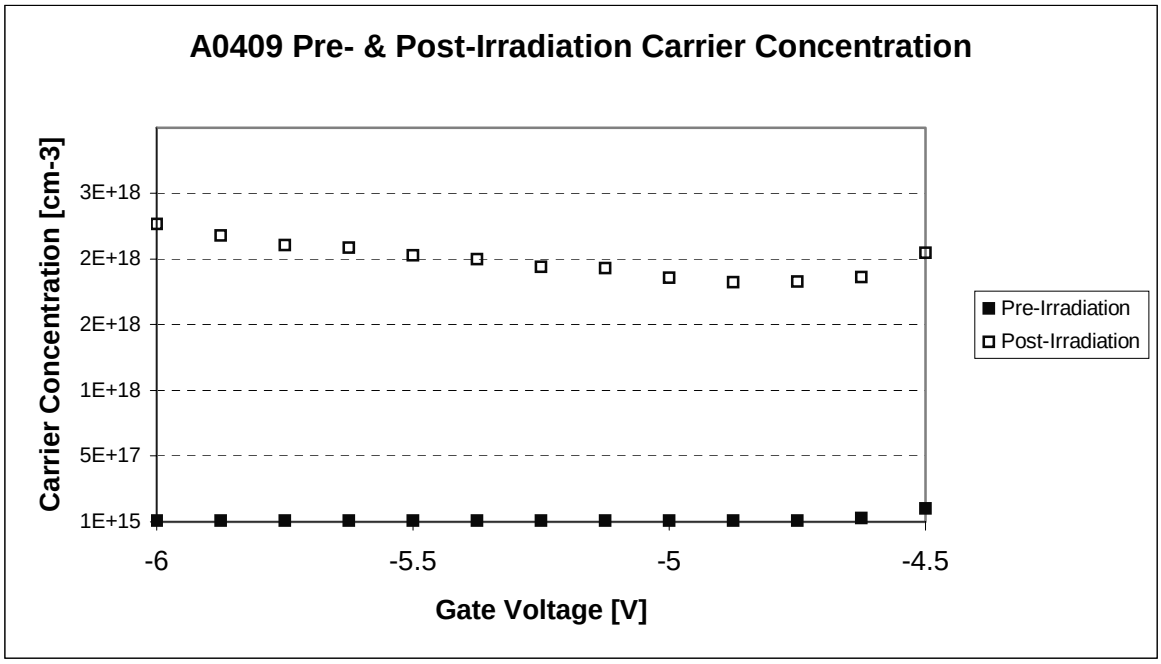

Figure 64. Sample A0409 Pre- and Post-Irradiation Carrier Concentration

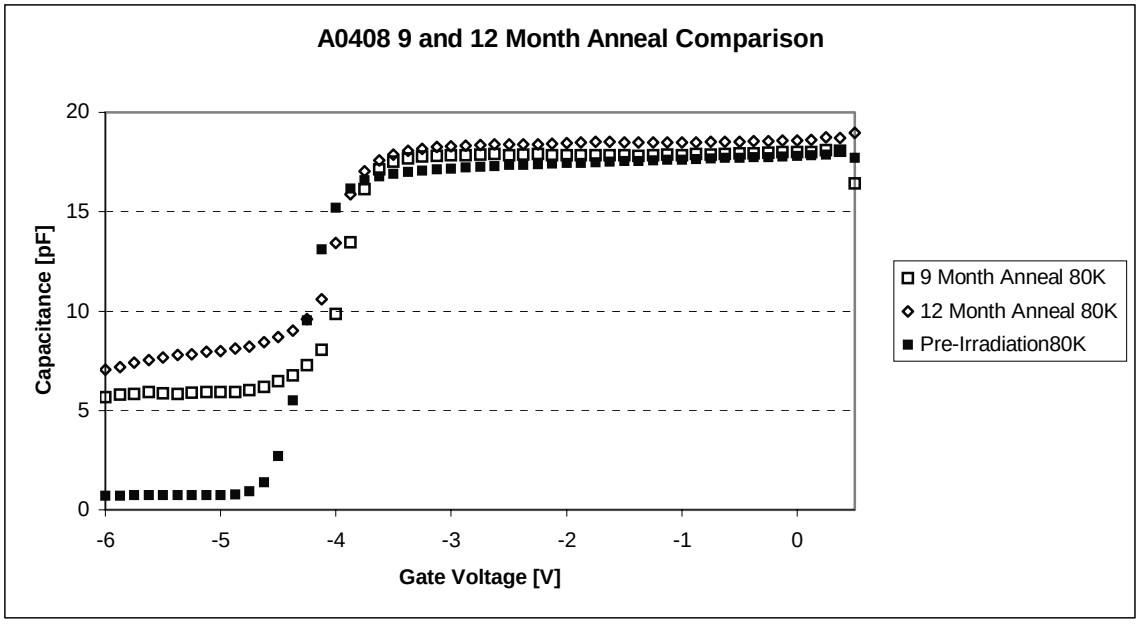

Figure 65: Comparison of CV curves for A0408 after a nine and twelve-month room temperature anneal measured at 80K.

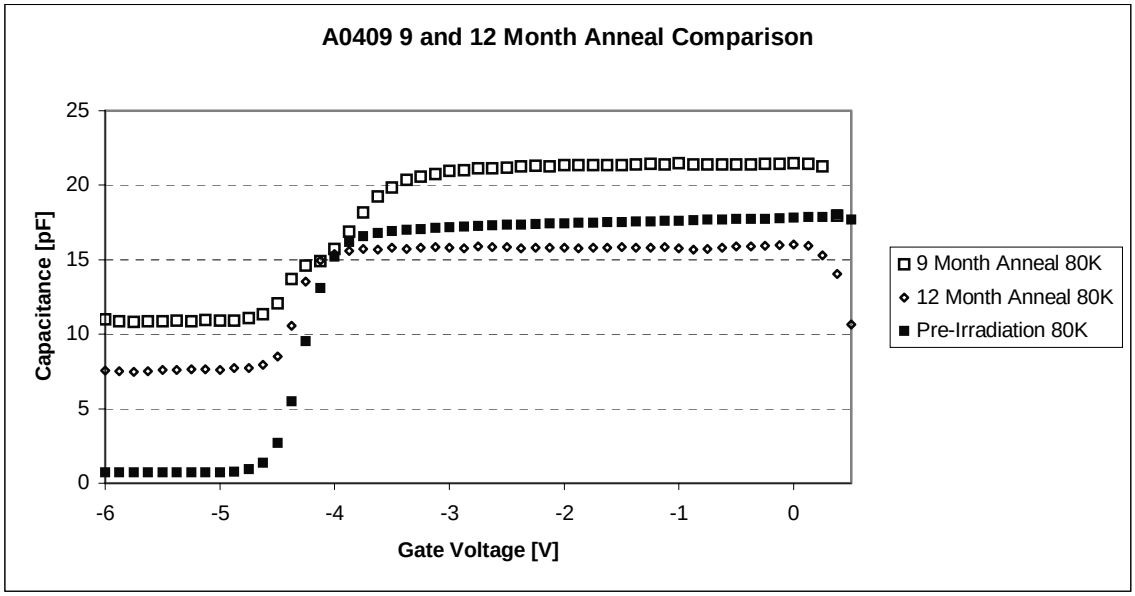

Figure 66: Comparison of CV curves for A0409 after a nine and twelve-month room temperature anneal measured at 80K.

As initially stated, device A0408 and A0409 annealed at room temperature conditions from the 28th of January 2003 until the 22nd of October 2004 when the first

capacitance-voltage measurements were conducted. The elapsed time was just under nine months. The expectation is that any of these devices left to anneal at room temperature would respond in a similar manner taking into account the incident electron energy and the total fluence experienced.

On the 16th of December 2004, twelve months after irradiation a second set of capacitance-voltage measurements were recorded in order to observe the effects of a 12-month room temperature anneal. Again, as with the previous measurements of A0408 and A0409, the results of both devices were different. As Figure 65 shows the capacitance increases in all regions of the curve for A0408 with a negative threshold voltage shift back toward the pre-irradiation curve. This would apparently show that hole traps in the AlGaN layer are increasing rather than annealing away. A0409 in Figure 66 shows a decrease in all areas of the curve with respect to the nine-month anneal curve and the accumulation region of the pre-irradiation curve. This demonstrates that the hole traps are annealing due to tunneling to a point that below that of the pre-irradiation capacitance level. A positive threshold voltage shift is noted in A0409 toward pre-irradiation levels that are consistent with the observations in A0408 in that both V_{TH} tend back toward the pre-irradiation V_{TH}. The fact that the accumulation region over annealed past the pre-irradiation capacitance for A0409 may be attributed to the fact that the pre-irradiation curve is an average of nine non-irradiated devices and may not reflect the exact nature of the pre-irradiation capacitance of A0409.

The results of A0408 and A0409 are consistent with the annealing of A1 and A2 in that A1 and A2 also over annealed and then showed a trend back to pre-irradiation levels.

Analysis and Discussion

In previous research [21], an unexplained result of irradiation was a large increase in drain current. At the time, the C-V measurements required to explain these results were unavailable. However, this research has conducted the required measurements needed to explain the phenomenon.

Using Equation (20) as the mathematical model that describes the drain current, I_{DS} is directly related to four variables: the charge of an electron, the width of the gate, the electron mean velocity in the channel, and the channel sheet charge density. Since both the charge of an electron and the gate width are constants, this indicates that any change in drain current must be caused by either a change in the channel sheet charge density (the 2DEG carrier concentration) or a change in the electron mean velocity in the channel. Capacitance measurements from experiment were used to calculate the carrier concentration before irradiation and after irradiation by electrons. The increase in capacitance resulted in an increase in carrier concentration indicating that the drain current increase was caused by a direct increase in carrier concentration in the 2DEG.

Device ID	Voltage [V]	Capacitance [F] *Pre-Irradiation*	Carrier Concentration [cm^{-3}] *Pre-Irradiation*	Capacitance [F] *Post-Irradiation*	Carrier Concentration [cm^{-3}] *Post-Irradiation*	Order Magnitude Of Change [cm^{-3}]
A0408	-5	7.375×10^{-13}	8.52×10^{15}	5.922×10^{-12}	5.49×10^{17}	*2*
A0409	-5	7.375×10^{-13}	8.52×10^{15}	1.089×10^{-11}	1.86×10^{18}	*3*
A16	-5	2.04×10^{-12}	6.53×10^{16}	1.66×10^{-12}	4.32×10^{16}	*0*
A1	-5	2.75×10^{-12}	1.19×10^{17}	4.11×10^{-12}	2.66×10^{17}	*0*

Table 9: Comparison of device Pre- And Post-Irradiation Carrier Concentration.

In three of the four devices observed during this research effort, the major effect was an increase in the capacitance in the inversion region after irradiation by 0.45 MeV electrons. Table 9 shows the effects of this level of irradiation in the carrier concentration of the 2DEG as calculated by equation (22).

The carrier concentration increase is caused by either an increase in positive charge in the AlGaN layer and/or an increase in donor electrons from a nitrogen vacancy in the gallium nitride.

The first explanation for the drain current increase is based on trapped charge in the AlGaN layer. The AlGaN layer is extremely thin at 25 nm and as such any charge trapped in the AlGaN layer would have an enormous effect on the electric field acting upon charge carriers in the GaN layer. Essentially, any trapped charge would appear to increase the gate voltage with respect to the charge carriers in the GaN. The result of an increase in gate charge would be an increase in negative charge drawn up from the GaN toward the interface to match the positive charge trapped in the AlGaN. This increase in equal but opposite charge would appear as more charge on a parallel plate capacitor resulting in increased capacitance in the accumulation region of the C-V curves. This is in fact what is observed in samples A0408, A0409 and A1.

Electron radiation interacting with atoms in the AlGaN layer ionizes a large amount of electrons. The massive amounts of ionization involved with this are supported by the fact that collisional stopping power, which causes ionization and excitation, accounts for the overwhelming majority of energy deposited in AlGaN [21]. The large amounts of ionization involved are produced by relatively low fluences (10^{13} e^-/cm^2 to 10^{14} e^-/cm^2). These ionized electrons are temporarily trapped in energy states near the

conduction band of AlGaN. However, due to the application of a high electric field through the gate voltage or the intrinsic electric field associated with the highly polarized AlGaN heterostructure, these trapped electrons are immediately made mobile and swept out of the AlGaN. In the first case, a positive applied gate voltage and the intrinsic electric field draw the electrons to the gate whereas a negative gate voltage pushes the electrons toward the GaN. The latter case results in negative charge collection at the AlGaN/GaN heterointerface, which would then be added into the 2DEG.

In any event, this process results in the removal of numerous electrons from the AlGaN layer, leaving behind a net stationary positive charge. This new stationary positive charge would add to the overall net positive charge in the AlGaN layer (created by polarization fields) resulting in an increase in the electric field seen by the potential 2DEG carriers in the GaN layer. The increased electric field (directed into the GaN layer) would draw an increased number of mobile electrons out of the GaN layer and deposit them into the 2DEG, yielding higher 2DEG carrier concentrations. As previously indicated, this proposed process essentially involves the creation of a virtual gate voltage similar to the threshold voltage shifting effect that occurs in electron irradiated MOSFETs and which is observed Figure 50 and Figure 60.

The second explanation for an increase in the carrier concentration in the 2DEG is through the formation of nitrogen vacancies that donate electrons to the GaN that are deposited into the 2DEG. The nitrogen vacancy has been proposed by numerous sources [18] [19] [27] as the impurity responsible for the *n*-type self-doping of gallium nitride and major contributor to the 2DEG.

This experiment measured the capacitance of transistor devices irradiated using 0.45 MeV low energy electrons. The post-irradiation capacitance increased with respect to the pre-irradiation capacitance levels. Through calculations these capacitance levels were used to show that the carrier concentration in the 2DEG increased in the same manner that doping concentration caused a vertical shift in the C-V curves of *n*-type MOSFETs in Figure 26.

In a previous study, Look *et al.* [27] irradiated gallium nitride with 0.42 MeV electrons and found that at that level of radiation only the nitrogen vacancy was a shallow donor. Since 0.42 MeV and 0.45 MeV electrons are relatively close in energy, it is proposed that the increase in carrier concentration observed in these devices is due to the nitrogen vacancy contributing electrons in the gallium nitride and that these electrons are subsequently drawn into the 2DEG by the inherent electric field in the AlGaN.

Look *et al.* [27] further state that the minimum energy required to produce nitrogen displacement is 0.32 MeV and the minimum energy required to produce a gallium displacement is 0.53 MeV. The when this displacement occurs a nitrogen atom can donate and electron and a gallium atom accepts an electron. Furthermore, the production of the nitrogen donors exceeds the formation of gallium acceptors up to energy of approximately 0.87 MeV.

The increase due to the nitrogen vacancy in GaN should be easily observed by irradiating the samples with various energy electrons from 0.4 MeV to 0.8 MeV. As the energy increases the effects of donor electrons from the nitrogen should decrease as the incoming electrons begin to interact with the gallium. Thus, the capacitance should decrease when the C-V curves at higher electron energies are plotted and compared to the

plots of C-V curves of incident electrons with lower energies. During the irradiation of sample A2, the incident electron energy was changed to 0.8 MeV in order to observe this effect.

A slight decrease in capacitance in the inversion region between the 0.45 MeV sample, A1, and the 0.8 MeV sample, A2, was initially expected; however, the complete change in sign of the capacitance readings of A2 was unexpected. The following explanation is proposed. The fact that the capacitance measurements for A2 were negative indicates that the capacitance measured is due to the creation of acceptors in the GaN layer whereas a measurement of positive capacitance indicates that the capacitance measured is due to the creation of donors in the GaN. The GaN is intrinsically *n*-type indicating a natural surplus of electrons. This explains why the initial capacitance measurements are not equal in magnitude to the positive capacitance measurements and why as the measurement cycles repeat the capacitance becomes less negative. The intrinsic electrons are slowly filling the acceptors (holes) as the inherent electric field between the AlGaN and GaN directs the electrons toward the GaN.

The effect of incident electrons (0.45 MeV) is ionization and the creation of electron/hole pairs in the AlGaN. Due to the intrinsic electric field in the AlGaN, the ionized electrons exit the heterostructure rapidly leaving behind a stationary and trapped positive charge in the AlGaN along the interface between the AlGaN and GaN (Figure 67). This trapped positive charge along the interface causes more electrons from the bulk GaN to populate the 2DEG requiring a more negative applied bias to turn the device off and collapse the quantum well. The observed result of this trapped charge in the CV curves is a negative curve shift along the gate voltage axis and a negative increase in the

threshold voltage (Figure 68). Also, Figures 37 and 39 clearly show this threshold voltage shift following irradiation; however, Figure 57 and 59 show that after a 9 month room temperature anneal, the curve has recovered to the pre-irradiation location. The defect centers have been filled due to recombination through tunneling during the annealing process.

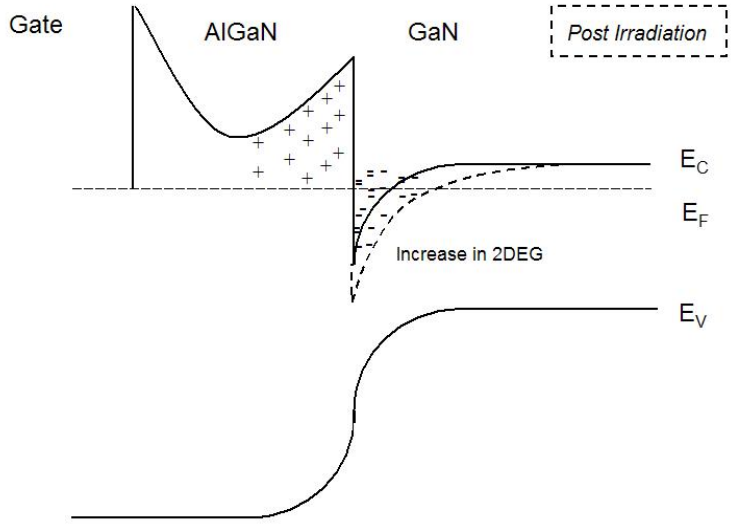

Figure 67. Band diagram of AlGaN/GaN MODFET after irradiation by 0.45 MeV electrons showing increase in carrier concentration due to formation of V_N in the GaN that donate electrons to the 2DEG.

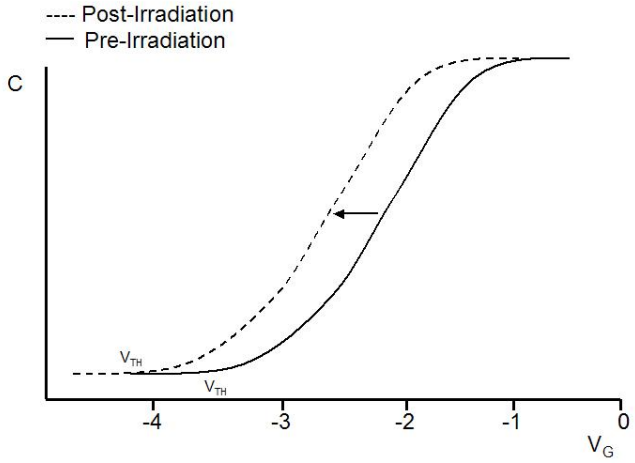

Figure 68. Negative threshold voltage shift in CV curve as a result of 0.45 MeV electron irradiation creating positive interface trapped charge.

The effect of incident electrons (0.8 MeV) is the formation of gallium vacancies in the GaN. These gallium vacancies act as acceptors and draw electrons from the 2DEG thus reducing the number of carriers and depopulating the quantum well. The gallium vacancy (acceptor) has the effect of lowering the E_F and depopulating the 2DEG.

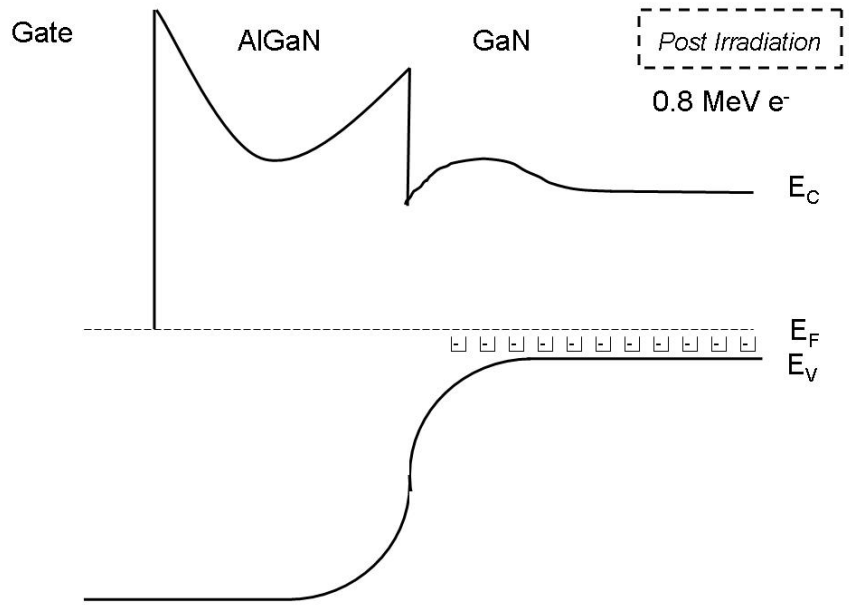

Figure 69. Band diagram of AlGaN/GaN MODFET after irradiation by 0.8 MeV electrons showing decrease in carrier concentration due to formation of V_{Ga} in the GaN that accept electrons from the heterostructure and 2DEG.

The capacitance in the Keithley 590 is calculated by the simple relationship,

$$C = I / fV \tag{23}$$

where I is the measured current, f is the measurement frequency and V is the source voltage. The frequency is a constant set by the operator depending on the output desired and can be either 100 kHz or 1 MHz on the Keithley 590.

The negative capacitance measurement obtained during the data recording of sample A2 is due to the way in which the Keithley 590 measures the capacitance through

equation (23). The only term in equation (23) that has the potential to change sign is V due to a measured potential difference between the conduction band and the Fermi level that is greater (Figure 69) compared to the measured potential from sample A1 (Figure 67). The Keithley 590 measures a current based on electrons inherently, and outputs a positive capacitance. However, the 0.45 MeV incident electrons create nitrogen vacancies (donors) in the AlGaN and GaN liberating electrons that populate the 2DEG and others that exit the AlGaN under the influence of the intrinsic electric field, $\mathcal{E}$. This is the normal or positive measured capacitance and results in a positive capacitance measurement through the Keithley 590. The 0.8 MeV incident electrons create gallium vacancies (acceptors) in the GaN liberating holes that depopulate the 2DEG and create a more positive charge in the normally n-doped GaN layer. Since the GaN is still under the influence of the intrinsic electric field, $\mathcal{E}$, the conduction band still bends somewhat at the heterojunction forming a quantum well (Figure 69), but the quantum well has been depopulated of electrons. This depopulation of the 2DEG and increase in positive charge in the GaN accounts for the negative capacitance measurement by the Keithley 590.

Additionally, just as the room temperature anneal of A1 resulted in an increase in measured capacitance as the annealing process progressed, the room temperature anneal of A2 resulted in a decrease in measured capacitance as the annealing progressed. This could indicate that the process liberating electrons and holes from the donors and acceptors, respectively, continues after irradiation ceases with the result that there is a net increase in stored charge in the donor case or a net decrease in stored charge in the acceptor case.

VI. Conclusions and Recommendations

Conclusions

Irradiation of AlGaN /GaN HEMTs by low energy electrons creates temperature-dependent damage that affects transistor operation. These effects have been observed in the transistor through capacitance-voltage measurements. The transistors show an increase in capacitance in the accumulation region and the inversion region as well as a negative shift and moderate flattening of the slope in the depletion region. The increase in capacitance in the inversion region indicates an increase in charge as a result of an increase in carrier concentration in the 2DEG, while the increase in the accumulation region indicates an increase in trapped positive charge in the AlGaN. The slope flattening in depletion indicates the presence of trapped interface charge between the AlGaN and GaN, which appears to be a permanent defect for the lower incident energy electron irradiation. The devices consistently fail to operate as designed at total fluences of 1.0×10^{15} e^-/cm^2 and do not recover completely to pre-irradiation operating parameters even after room temperature annealing.

The increase in carrier concentration in the 2DEG is due to low energy electron irradiation of 0.45 MeVs most likely resulting in displaced nitrogen atoms creating nitrogen vacancies. The nitrogen vacancies donate an electron to the GaN, which (due to the inherent electric fields in the highly polarized AlGaN layer) is drawn into the 2DEG. A second mechanism increasing the carrier concentration in the 2DEG is the deposition of large amounts of energy into the AlGaN resulting in a huge amount of ionization. This ionization results in the creation of electron-hole pairs in the AlGaN. Due to the intrinsic

electric field in the AlGaN, the electrons are swept out of the AlGaN and into the 2DEG leaving behind a large amount of trapped positive charge. This trapped positive charge increases the effect on the 2DEG by drawing more carriers from the bulk GaN increasing the concentration of the carriers. Essentially, both processes play an integral role in increasing the carrier concentration. The measurements obtained in this research do not provide the requisite information to definitively state which process dominates and under what conditions one dominates the other.

By conducting experiments at various energy levels ranging from energy that creates nitrogen vacancies to energy that favors gallium vacancies, the effects on carrier concentration were observed. The results indicate that the 2DEG increases at low electron energies due to nitrogen vacancies acting as donors, and decreases at higher electron energies due to gallium vacancies acting as acceptors.

Recommendations for Further Work

Due to the maintenance required by the VDG and the subsequent time constraints to complete data collection, not all of the 9 samples prepared for irradiation were irradiated. This leads to the requirement for additional research to validate the findings of this research with more corroborative data. Ideally, two additional samples irradiated at 0.45 MeV that duplicated the results of A1 would reinforce the conclusion that carrier concentration is indeed increasing due to irradiation. Likewise, at least two more irradiations at 0.8 MeV are required to duplicate the negative capacitance measurements and offer validation of the premise that gallium displacements are creating acceptors at 0.8 MeV while nitrogen vacancies are providing donors at a lower energy of 0.45 MeV.

Then, the proposed cause of the carrier concentration increase in the 2DEG can be attributed to the nitrogen vacancy as a result of incident electron energy. Further research should attempt to irradiate at a minimum with incident electrons at energies of 0.3, 0.5 and 0.7 MeV to observe changes in capacitance and determine where positive and negative capacitance thresholds occur as well as where there is no change.

A study using DLTS to determine if low incident electron energy causes nitrogen displacements and higher incident electron energy causes gallium displacements would add further credence to the results presented and theory proposed in the preceding pages.

Another possible avenue of investigation would be positron annihilation spectroscopy performed on samples irradiated with incident electron energy of 0.8 MeVs or greater in order to determine if gallium vacancies are actually formed in the GaN.

Additionally, a combined study involving both I-V and C-V low temperature measurements repeating both previous work and this research would produce concurrent results that when compared would provide a more complete picture than that of the two separate studies.

Finally, a computer simulation or model that replicates the device functioning would be beneficial in analyzing and predicting the various radiation effects on the HEMT devices. Specifically, the model should include the ability to input heterostructure parameters such as those listed on Figure 30. Additionally, by inputting incident electron energy, fluence and beam current, the output would yield capacitance information relative to all three regions of interest (accumulation, depletion and inversion) as a result of the effects of radiation.

Appendix A – Visual Basic Data Acquisition Program

This program was used to control the data acquisition device(s) used in this experiment to obtain capacitance-voltage measurements both during the pre-characterization of the devices and the actual experimental phase of irradiation.

****

```
Option Explicit
'CV measurements program Version 13 October 2004

Dim cycles As Integer
Dim startsumsec As Long
Dim elapsedtime As Integer
Dim temperature As Single

Dim CVFileName As String
Private Sub CWGPIB1_DataReady(ByVal taskNumber As Integer, data As Variant)

End Sub
```

```
Private Sub clrplot_Click()
CWGraph.ClearData
CWGraph1.ClearData
CWGraph2.ClearData
End Sub
```

```
Private Sub iDevice_OnReceivedData(data As String, DataTag As String, DateTime As
String, Quality As Long)
  Select Case DataTag
   Case "MainReading"
     templabel.Caption = data
  End Select
End Sub
```

```
Private Sub QuitButton_Click()
GPIBCAP.Write ("N0X")  'Place Capacitance SMU in Bias-off Mode
Unload Me
End
End Sub
```

```
Private Sub ResetFields_Click()

'Gate Voltage Frame
StartVgBox.Text = "-6.0"
StopVgBox.Text = "0.5"
StepVgBox.Text = ".125"

Vglabel.Caption = "0.000"
Caplabel.Caption = "0.0"
Transbox.Caption = "0.0"

'Cycle Label
CyclesBox.Text = "1"

dateofstart.Caption = "00"
timeofstart.Caption = "00:00:00"
dateofend.Caption = "00"
timeofend.Caption = "00:00:00"

'Comment Box
CommentBox.Text = "No File Comments"
deviceID.Text = "Enter device ID"
'powerkW.Text = "0"
'irradtime.Text = "0"
'desiredfluence.Text = "0"

GPIBCAP.Write ("X")

CWGraph.ClearData
CWGraph1.ClearData
CWGraph2.ClearData

End Sub
```

```
Private Sub Form_Load()

Call SetupGPIB
Call ResetFields_Click
elapsedtime = 0
CWGraph.ChartLength = 10000       ‘Graph of C vs. Vg
CWGraph1.ChartLength = 10000      ‘Graph of Conductance vs. Vg
CWGraph2.ChartLength = 10000      ‘Graph of 1/C^2 vs. Vg

'Setup CNi16D for use over Ethernet port with TCP/IP
iDevice.Command485Mode = RS485
```

```
iDevice.CommStatusEnable = True
iDevice.DataAccessMode = Asynchronous
iDevice.MeasDisplayEnable = False
iDevice.MeasIdleText = "No Read Available"
iDevice.ServerType = TCP_IP
iDevice.ServerServer = "128.100.101.254"
iDevice.ServerSource = 1000

temperature = iDevice.MainReading

End Sub
```

```
Private Sub DirSetup()

Dim today As String
Dim dirExist As String
Dim filedir As String

CurDir ("C:\")
ChDir "C:\"

filedir = "CV Thesis 2004 Output Data"
dirExist = Dir(filedir, vbDirectory)
If (Len(dirExist) = 0) Then
  MkDir filedir
End If

ChDir filedir

filedir = "Raw Data Files"
dirExist = Dir(filedir, vbDirectory)
If (Len(dirExist) = 0) Then
  MkDir filedir

End If

ChDir filedir

today = Format(Now, "mmddyy")       ' String of Today's Date
dirExist = Dir(today, vbDirectory)     ' Check that directory exist

If (Len(dirExist) = 0) Then         ' If not, create it
  MkDir today

End If
```

```
ChDir today

workdir.Caption = CurDir("C:")
End Sub
```

```
Private Sub SetupGPIB()

'CV Analyzer Setup
GPIBCAP.Reset
GPIBCAP.BoardNumber = 0
GPIBCAP.PrimaryAddress = 15
GPIBCAP.SecondaryAddress = 0
GPIBCAP.Configure


End Sub
```

```
Private Sub StartButton_Click()
Call DirSetup
Dim startmonth As Long
Dim startday As Long
Dim starthrs As Long
Dim startmin As Long
Dim startsec As Long

Dim duration As Integer
Dim Endtime As String

Dim starttime As String

'Record the start time of the experiment on click
starttime = Format(Now, "hh.mm.ss")
startmonth = Month(Now)
startday = Day(Now)
starthrs = Hour(starttime)
startmin = Minute(starttime)
startsec = Second(starttime)
startsumsec = startsec + (60 * startmin) + (60 * 60 * starthrs) '+ (60 * 60 * 24 * startday)

'Initialize temperature timer to record temperatures every second
TempTimer.Interval = 500
TempTimer.Enabled = True

dateofstart.Caption = Date
timeofstart.Caption = starttime
```

```
dateofend.Caption = "00"
timeofend.Caption = "00:00:00"

'Set up Capacitance Voltage
GPIBCAP.Write "B0X"   'Store Current Reading only in Buffer
'GPIBCAP.Write "F0X"   '100 kHz type measure
GPIBCAP.Write "F1X"   '1 MHz type measure
GPIBCAP.Write "G2X"   'Data Format Output
'GPIBCap.Write "O2,0,0X" 'Operation
GPIBCAP.Write "P0X"   'Filter OFF
GPIBCAP.Write "R0X"   'Auto Range
'GPIBCAP.Write "S0X"   'Reading Rate = 1000/sec
'GPIBCAP.Write "S1X"   'Reading Rate = 75/sec
GPIBCAP.Write "S2X"   'Reading Rate = 18/sec
'GPIBCAP.Write "S3X"   'Reading Rate = 10/sec
'GPIBCAP.Write "S4X"   'Reading Rate = 1/sec
GPIBCAP.Write "T2,0X"  'Trigger on X Command

Call RecordDataSweep

End Sub
```

```
Private Sub RecordDataSweep()

Dim Cap As Single
Dim Cap2 As Single
Dim Cond As Single
Dim Vg As Single

Dim StartVg As Single
Dim StopVg As Single
Dim StepVg As Single

Dim currentmonth As Long
Dim currenttime As String
Dim currentday As Long
Dim currenthrs As Long
Dim currentmin As Long
Dim currentsec As Long
Dim currentsumsec As Long
Dim diffsumsec As Integer

Dim i_cycle As Integer

Dim totalhrs As Integer
```

```
Dim totalmin As Integer
Dim totalsec As Integer

Dim printtime As String
Dim data(1, 0) As Variant

  StartVg = StartVgBox.Text
  StopVg = StopVgBox.Text
  StepVg = StepVgBox.Text

  cycles = CyclesBox.Text

  CVFileName = Format(Date, "mmd") & "_" & Format(Time, "hhmmss") & "_" &
deviceID.Text & "_" & irradtime.Text & "_" & desiredfluence.Text & ".txt"
  Open CVFileName For Output As #1

  'Write CV Data File Header
  Print #1, "Filename: " & CVFileName
  Print #1, "Device ID: " & deviceID.Text
  'Print #1, "Power [kW:] " & powerkW.Text
  'Print #1, "Time of Irradiation: " & irradtime.Text
  'Print #1, "Desired Fluence: "; desiredfluence.Text
  Print #1, "Misc Comments: " & CommentBox.Text
  Print #1,
  Print #1, "Cycle;Time;Temp;Vg;Cap;Trans"

'Perform CV Measurements
For i_cycle = 1 To cycles
  For Vg = StartVg To StopVg Step StepVg

  GPIBCAP.Write ("V" & Vg & "," & Vg & ",0,0,250X")  'Set Bias Voltage
  GPIBCAP.Write "N1X"     'Turn on Bias Voltage        'Trigger and Execute


     printtime = Format(Now, "hh.mm.ss")

     GPIBCAP.Write "O1,0,0X" 'Operation capacitance
     Cap = Mid(GPIBCAP.Read, 5, 11)
     GPIBCAP.Write "O2,0,0X" 'Operation conductance
     Cond = Mid(GPIBCAP.Read, 5, 11)


     'Check the temptimer to read new temperature
     DoEvents
```

```
    Print #1, i_cycle & ";" & printtime & ";" & temperature & ";" & Vg & ";" & Cap &
";" & Cond

    'Plot capacitance vs. gate voltage
    data(0, 0) = Vg
    data(1, 0) = Cap
    CWGraph.ChartXY data

    'Plot conductance vs. gate voltage
    data(1, 0) = Cond
    CWGraph1.ChartXY data

    'Plot 1/C2

    GPIBCAP.Write "O4,0,0X" 'Operation capacitance
    Cap2 = Mid(GPIBCAP.Read, 5, 11)
    data(1, 0) = Cap2
    CWGraph2.ChartXY data

    'Refresh the Information Panel
    Vglabel.Caption = FormatNumber(Vg, 3)

    Caplabel.Caption = Cap
    Condbox.Caption = Cond

    cyclelabel.Caption = i_cycle
    Panel.Refresh


  Next

    GPIBCAP.Write ("N0X")  'Place CV Analyzer in Inoperate Mode
     cyclelabel.Caption = i_cycle
    Panel.Refresh

Next i_cycle

Panel.Refresh
currenttime = Format(Now, "hh.mm.ss")
dateofend.Caption = Date
timeofend.Caption = currenttime

Print #1,
Print #1, dateofstart
Print #1, timeofstart
Print #1, dateofend
```

```
Print #1, timeofend
Close #1
End Sub
```

```
Private Sub Stop_Click()
GPIBCAP.Write ("N0X")  'Place Gate SMU in Inoperate Mode
'Unload Me

End Sub

' TempTimer controls how often temperature is updated
' Requests an updated temperature from CNi16D Controller, and updates
' total amount of elapsed time in seconds of experiment.
Private Sub TempTimer_Timer()

temperature = iDevice.MainReading        'Request Temperature Reading
End Sub
```

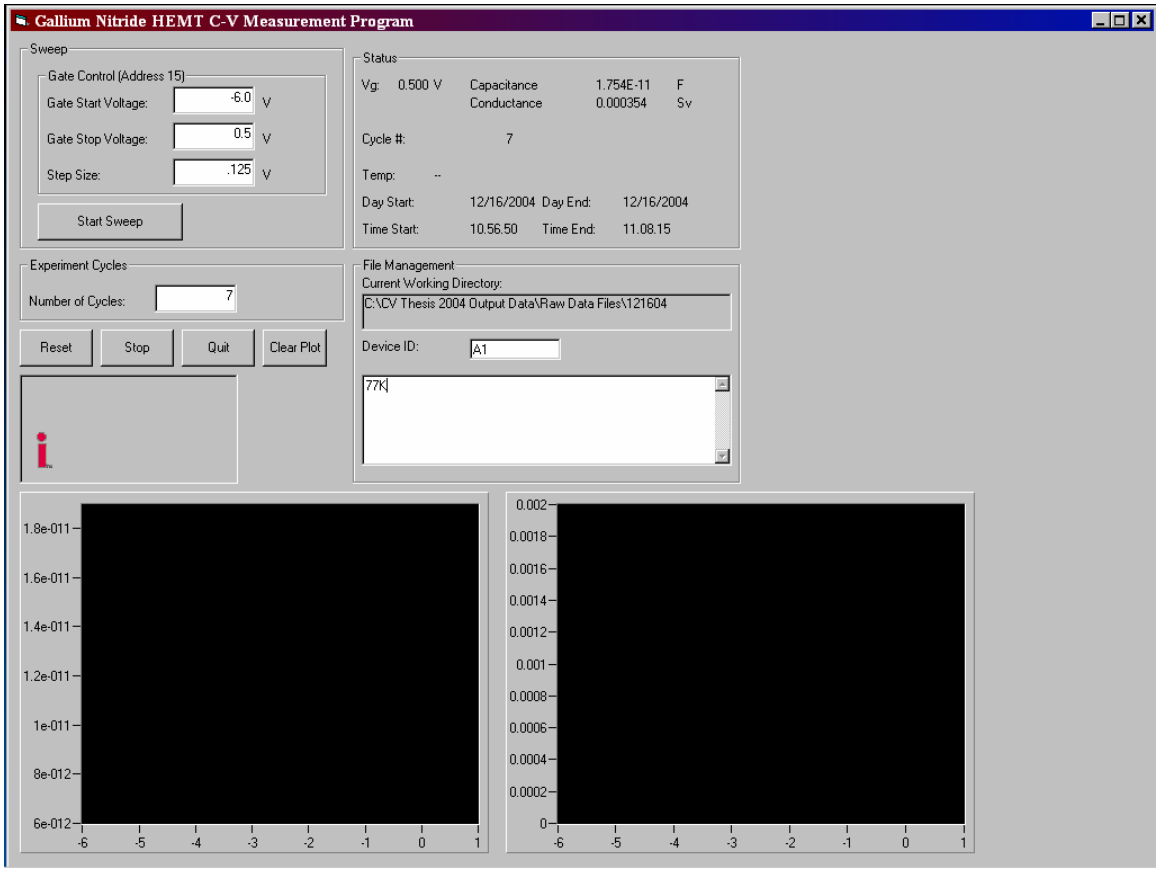

Figure 70: Screen capture image of program graphic user interface.

Appendix B – Pre-characterization C-V Plots (80K / 330K)

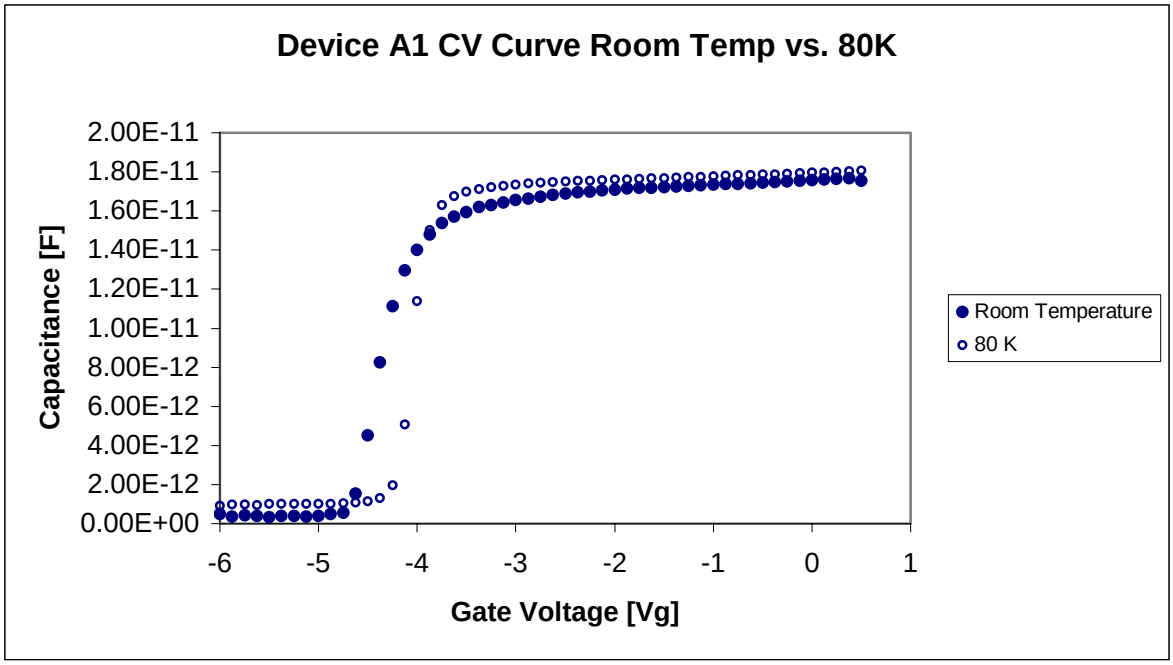

Figure 71: Pre-characterization plots of device A1 (80K and 300K)

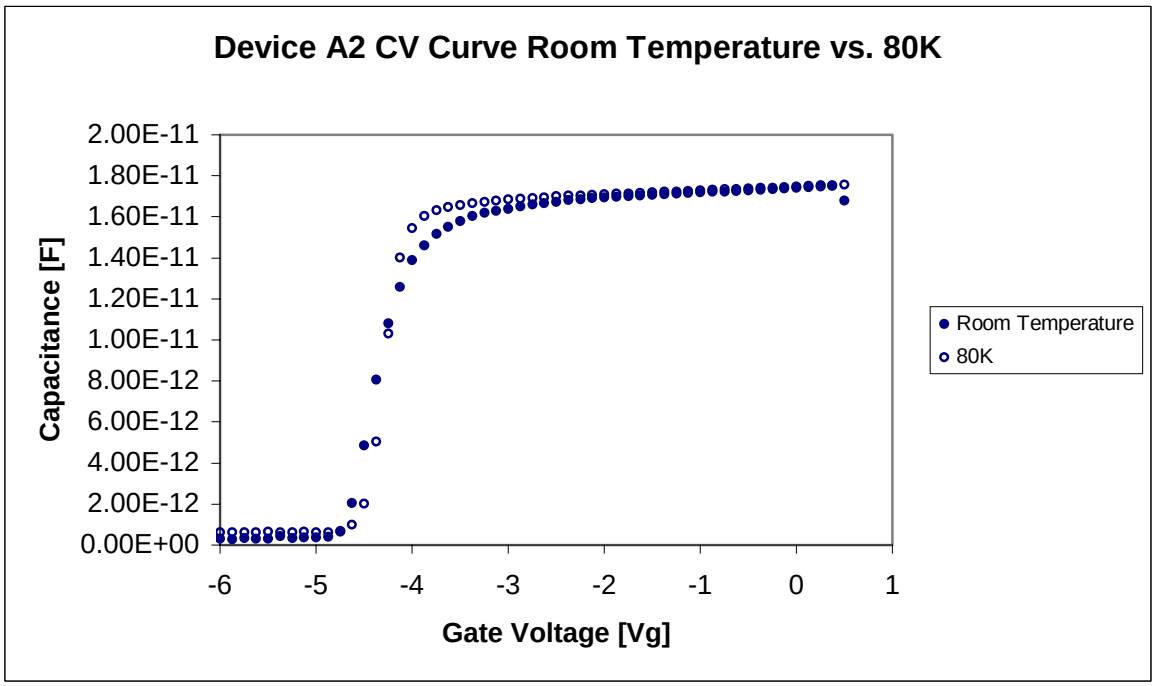

Figure 72: Pre-characterization plots of device A2 (80K and 300K)

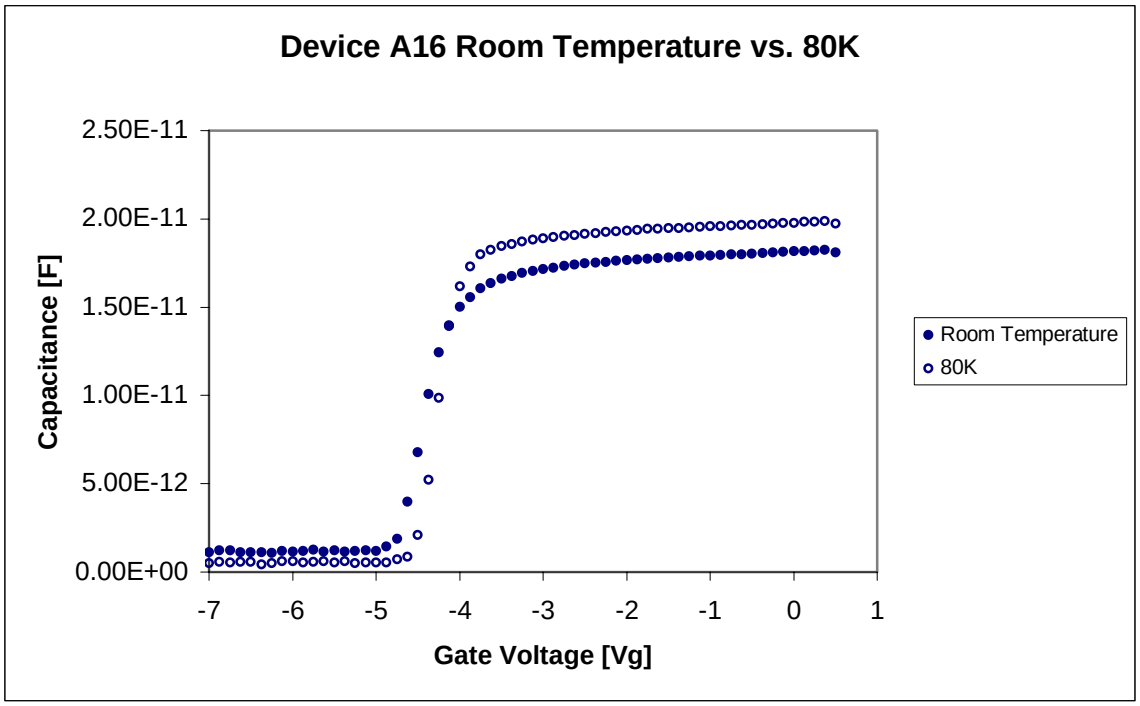

Figure 73: Pre-characterization plots of device A16 (80K and 300K)

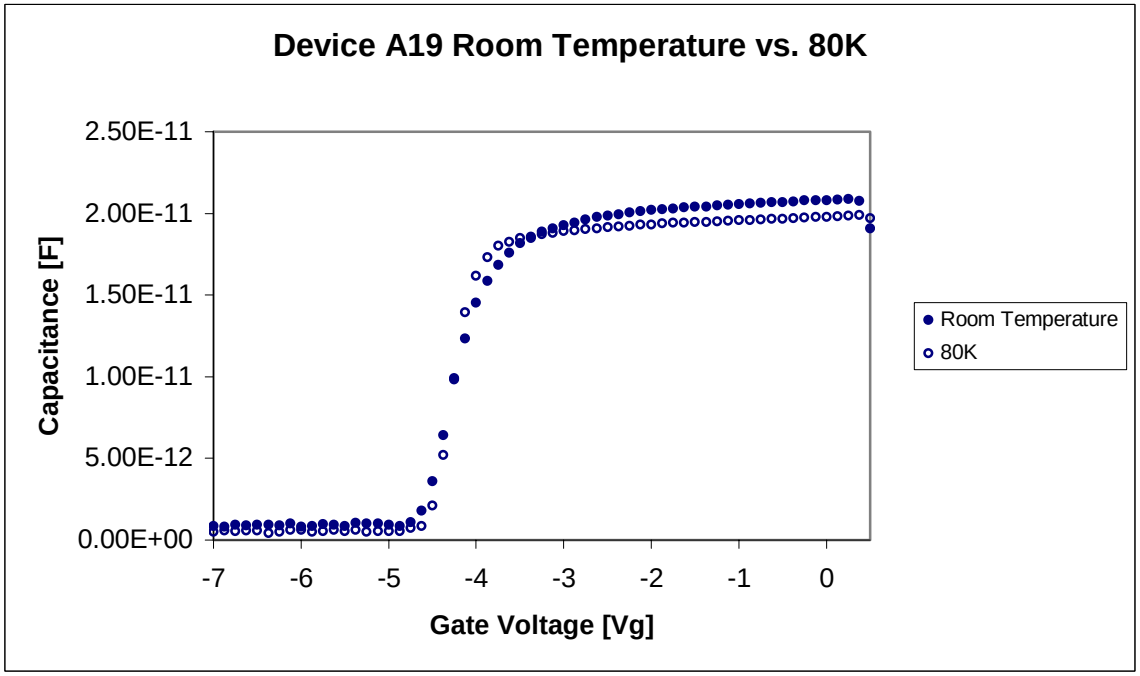

Figure 74: Pre-characterization plots of device A19 (80K and 300K)

Appendix C – Carrier Concentration Calculations

This worksheet compares the pre-irradiation device A1 with the post-irradiation devices A0409 and A0408. The carrier concentration before irradiation in device A1 is 1.51601×10^{15} cm^{-3} while the post-irradiation carrier concentration is 7.94587×10^{17} cm^{-3} and 2.37133×10^{18} cm^{-3} for A0409 and A0408 respectively.

$CapA1 = 3.11 * 10^{-13}$

$V = 5$

$q = 1.602 * 10^{-19}$

$\epsilon_\circ = 8.85 * 10^{-14}$

$\epsilon = 9.0$

$CapAreaA1 = CapA1 / (50 * 10^{-4} * 100 * 10^{-4})$

6.22×10^{-9}

$$N_{CV} = \frac{CapAreaA1^3}{q * \epsilon_\circ * \epsilon} * \frac{V}{CapAreaA1}$$

1.51601×10^{15}

$Cap409 = 7.12 * 10^{-12}$

$V = 5$

$q = 1.602 * 10^{-19}$

$\epsilon_\circ = 8.85 * 10^{-14}$

$\epsilon = 9.0$

$CapArea409 = Cap409 / (50 * 10^{-4} * 100 * 10^{-4})$

1.424×10^{-7}

$$N_{CV} = \frac{CapArea409^3}{q * \epsilon_\circ * \epsilon} * \frac{V}{CapArea409}$$

7.94587×10^{17}

$Cap408 = 1.23 * 10^{-11}$

$V = 5$

$q = 1.602 * 10^{-19}$

$\epsilon_\circ = 8.85 * 10^{-14}$

$\epsilon = 9.0$

$CapArea408 = Cap408 / (50 * 10^{-4} * 100 * 10^{-4})$

2.46×10^{-7}

$$N_{CV} = \frac{CapArea408^3}{q * \epsilon_\circ * \epsilon} * \frac{V}{CapArea408}$$

2.37133×10^{18}

Multiply by the thickness of the 2DEG(assume 1 nm) to get cm^{-2}

$n_s = N_{CV} * 10^{-7}$

2.37133×10^{11}

Multiply by the thickness of the 2DEG(assume 10 nm) cm^{-2}

$n_s = N_{CV} * 10 * 10^{-7}$

2.37133×10^{12}

Bibliography

[1] J. Petrosky. *Radiation Effects Book: Class Notes NENG 664.* Unpublished. 2004

[2] C. Claeys and E. Simoen. "Radiation Effects in Advanced Semiconductor Materials and Devices," Springer-Verlag, Berlin (2002).

[3] P.S.Winokur. "Total-dose Radiation Effects (From the Perspective of the Experimentalist)," *IEEE Nuclear and Space Radiation Effects Conference Short Course,* New Orleans, 13 July 1992. (1999)

[4] Robert F. Pierret. *Semiconductor Device Fundamentals*. Addison-Wesley Publishing Company, Reading, MA, 1996.

[5] M. Stutzmann, *et al*. "GaN-based heterostructures for sensor applications," *Diamond and Related Materials*, 11: 886-891 (2002).

[6] Stephen A. Campbell. *The Science and Engineering of Microelectronics Fabrication*. Oxford University Press, New York, 2001.

[7] K. Linthicum. "GaN Overview." Excerpt from unpublished article. n. pag. http://www.nitronex.com/education/ganOverview.html. 15 July 2004.

[8] L. Shen, *et al.* "AlGaN/AlN/GaN high-power microwave HEMT," *IEEE Electron Device Letters,* Vol. 22, No. 10: 457-459 (2001).

[9] Hadis Markoc. "Potential applications on III-V nitride semiconductors," *Materials Science and Engineering*, B43: 137-146 (1997).

[10] Mohamed Henini. "III-V nitrides for electronic and UV applications," *III-Vs Review*, Vol. 12, No. 5: 28-32 (1999).

[11] B. Luo, *et al*. "High-energy proton irradiation effects on AlGaN/GaN high-electron mobility transistors," *Journal of Electronics Materials*, 31: 437-441 (2002).

[12] A. Ionascut-Nedelcescu, *et al*. "Radiation hardness of gallium nitride," *IEEE Transactions on Nuclear Science*, 49: 2733-2738 (December 2002).

[13] B. D. White, *et al*. "Characterization of 1.8 MeV proton-irradiated AlGaN/GaN field-effect transistor structures by nanoscale depth-resolved luminescence spectroscopy," *IEEE Transactions on Nuclear Science* 49: 2695-2701 (December 2002).

[14] Gaudreau, *et al*. "Transport Properties of Proton-Irradiated Gallium Nitride-Based Two-Dimensional Electron-Gas System," *IEEE Transactions on Nuclear Science*, 49: 2702-2707 (December 2002).

[15] S. M. Sze. *Semiconductor Devices: Physics and Technology.* 2nd Edition, John Wiley & Sons, Inc. New York, 2002.

[16] S. Hiyamizu, *et al.* "High mobility of two-dimensional electrons at the GaAs/n-AlGaAs heterojunction interface," *Applied Physics Letters*, Vol. 37, No. 9: 805-807 (1980).

[17] Umesh K. Mishra, *et al*. "AlGaN/GaN HEMTs – An Overview of Device Operation and Applications," *Proceedings of the IEEE*, Vol. 90, No. 6: 1022-1031 (2002).

[18] Kevin D. Greene. *Electron Paramagnetic Resonance Spectroscopy and Hall Effect Studies of the Effects of Low Energy Electron Irradiation on Gallium Nitride (GaN).* Air Force Institute of Technology (AU), Wright-Patterson AFB OH, September 2003.

[19] H. Morkoç. "Nitride Semi-conductors and Devices," Springer-Verlag, Berlin, 1999.

[20] Andrew Holmes-Siedle, Len Adams. *Handbook of Radiation Effects*. 2nd Edition, Oxford University Press, Oxford, 2002.

[21] James M. Sattler. *An Analysis of the Effects of Low Energy Electron Radiation on AlGaN/GaN Modulation-Doped Field Effect Transistors*. Air Force Institute of Technology (AU), Wright-Patterson AFB OH, March 2004.

[22] M. S. Shur, *et al.* "Wide band gap electronic devices," *Fourth IEEE International Caracas Conference on Devices, Circuits and Systems*, Aruba, April 17-19, 2002.

[23] Q. Chen, *et al*. "Microwave Electronic Device Applications of AlGaN/GaN Heterostructures," *Materials Science and Engineering*, B59: 395-400 (1999).

[24] S. Goodman, *et al.* "Electron irradiation induced defects in n-GaN," *Semiconducting and Insulating Materials Conference 2000*, SIMC-XI International, 43-46 (2000).

[25] C. Coskun, *et al.* "An experimental set-up for *in situ* Hall measurements under high-energy electron irradiation for wide-bandgap materials," *Measurement Science and Technology,* Vol. 15: 297-302 (2004).

[26] Z-Q. Fang, *et al*. "Deep centers in as-grown and electron-irradiated n-GaN," *IEEE*, 35-42 (2000).

[27] D. C. Look, *et al*. "On the Nitrogen Vacancy in GaN," *Applied Physics Letters*, Vol. 83, No. 17: 3525-3527 (2003).

[28] R. Wilkins, *et al.* "Ionization and displacement damage irradiation studies of quantum devices: Resonant tunneling diodes and two-dimensional electron gas transistors," *IEEE Transactions on Nuclear Science,* Vol. 46, No. 6: 1702-1707 (1999).

[29] A. Y. Polyakov, *et al*. "Effects of proton implantation on electrical and recombination properties of n-GaN," *Solid State Electronics*, 44: 1971-1983 (2000).

[30] X. Hu, *et al.* "Proton-irradiation effects on AlGaN/AlN/GaN high electron mobility transistors," *IEEE Transactions on Nuclear Science,* Vol. 50. No. 6: 1791-1796 (2003).

[31] X. Hu, *et al.* "The energy dependence of proton-induced degradation in AlGaN/GaN high mobility electron transistors," *IEEE Transactions on Nuclear Science,* Vol. 51, No. 2: 293-297 (2004).

[32] D. C. Look, *et al*. "Defect Donor and Acceptor in GaN," *Physical Review Letters*, Vol. 79, No. 12: 2273-2276 (1997).

[33] N. Shaar *et al.* "Use of Capacitance-Voltage Measurement for characterization of a new poly-gate MOS process," (2004).

[34] P. Notinger Jr., *et al.* "Characterization of Electric Charge in Non Irradiated and Irradiated MOS Structures by Thermal Step and Capacitance-Voltage Measurements," 2002 Annual Report Conference on Electrical Insulation and Dielectric Phenomena.

[35] T. Hashizume *et al.* "Capacitance-Voltage characterization of AlN/GaN metal-insulator-semiconductor structures grown on sapphire substrate by metalorganic chemical vapor deposition, *Journal of Applied Physics*, Vol. 88, No. 4: 1983-1986 (2000).

[36] O. Ambacher *et al.* "Two-dimensional electron gases induced by spontaneous and piezoelectric polarization charges in N- and Ga-face AlGaN/GaN heterostructures," *Journal of Applied Physics*, Vol. 85, No. 6: 3222-3233 (1999).

[37] P. Pisecny *et al.* "Determination of Interface Trap Density in Unipolar Structures Using Quasistatic C-V Method," *Journal of Electrical Engineering,*Vol. 55, No. 3-4: 95-99 (2004).

[38] E. F. De Silva, Jr. *et al.* "Time evolution of SiO2 / Si interface defects and dopant passivation in MOS capacitors," *Microelectronic Engineering,* Vol. 51-52: 567-574 (2000).

[39] B. J. Gordon. "C-V plotting myths and methods," Solid State Technology 1993 (January): 57-61.

[40] Ron Schrimpf. "Radiation Effects on MOS devices," *Vanderbilt Radiation Effects Short Course,* 15 August 2001.

[41] E.F.Schubert. "Chapter 16-3. MOS C-V characteristics," Class Notes retrieved from the internet. http://www.ecse.rpi.edu/~schubert/course-ECSE-2210%20MT/MT-26-Ch16-3.ppt. 2 November 2004.

[42] H. Morkoç, *et al.* "Review: GaN-based modulation doped FETs and UV detectors," *Solid-State Electronics,* 46: 157-202 (2002).

[43] Hsu, L. *et al*. "Electron mobility in AlxGa1-xN/GaN heterostructures," Physical Review B, Vol. 56, No. 3: 1520-1528 (1997).

REPORT DOCUMENTATION PAGE

Form Approved
OMB No. 074-0188

The public reporting burden for this collection of information is estimated to average 1 hour per response, including the time for reviewing instructions, searching existing data sources, gathering and maintaining the data needed, and completing and reviewing the collection of information. Send comments regarding this burden estimate or any other aspect of the collection of information, including suggestions for reducing this burden to Department of Defense, Washington Headquarters Services, Directorate for Information Operations and Reports (0704-0188), 1215 Jefferson Davis Highway, Suite 1204, Arlington, VA 22202-4302. Respondents should be aware that notwithstanding any other provision of law, no person shall be subject to an penalty for failing to comply with a collection of information if it does not display a currently valid OMB control number.
PLEASE DO NOT RETURN YOUR FORM TO THE ABOVE ADDRESS.

1. REPORT DATE *(DD-MM-YYYY)*	**2. REPORT TYPE**	**3. DATES COVERED** *(From – To)*
21-03-2005	**Master's Thesis**	Jun 2004 – Mar 2005

4. TITLE AND SUBTITLE

CAPACITANCE-VOLTAGE STUDY ON THE EFFECTS OF LOW ENERGY ELECTRON RADIATION ON $Al_{0.27}Ga_{0.73}N$ / GaN HIGH ELECTRON MOBILITY TRANSISTOR

5a. CONTRACT NUMBER

5b. GRANT NUMBER

5c. PROGRAM ELEMENT NUMBER

6. AUTHOR(S)

Jarzen, Thomas D., Major, USA

5d. PROJECT NUMBER

5e. TASK NUMBER

5f. WORK UNIT NUMBER

7. PERFORMING ORGANIZATION NAMES(S) AND ADDRESS(S)

Air Force Institute of Technology
Graduate School of Engineering and Management (AFIT/ENP)
2950 Hobson Way
WPAFB OH 45433-7765

8. PERFORMING ORGANIZATION REPORT NUMBER

AFIT/GNE/ENP/05-05

9. SPONSORING/MONITORING AGENCY NAME(S) AND ADDRESS(ES)

DTRA/CSNP
DTRA HEADQUARTERS
ATTN:
8725 John J. Kingman Road
Ft. Belvoir, VA 22060-6201

10. SPONSOR/MONITOR'S ACRONYM(S)

11. SPONSOR/MONITOR'S REPORT NUMBER(S)

12. DISTRIBUTION/AVAILABILITY STATEMENT

APPROVED FOR PUBLIC RELEASE; DISTRIBUTION UNLIMITED

13. SUPPLEMENTARY NOTES

14. ABSTRACT

The effects of radiation on semiconductors are extremely important to the Department of Defense since the majority of the defense informational, navigational and communications systems are now satellite-based. Due to the high radiation tolerance of gallium nitride and a plethora of high temperature, high power and high frequency applications, the prospect that gallium nitride based devices will become key components in a multitude of military satellite-based systems is highly probable. $Al_xGa_{1-x}N$/GaN HEMTs were irradiated at low temperature (~80 K) by 0.45 – 0.8 MeV electrons up to fluences of 1×10^{15} e^-/cm^2. Following irradiation, low temperature capacitance-voltage measurements were recorded providing fluence-dependent measurements; additionally low-temperature post-irradiation capacitance-voltage measurements were recorded at twenty-four hour intervals up to 168 hours in order to investigate the room temperature annealing process. Using previously irradiated devices, the effects of a 9 month room temperature anneal were also considered. Capacitance-voltage measurements indicate that low energy electron radiation results in an increase in the transistor channel drain current. These increases occur both at low and room temperature. The mechanism, clearly shown through capacitance-voltage measurements, causing the increase in drain current is an increase in the carrier concentration in the 2DEG. This result is due to donor electrons from a nitrogen vacancy in the gallium nitride. The devices begin to anneal immediately and show almost complete recovery after 72 hours.

15. SUBJECT TERMS

Aluminum Gallium Nitride, Gallium Nitride, Transistors, Heterojunctions, High Electron Mobility Transistors, Field Effect Transistors, Electron Irradiation, Radiation Effects, Radiation Damage, Semiconductors, Capacitance-Voltage Measurements

16. SECURITY CLASSIFICATION OF:			**17. LIMITATION OF ABSTRACT**	**18. NUMBER OF PAGES**	**19a. NAME OF RESPONSIBLE PERSON**
REPORT	**ABSTRACT**	**c. THIS PAGE**			Dr. James C. Petrosky, (ENP)
U	**U**	**U**	**UU**	143	**19b. TELEPHONE NUMBER** *(Include area code)* (937) 255-6565, ext 4600 (James.Petrosky@afit.edu)

Standard Form 298 (Rev: 8-98)
Prescribed by ANSI Std. Z39-18